JMO

Journal for Modeling in Ophthalmology

Journal for Modeling in Ophthalmology (JMO) was created in 2014 with the aim of providing a forum for interdisciplinary approaches integrating mathematical and computational modeling techniques to address open problems in ophthalmology.

The Editorial Board members include experts in ophthalmology, physiology, mathematics, and engineering, and strive to ensure the highest scientific level of the contributions selected for publication. JMO aims to be the voice for this rapidly growing interdisciplinary research and we hope you will join us on this exciting journey.

JMO welcomes articles that use modeling techniques to investigate questions related to the anatomy, physiology, and function of the eye in health and disease.

For further information on JMO's focus and scope as well as manuscript submissions:

www.modeling-ophthalmology.com
info@modeling-ophthalmology.com

Copyright

Manuscript submissions
Author guidelines and templates are available via the website, through which all manuscripts should be submitted. For inquiries please contact us via e-mail.

Publication frequency
JMO is published four issues per year (quarterly) electronically. A selection is published in print twice a year and distributed free of charge at congresses through Kugler Publications or partners.

Advertising inquiries
JMO offers online and in print sponsorship and advertising opportunities. Please contact Kugler Publications to for inquiries.

b. After 12 months from the date of publication, authors are able to enter into separate, additional contractual arrangements for the non-exclusive distribution of JMO's published version of the work, with an acknowledgement of its initial publication in JMO.

Open access policy

The first volume of JMO is fully open access (after registration) without requiring any publication fee from the authors. However, we are currently evaluating various models to cover the publications costs while keeping knowledge as accessible as possible, which remains our first priority. Possible models include subscription fees, publication fees, and advertisement venues, or a combination. Please share your thoughts with us on this hot topic via e-mail.

Disclaimers

Table of contents

Editorial ESB-ITA 2017 special issue

Anna Pandolfi[1], Giuseppe Vairo[2]

[1]Department of Civil and Environmental Engineering, Politecnico di Milano (Polytechnic University of Milan), Milan, Italy; [2]Department of Civil Engineering and Computer Science, Università degli Studi di Roma "Tor Vergata", Rome Italy

This special issue of the *Journal for Modeling in Ophthalmology* collects, in the form of extended abstracts, contributions presented during the Thematic Symposium on Eye Biomechanics, organized within the VII Annual Meeting of the Italian Chapter of the European Society of Biomechanics (ESB-ITA 2017) held on September 28-29, 2017 in Rome, Italy. The scientific and administrative organization of the general meeting was committed to the Università degli Studi di Roma "Tor Vergata", while the scientific coordination of the thematic symposium was assigned to the Politecnico di Milano.

The thematic symposium addressed the behavior of heathy and diseased eyes involving diverse areas of physics such as solid mechanics, fluid mechanics, and electro-chemistry. The focus was on modeling the complex physics of the eye, regarded as a fundamental point to improve patient outcomes in current clinical practice. Clinical experiences in ophthalmology, consistent theoretical formulations, and advanced computational modeling methods have been presented as the results of a successful cooperation between clinicians, engineers, and physicists.

In recognition of the high quality of the thematic symposium, approaching topics at the cutting edge of research in ocular biomechanics, this issue collects posters and oral presentations. Contributions describe computational models for the analysis of ocular biomechanics, useful for simulating, planning and optimizing surgical procedures (Sala *et al.* and Ariza-Gracia *et al.*); theoretical models and experimental strategies for the investigation of the biomechanical etiology of eye diseases, *e.g.,* glaucoma, age-related macular degeneration, vitreoschisis, myopia, and diabetic retinopathy (Stefanoni *et al.*, Sacco *et al.*, and Salerni *et al.*), as well as for the optimization of possible therapeutic strategies (Ferroni *et al.* and Davvalo Khongar *et al.*); experimental studies for the identification of the mechanical properties of the tissues (Zhoula *et al.*, Kazaili and Akhtar, and Lipari *et al.*) and the optimization of surgical procedures (Romano *et al.*, Nepita *et al.*, and Stocchino *et al.*); constitutive models of ocular tissues (Vasta *et al.* and Recrosi *et al.*); and computational approaches for the simulation of mechanical-based diagnostic procedures (Montanino *et al.* and Ariza-Gracia *et al.*).

Correspondence: Anna Pandolfi, Department of Civil and Environmental Engineering, Politecnico di Milano, Piazza Leonardo da Vinci 32, 20133 Milano, Italy.
E-mail: anna.pandolfi@polimi.it

Although the summaries collected here refer to selected front-line studies developed mainly within the Italian community, all contributions testify explicitly that the efforts arising from the Italian scientists in the field of ocular biomechanics are strongly intertwined with the international research network, and that Italian research plays a major role in the international scene.

Towards a full model for ocular biomechanics, fluid dynamics, and hemodynamics

Lorenzo Sala[1], Christophe Prud'Homme[1], Marcela Szopos[1], Giovanna Guidoboni[2]

[1]*Institute for Advanced Mathematical Research, Unité Mixte de Recherche 7501, National Center for Scientific Research, University of Strasbourg, Strasbourg, France;* [2]*Department of Electrical Engineering and Computer Science, University of Missouri, Columbia, MO, USA*

Abstract

This contribution presents an ongoing work to implement a patient-specific mathematical virtual simulator for the eye. The aim is to create a multiscale and multiphysics model for the description of ocular biomechanics, fluid dynamics, and hemodynamics. This instrument may serve to illustrate and estimate some clinically relevant parameters, as well as predict their spatial and temporal evolution adopting forward-looking numerical techniques.

Keywords: hybridizable discontinuous Galerkin method, multiphysics, multiscale, ocular virtual simulator

1. Introduction

Our purpose is to develop a patient-specific Mathematical Virtual Simulator (MVS) that can describe and quantify the interaction between biomechanics, fluid dynamics, and hemodynamics in the eye. The aim is to couple all the various physical aspects in the same model in order to have a full overview of the ocular system. To reach this ambitious goal, we have identified four main modeling steps:
1. blood circulation in the eye from a systemic viewpoint;

Correspondence: Lorenzo Sala, Université de Strasbourg, CNRS, IRMA UMR 7501, Strasbourg, France.
E-mail: sala@unistra.fr

2. biomechanics and tissue perfusion in the optic nerve head and the lamina cribrosa;[1]
3. biomechanics for the sclera, retina, choroid, and cornea; and
4. fluid dynamics of the vitreous and aqueous humor.

Each step is naturally coupled with the others, giving rise to challenging problems from both the modeling and computational perspectives. In this abstract, we focus our attention on the second and third steps.
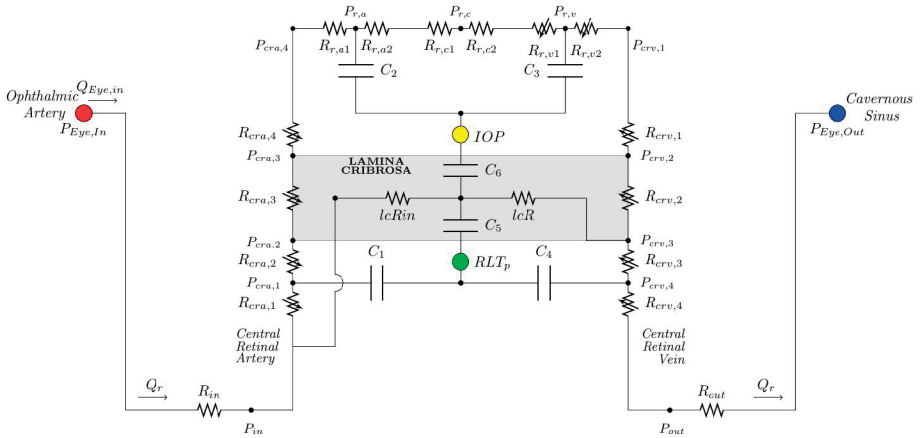
Fig. 1. Circuit-based model retinal and retrobulbar flow.
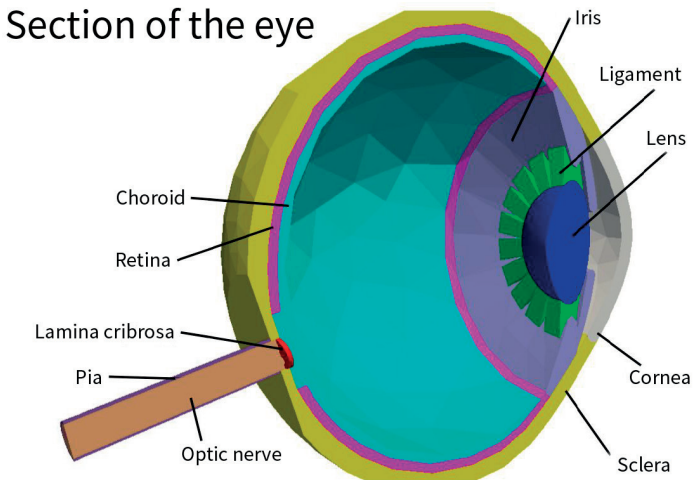
Fig. 2. The 3-D geometry generated with Salome.

2. Model and methods

The MVS has a multiscale architecture that aims at preserving the natural systemic features of blood circulation, while providing detailed views on sites of particular interest from the clinical viewpoint, such as the lamina cribrosa. Thus, MVS combines:

1. a circuit-based model for blood flow in the retinal vasculature, central retinal artery (CRA), and central retinal vein (CRV);
2. a 3-D porous media model for the perfusion of the lamina cribrosa; and
3. a 3-D isotropic elastic model for the biomechanics in the lamina cribrosa, retina, choroid, sclera, and cornea.

Figure 1 illustrates the circuit-based model in which we are substituting the lumped-parameters description of the lamina with a poroelastic spatial distribution model of the lamina. The elastic system of the lamina is also influenced by the biomechanics of the sclera, retina, choroid, and cornea. The novelty of the methods in the current work comes from two complementary perspectives. On the one hand, from a clinical perspective, the model inputs (*e.g.*, blood pressure, intraocular pressure, and ocular geometry) are easily accessible with standard instruments and can therefore be tailored to patient-specific conditions. In particular, starting from an initial computer-aided design (CAD) geometrical model, the structure of the geometry is further elaborated using Salome (OPEN CASCADE SAS, Guyancourt, France)[1] with the help of a Python (Python Software Foundation, The Netherlands) script that incorporates some parameterized values (*e.g.*, thickness of the lamina cribrosa) into the final meshed geometry (Fig. 2). On the other hand, from a numerical viewpoint, the problem involves a non-trivial coupling between biomechanics and hemodynamics in the tissue of the lamina cribrosa, which calls for:

1. high accuracy in the approximation for both primal variables (*i.e.*, displacement and pressure) and dual variables (*i.e.*, stress and perfusion velocity); and
2. integral boundary conditions to account for the coupling between 0-D and 3-D model components.

2.1. Coupling between biomechanics and hemodynamics

The two-way coupling between biomechanics and hemodynamics contributing to tissue perfusion in the lamina cribrosa is taken into account by means of the following poroelastic model:

$$\nabla \cdot \underline{\underline{\sigma}} = f_{el} \tag{1}$$

$$\underline{\underline{\sigma}} = \underline{\underline{\sigma}}_{el} - p\underline{\underline{I}} \tag{2}$$

$$\underline{\sigma}_{el} = \mu\left(\nabla \underline{u} + \nabla^{\top}\underline{u}\right) + \lambda(\nabla \cdot \underline{u})\underline{\underline{I}} \tag{3}$$

$$\nabla \cdot \underline{u}t + \nabla \cdot \underline{v} = f_{fl} \tag{4}$$

$$\underline{v} + \kappa\nabla p = 0 \tag{5}$$

where $\underline{\underline{\sigma}}$ is the total stress tensor, $\underline{u}$ is the solid displacement, p is the fluid pressure, $\underline{v}$ is the discharge velocity, λ and μ are the elastic parameters, κ is the permeability, and $\boldsymbol{f}_{el}$ and f_{fl} are volumetric sources of linear momentum and fluid mass, respectively. The poroelastic system, illustrated in Equations (1-5), has been already studied and presented in Causin *et al.*[2] and Prada.[3] Here, we highlight the importance of the two terms in red, since they are responsible for the biomechanical/hemodynamical coupling. Indeed, the presence of capillaries within the lamina collagen beams may influence the biomechanical behavior of the tissue, as expressed in Equation (2). In turn, structural deformations may induce local changes in blood flow, as expressed in Equation (4).

2.2. Hybridizable discontinuous Galerkin method and integral boundary condition

To numerically solve the coupled system of Equations (1-5), we implemented a hybridizable discontinuous Galerkin (HDG) method[4] in the multiphysics open-source platform Feel++ (Cemosis; Strasbourg, France).[5] The HDG method has several attractive features:

1. it provides optimal approximation of both primal (pressure, displacement) and dual (velocity, stress) variables;
2. it requires less globally coupled degrees of freedom than DG methods of comparable accuracy using static condensation; and
3. it allows local element-by-element post-processing to obtain new approximations with enhanced accuracy and conservation properties.

Furthermore, to handle the multiscale nature of this problem, we coupled the 3-D system of partial differential Equations (1-5) with a 0-D circuit model implemented in OpenModelica (Open Source Modelica Consortium; Linköping, Sweden). The complex coupling between the HDG system and the circuit has been achieved using integral boundary condition (IBC) and a time-splitting energy-based scheme in the spirit of a recent method presented in Carichino *et al.*[6] The combination of IBC with the high accuracy in dual variables of the HDG method revealed to be determinant for the proper resolution of the coupled multiscale problem. A detailed explanation of this procedure can be found in Sala *et al.*[7]
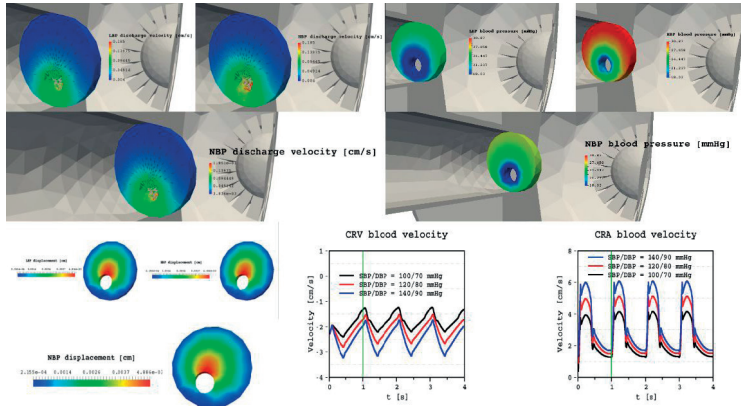
Fig. 3. Lamina cribrosa and CRA/CRV results simulated via MVS.
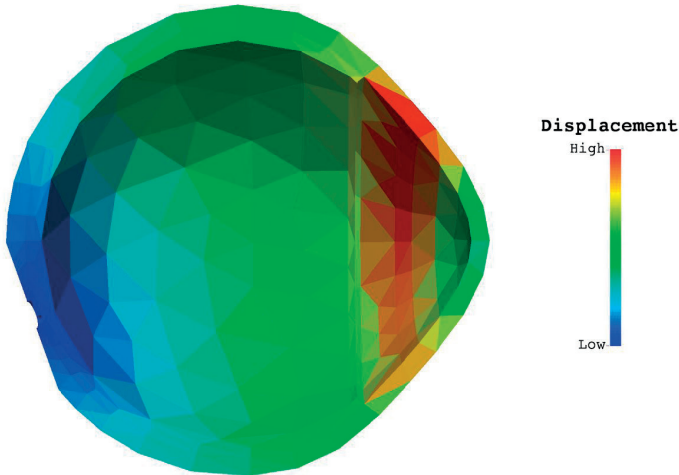
Fig. 4. Qualitative displacement on retina, choroid, sclera, and cornea simulated via MVS.

3. Results

Simulated distributions of velocities and pressure within the lamina, and of blood velocity within the CRA and CRV obtained via the MVS (see Fig. 3) exhibit a satisfactory agreement with reported experimental data,[8-10] with a special focus on the blood pressure computed on the lateral boundary of the lamina, where we have applied the integral interface condition between the 0-D and the 3-D models.

Moreover, some outcomes (Fig. 3, two bottom right figures) of MVS can be directly compared to those obtained via direct imaging modalities.[11]

In Figure 4, we show an overview of the qualitative behavior of the displacement for the lamina, retina, choroid, sclera, and cornea.

4. Conclusion

In conclusion, MVS combines innovative and complex methods such as integral boundary condition for HDG in order to be able to address the increasing demand of information on parts of the eye that are not easily accessible with standard research methods, such as those regarding the perfusion of the lamina cribrosa in the optic nerve head. Furthermore, the proposed model develops an interesting multiphysics and multiscale approach to connect different characters such as biomechanics and hemodynamics.

Acknowledgements

References

1.   Sala L, Prudhomme C, Prada D, et al. Patient-specific virtual simulator of tissue perfusion in the lamina cribrosa. In: Annual Meeting of the Association for Research in Vision and Ophthalmology. 7-11 May 2017. Baltimore, MD, USA.

2.   Causin P, Guidoboni G, Harris A, Prada D, Sacco R, Terragni S. A poroelastic model for the perfusion of the lamina cribrosa in the optic nerve head. Math Biosci. 2015; 257:33-41.

3.   Prada D. A hybridizable discontinuous Galerkin method for nonlinear porous media viscoelasticity with applications in ophthalmology. PhD thesis at IUPUI. 2016. Indianapolis (IN) USA.

4.   Cockburn B, Gopalakrishnan J, Lazarov R. Unified hybridization of discontinuous Galerkin, mixed, and continuous Galerkin methods for second order elliptic problems. SIAM J Numer Anal. 2009;47(2):1319–1365.

5.   Prud'Homme C, Chabannes V, Doyeux V, Ismail M, Samake A, Pena G. Feel++: A Computational Framework for Galerkin Methods and Advanced Numerical Methods ESAIM: Proceedings, EDP Sciences. 2012; 38: pp. 429-455. doi: 10.1051/proc/201238024

6.   Carichino L, Guidoboni G, Szopos M. Operator splitting approach for coupling Stokes flow and non-linear systems of ODEs. In: 7th International Conference on Computational Methods for Coupled Problems in Science and Engineering. 2017. Rhodes, Greece.

7.   Sala L, Hild R, Prud'Homme C, et al. An implementation of HDG methods with Feel++. Application to problems with integral boundary condition. In preparation. 2017.

8.   Yan DB, Coloma FM, Metheetrairut A, Trope GE, Heathcote JG, Ethier CR. Deformation of the lamina cribrosa by elevated intraocular pressure. Br J Ophthalmol. 1994;78(8):643-648.

9.   Sigal IA, Flanagan JG, Tertinegg I, Ethier CR. Finite element modeling of optic nerve head biomechanics. Invest Ophthalmol Vis Sci. 2004;45(12):4378-4387.

10. Guidoboni G, Harris A, Cassani S, et al. Intraocular pressure, blood pressure, and retinal blood flow autoregulation: A mathematical model to clarify their relationship and clinical relevance. Invest Ophthalmol Vis Sci. 2014;55(7):4105-4118.

11. Williamson TH, Harris A. Color Doppler ultrasound imaging of the eye and orbit. Surv Ophthalmol. 1996;40(4):255-267.

Nanostructural and mechanical changes in the sclera following proteoglycan depletion

Zhuola[1], Steve Barrett[2], Yalda Ashraf Kharaz[3], Eithne Comerford[3], Riaz Akhtar[1]

[1]*Department of Mechanical Materials and Aerospace Engineering, University of Liverpool, Liverpool, UK;* [2]*Department of Physics, University of Liverpool, Liverpool, UK;* [3]*Institute of Ageing and Chronic Disease, University of Liverpool, Liverpool, UK*

Abstract

The mechanical properties of ocular tissues, such as the sclera, have a major impact on healthy eye function, and are governed by the properties and composition of the microstructural components. For example, biomechanical degradation associated with myopia occurs alongside a reduction of proteoglycans (PGs). In this study, the role of PG degradation in the nanomechanical properties of the porcine sclera is explored. *In-vitro* enzymatic degradation of PGs was conducted with α-amylase and chondroitinase ABC enzymes. Collagen fibril morphology and nanomechanical stiffness were measured with atomic force microscopy (AFM). The elastic modulus of the tissue was reduced in all enzyme-treated samples relative to controls. In addition, collagen fibril organization was disrupted by PG depletion. Our data demonstrate that PGs play an important role in determining not only the mechanical properties at these length scales, but also collagen fibril arrangement.

Keywords: collagen structure, proteoglycan depletion, scleral mechanical properties

1. Introduction

The sclera is the dense outer coating of the eye, which provides the structural framework that defines the shape of the eye. It is mainly composed of collagen, elastin, and interfibrillar PGs. There is substantial evidence that profound bio-

Correspondence: Zhuola, Department of Mechanical Materials and Aerospace Engineering, University of Liverpool, Brownlow Hill, Liverpool L69 3GH, UK.
E-mail: zhuola@liverpool.ac.uk

mechanical changes occur in the sclera with conditions such as myopia, which is characterized by scleral weakening. Alongside biomechanical changes, a reduction of collagen fibril diameter and PG content have been reported in myopic eyes. However, few studies to date have determined how PG content in the sclera affects its mechanical properties and nanostructure. In this study, *in-vitro* degradation of PGs in the porcine sclera was conducted in order to determine how this affects nanoscale changes in its structure and mechanical properties.

2. Materials and methods

Porcine eyes were obtained from a local abbatoir (n = 5). The sclerae were dissected and cryosectioned for AFM testing following the methods and experimental procedure described previously.[1] The cryosectioned samples were treated with the following solutions: 2mg/ml α-amylase in phosphate buffered saline (PBS), 2mg/ml α-amylase in ultra-clean distilled water, chondroitinase ABC buffer, 100% ultra clean distilled water (control group), and 100% PBS (control group). The nanotopography and elastic modulus were measured before and after one-hour treatment at the same locations with AFM using the Peakforce QNM method.[1] All tests were conducted in liquid.

As shown in Figure 1, chondroitinase ABC depletes two types of major sulphated PGs in the sclera:[1] chondroitin sulfate PGss and dermatan sulfate PGs.[2] Sulphated glycosaminoglycan (sGAG, a major component of PGs) content was analyzed with the dimethylmethylene blue (DMMB) assay before and after α-amylase treatment.
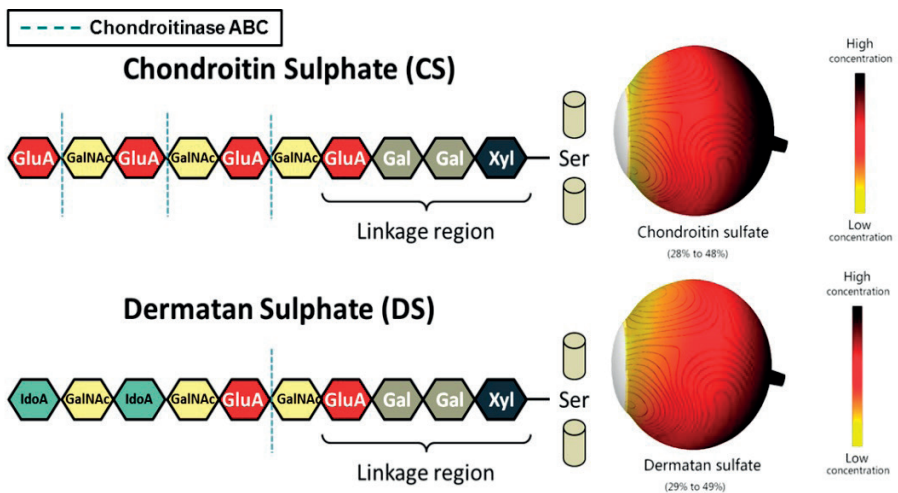
Fig. 1. PG depletion by using chondroitinase ABC.

Although α-amylase is one of the major enzymes found in tear fluid, few studies have shown which PGs in the eye are affected by α-amylase.

Nanomechanical properties were determined off-line by using NanoScope Analysis 1.7 (Bruker Nano Inc.; Nano Surfaces Division, Santa Barbara, CA, USA). AFM images from the height channel (topography images) were analyzed using Image SXM 1.99 (Steve Barrett, Image J; http://www.liv.ac.uk/~sdb/ImageSXM/) and Matlab 2013a (The MathWorks; Natick, MA, USA) for measuring scleral collagen fibril structure and distribution.

3. Results

DMMB assays indicated that sGAG content was reduced after α-amylase treatment in all three regions (8.9% to 22.6%). Collagen fibril diameter was significantly reduced in all groups incubated with enzyme solutions, and remained unchanged in control groups. Collagen fibril D-periodicity remained unchanged in all groups after incubation. The gap zone depth increased significantly in all groups after incubation with enzymes, decreasing after 100% PBS incubation. As shown in Figure 2, the elastic modulus decreased in all groups after incubation with enzyme solutions and significantly increased after incubation with 100% PBS buffer.
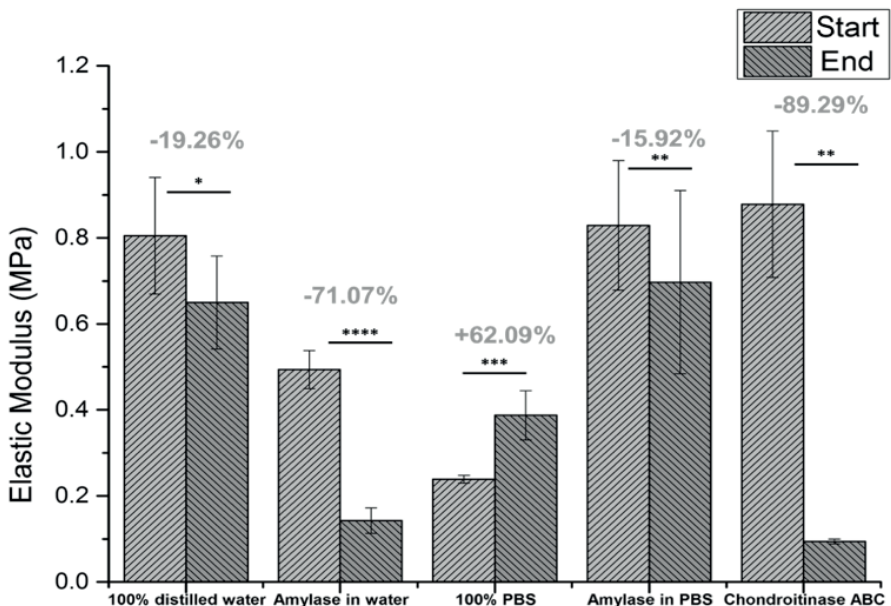
Fig. 2. Results of mechanical properties measured with AFM Peakforce QNM.

4. Conclusion

These data demonstrate that collagen fibril mechanical properties are substantially altered by salt concentration and that PGs play an important role in determining the nanostiffness and structure of the sclera. Collagen D-periodicity remained unchanged in all groups after treatment, indicating that PG depletion does not degrade collagen fibrils. Elastic properties were reduced in samples incubated with amylase solutions, decreasing even further in those incubated with chondroitinase solution. This result indicated that PG degradation will cause a reduction in the elastic modulus of collagen fibrils.

References

1. Papi M, Paoletti P, Geraghty B, Akhtar R. Nanoscale characterization of the biomechanical properties of collagen fibrils in the sclera. Appl Phys Lett. 2014;104(10):103703.
2. Murienne BJ, Chen ML, Quigley HA, Nguyen TD. The contribution of glycosaminoglycans to the mechanical behaviour of the posterior human sclera. J R Soc Interface. 2016;13(119):20160367.
3. Trier K, Olsen EB, Ammitzbøll T. Regional glycosaminoglycans composition of the human sclera. Acta Ophthalmol. 1990;68(3):304-306.

Clinical assessment of intraocular pressure: a whole-eye dynamic model

Francesca Stefanoni[1], Alon Harris[3], Marcela Szopos[2], Christophe Prud'homme[2], Riccardo Sacco[1], Dario Messenio[4], Maria Laura Costantino[1], Giovanna Guidoboni[2]

[1]Department of Mathematics, Politecnico di Milano (Polythecnic University of Milan), Milan, Italy; [2]Institute for Advanced Mathematical Research, UMR 7501, National Center for Scientific Research, University of Strasbourg, Strasbourg, France; [3]Eugene and Marilyn Glick Eye Institute, Indiana University School of Medicine, Indianapolis, IN, USA; [4]Eye Clinic, Department of Clinical Science - ASST Fatebenefratelli Sacco, University of Milan, Milan, Italy

Abstract

The aim of this work is to provide a quantitative description of how geometrical and material properties of ocular tissues and fluids influence intraocular pressure (IOP).

Keywords: intraocular pressure (IOP), glaucoma management, mathematical modeling, sensitivity analysis

1. Introduction

IOP assessment is a simple, quick and non-invasive test that can be performed in any ophthalmology clinic. IOP alterations are associated with many diseases, such as glaucoma, and it is therefore of great clinical interest to identify the factors influencing IOP levels. Indeed, it is well known that geometrical and material properties characterizing ocular tissues and fluids influence IOP. In this context, the main goal of this work is to address the need for quantitative understanding of the influence of patient-specific geometrical and material properties of ocular tissues and fluids on IOP by means of mathematical modeling.

Correspondence: Francesca Stefanoni, Department of Mathematics, Politecnico di Milano, via Bonardi 9, Milano, Edificio 14 "La Nave" Campus Leonardo del Politecnico di Milano, Milan, Italy.
E-mail: Francesca.stefanoni91@gmail.com

2. Methods and results

The model aims to be an electrical analog of the physiology of the eye, including various details regarding structural mechanics and fluid dynamics. Interestingly, pressure values inside the eye exhibit a static component, mainly due to the balance of aqueous humor (AH) inflow and outflow, and a dynamic component, mainly due to blood flow oscillations. We considered both static and dynamic components, and in particular, we investigated and quantified the influence of tissue (vitreous humor, cornea, and sclera) deformability and blood flow pulsatility on the dynamic measurements of IOP. Model calibration and validation have been performed using published data. The model has been implemented using the open access software OpenModelica (Open Source Modelica Consortium: Linköping, Sweden) in order to facilitate further model extensions and connections with other models already available for different parts of the eye.

2.1. Basic modeling assumptions

We defined the total volume of the eye as the sum of volumes of aqueous humor (anterior chamber), choroidal blood, and internal structures (vitreous humor, lens, and iris):

$$V_{tot} = V_{AH} + V_{blood} + V_{struc} \tag{1}$$

In our model, the analog of volume is the electrical charge, whereas the analog of volumetric flow rate is the electrical current. In the following sections, we review three models that simulate IOP under different assumptions. The models can be thought of as successive steps towards the modeling of whole-eye dynamics.

2.2. Static conditions

As a first step, pressure is assumed to be uniform inside the eye, while choroid and structure volumes are assumed to be given constants. The steady-state value of IOP is computed as the solution of the equaticon that describes the balance between AH production and drainage, as in Szopos et al.:[1]

$$\frac{dV_{AH}}{dt} = J_{in} - J_{out} = 0 \tag{2}$$

AH inflow is due to the processes of ultrafiltration and ionic secretion, whereas the outflow occurs through the trabecular and uveoscleral pathways. The balance leads to a scalar third order polynomial equation in the sole unknown IOP:

$$L\left[(cBP - IOP) - \sigma_p \Delta\pi_p - \sigma_s \Delta\pi_s\right] = \frac{1}{R_0[1 + Q(IOP - EVP)]}(IOP - EVP) + \frac{k_1}{k_2 + IOP}IOP \tag{3}$$

Using published data for the parameters (see Table 1), the value for the steady-state

Table 1. Control state values for the parameters

Parameter	Value and Unit	Meaning
L	0.3μl/min/mmHg	hydraulic conductance
cBP	27.5 mmHg	ciliary blood pressure
$\Delta\pi_p$	25 mmHg	oncotic pressure difference
σ_p	1 [-]	protein reflection coefficient
$\Delta\pi_s$	-450 mmHg	osmotic pressure difference
σ_s	0.0515 [-]	low-molecular component coefficient
EVP	8 mmHg	episcleral vein pressure
R_o	2.2 mmHg min/μl	resistance when pressure gradient equals zero
Q	0.012 mmHg	outflow obstruction coefficient
k_1	0.4 μl/min	maximum uvosclerar flow rate
k_2	5 mmHg	pressure corresponding to half max uveoscleral flow rate

Baseline values for the parameters: typical conditions of a healthy eye.

IOP found by OpenModelica is 14.9527 *V*, which is perfectly in the range of physiological IOP measured in the clinics. We performed a deterministic sensitivity analysis on Equation (3) showing that the major influence on IOP is given by $\Delta\pi_p$, $\Delta\pi_s$, and cBP, as shown in Figure 1.

2.3. Dynamic conditions

2.3.1. Ocular hemodynamics
We introduced a non-stationary component in the model starting from the model presented in Kiel *et al.*[2] The new assumption with respect to the previous model is that IOP depends on V_{tot} as in Equation (4), the given functions of time, $V_{ch}(t)$, and its first derivative, $G_{ch}(t)$, estimated as in Krakau.[3] The new model is thus described by the following system of equations:

$$\begin{cases} \dfrac{dV_{tot}}{dt} = J_{in} - J_{out} + G_{ch} \\ IOP = \overline{IOP}\,10^{\gamma(V_{tot} - \overline{V_{tot}})} \end{cases} \qquad (4)$$

where γ is a constant equal to 0.0215 μl^{-1} and overlined variables indicate baseline values according to literature (15 mmHg and 7 ml, respectively, for $\overline{IOP}$ and $\overline{V_{tot}}$). Changes in choroidal volume due to blood flow variations, namely $G_{ch}(t)$, are given by a sinusoidal current source. Changes in total volume, namely dV_{tot}/dt, are modeled by a capacitor, accounting for energy storage due to structural deforma-

(a) Variations in cBP (b) Variations in L (c) Variations in C_0

(d) Variations in k_1 (e) Variations in EVP (f) Variations in $\Delta\pi_s$

(g) Variations in k_2 (h) Variations in $\Delta\pi_p$
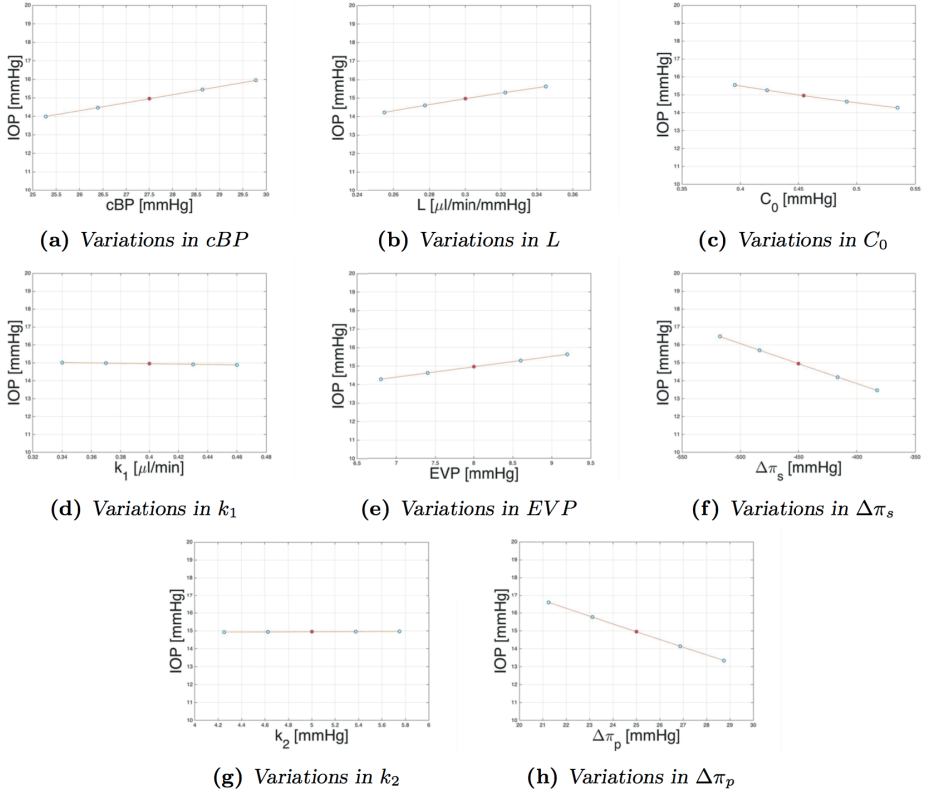
Fig. 1. Influence of different factors on IOP. Red dots indicate control state values for the variables and IOP; blue dots indicate samples used in the circuit.

bility of the eye. For the calibration of the current generator, we chose a frequency equal to the one of the clinically-measurable IOP wave, namely $1.1\overline{3}\ S^{-1}$. Oscillations in IOP indeed reflect changes in eye volume due to changes in the intraocular blood volume induced by the arterial blood pulse; thus, this frequency is that of the cardiac cycle. The amplitude value has been chosen to be 10.3166 µlS⁻¹, as in Krakau.[3]

2.3.2. Ocular deformability
As a first step, we estimated a constant value for the capacity by means of a linearization of the relationship between *IOP* and V_{tot} shown in Equation (4):

$$C = \frac{\Delta V_{tot}}{\Delta IOP} = \frac{1}{\gamma \overline{IOP}} = 1.35 \ \mu l \ mmHg^{-1} \tag{5}$$

Note that γ in Equation (5) is the same as in Equation (4), but with the relation expressed in natural logarithm. γ accounts for the elastic proprieties of the cornea,
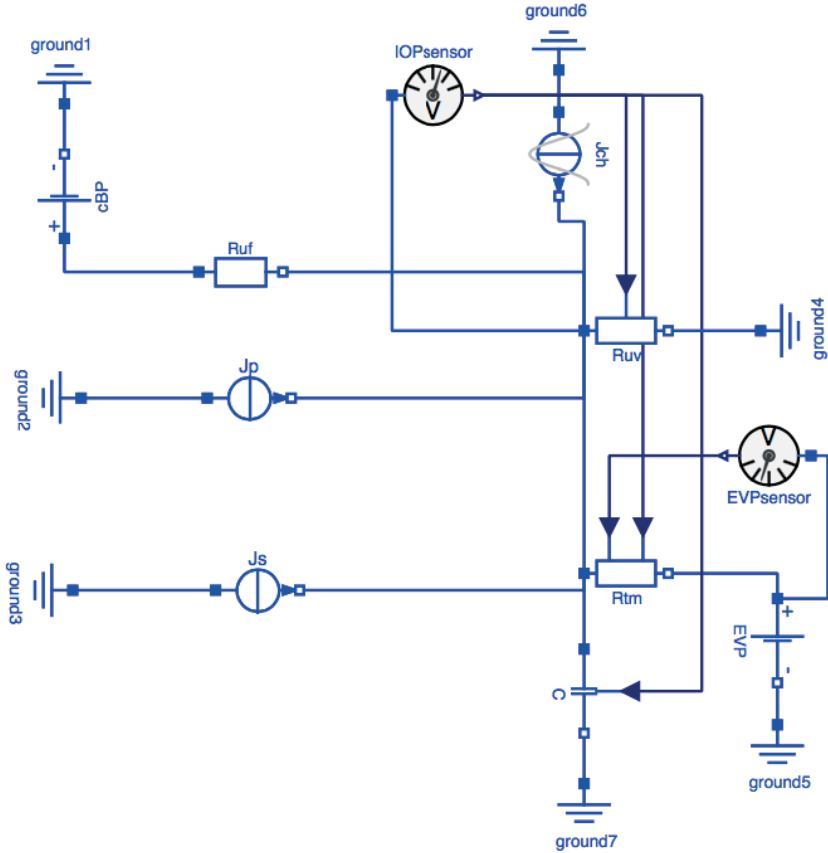
Fig. 2. OpenModelica electrical circuit for the dynamic component of IOP.

sclera, and other boundary structures of the eye, and is named ocular rigidity as in Friedenwald.[4]

Then we estimated a more precise non-linear value of the capacity as a function of *IOP*:

$$C = \frac{1/\gamma \log\left(\frac{IOP}{\overline{IOP}}\right)}{IOP - \overline{IOP}} \tag{6}$$

The circuit implemented in OpenModelica and the resultant IOP wave are shown in Figures 2 and 3, respectively. The sinusoidal IOP has an average value of 15.0179 mmHg and a range of variability of ± 2.12 mmHg, both increased with respect to the results found with the constant capacitance.
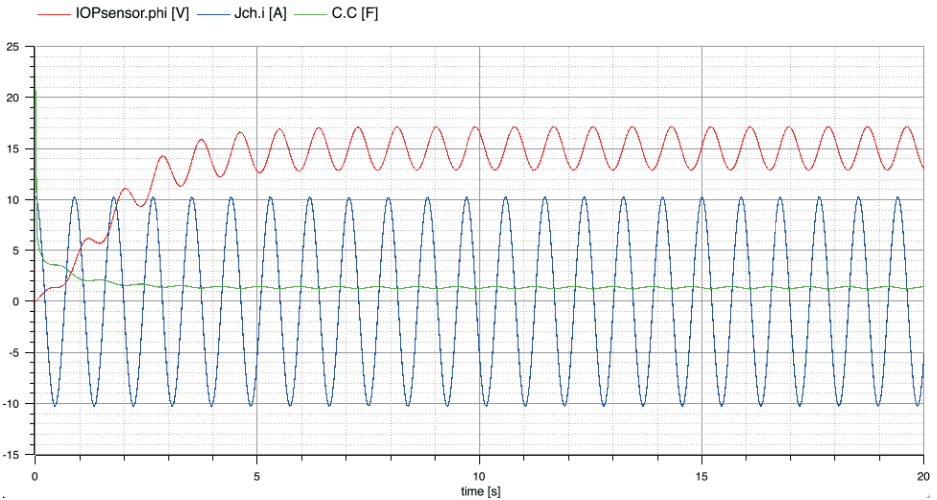
Fig. 3. OpenModelica simulation output: IOP, current generator Jch, and capacitor C.

3. Conclusions

This project provides a first attempt to consistently combine the static and dynamic components contributing to the pressure distribution inside the eye. It will help elucidate the relationship between the measured values of IOP and some important factors that may vary among patients. In a long-term perspective, the software developed within this project will be integrated within a larger virtual simulator for ocular biophysics, which may lead to a new tool for clinical use aimed at providing physicians with an integrated view of the patient's status to monitor, prevent, and treat diseases in a patient-specific manner.

References

1.   Open Source Modelica Consortium (OSMC), Linköping, Sweden.
2.   Szopos M, Cassani S, Guidoboni G, Prud'homme C, Sacco R, Siesky B, Harris A. Mathematical modelling of aqueous humor flow and intraocular pressure under uncertainty: towards individualized glaucoma management. Journal for Modeling in Opthalmology. 2016;1(2):29-39.
3.   Kiel JW, Hollingsworth M, Rao R, Chen M, Reitsamer HA. Ciliary blood flow and aqueous humor production. Prog Retin Eye Res. 2011;30(1):1-17.
4.   Krakau CE. Calculation of the pulsatile ocular blood flow. Invest Ophthalmol Vis Sci. 1992;33(9):2754-2756.
5.   Friedenwald JS. Contribution to the theory and practice of tonometry. Am J Ophthalmol. 1937;20(10):985-1024.

Ultrastructural and nanomechanical changes of the cornea following enzymatic degradation

Ahmed Kazaili[1,2], Riaz Akhtar[1]

[1]*Department of Mechanical, Material and Aerospace Engineering, School of Engineering, University of Liverpool, Liverpool, UK;* [2]*Department of Biomedical Engineering, School of Engineering, University of Babylon, Babylon, Iraq*

Abstract

Understanding of the ultrastructure and nanomechanical behavior of the cornea is important for a number of ocular disorders. In this study, atomic force microscopy (AFM) was used to determine nanoscale changes in the porcine cornea following enzymatic degradation. Different concentrations of amylase were used to degrade the cornea. A reduction in elastic modulus at the nanoscale, along with disrupted collagen morphology, was observed following enzymatic treatment. This study highlights the interplay between mechanical properties and collagen organization in the healthy cornea.

Keywords: amylase, corneal biomechanics, keratoconus

1. Introduction

There is a need to explore and develop a better understanding of corneal biomechanics at the nanolevel. Collagen fibrils are the main load-bearing components of the cornea, which are embedded in extracellular matrix, that is mainly formed of proteoglycans.[1] The structural organization and mechanical properties of collagen fibrils and proteoglycans play an important role in exhibiting normal corneal

Correspondence: Ahmed Kazaili, Department of Mechanical, Material and Aerospace Engineering, School of Engineering, University of Liverpool, Liverpool, L69 39H, UK.
E-mail: Ahmed.Kazaili@liverpool.ac.uk

curvature.[2] With certain diseases, such as keratoconus, these properties are compromised.[3] This study aims to use *in-vitro* enzymatic degradation to understand how the ultrastructural and nanomechanical changes in collagen fibril networks and extracellular matrix may affect corneal properties.

2. Materials and methods

Sixteen porcine corneas obtained from a local abattoir. They were grouped into a control group (8 corneas) and amylase-treated group (8 corneas). Corneal samples were chosen from the apex after desquamating the epithelial layer. A previous study has suggested that tissue samples for AFM should be 5 μm.[4] Samples from the anterior one-third of the stroma were chosen for this study. For the control group, each cornea was cryosectioned to produce six slices (5 μm thick): three of these slices were washed with distilled water (DW), and the other three slices were washed with phosphate buffer saline solution (PBS). For the amylase test group, each cornea was cryosectioned to produce 24 slices (5 μm thick). The samples from each cornea were then sub-divided into two subgroups: 16 slices were treated with amylase dissolved in DW and the other 16 slices were treated with amylase dissolved in PBS. The slices of each subgroup underwent enzymatic degradation (n = 2 slices/subgroup) at the following concentrations: 0.2, 0.4, 0.8, 1, 1.2, 2 mg/ml amylase. Each slice was incubated for 40 min.

Stromal samples were tested by using Bruker Multimode-8 AFM (Bruker; Santa Barbara, CA, USA); a schematic of the AFM is shown in Figure 1. The AFM method and instrument used have been described previously by Papi *et al.*[5] The elastic modulus and topographical properties were determined by using Peak Force Quantitative
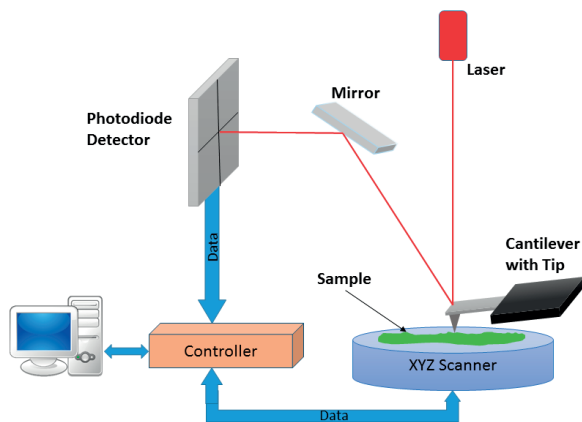
Fig. 1. Schematic of AFM.[5]

Nanomechanical Mapping (PF-QNM) mode in air. This AFM has been well-described in the literature.[6] The Derjaguin-Muller-Toporov (DMT) model was used to calculate elastic modulus. This model uses the loading force plus the adhesive force between the tip and the surface of the sample.[7] Aluminum-coated silicon probes (Bruker RTESPA-300) were used for all measurements. The AFM was calibrated to measure the tip radius and the spring constant of the cantilever by using a Vishay Photostress PS1 Polymer (Vishay; Wendell, NC, USA) reference sample with an elastic modulus of 2.7 GPa. The Poisson's ratio of the corneas was assumed to be 0.5. AFM images were analyzed and processed by using Bruker NanoScope Analysis Software, version 1.70. The temperature and humidity of the testing room were recorded as approximately 22.4 C° and 41%, respectively. All chemicals and reagents were obtained from Sigma-Aldrich (Dorset, UK).

3. Results and discussion

3.1. Topography

Topographical images revealed distinct collagen fibrils (type I) in the stroma when the samples were washed with either DW/PBS or treated by amylase (Fig. 2). The collagen fibrils had diameters ranging from 32–50 nm. The axial D-periodicity of collagen fibrils ranged from 64–70 nm.

Collagen fibril diameter was slightly higher in samples washed with DW as compared to PBS-washed. Deterioration in the collagen fibrils in samples treated with amylase was seen in some points (arrow in the zoomed image in Fig. 2). In addition, there was clear deterioration in the extracellular matrix.
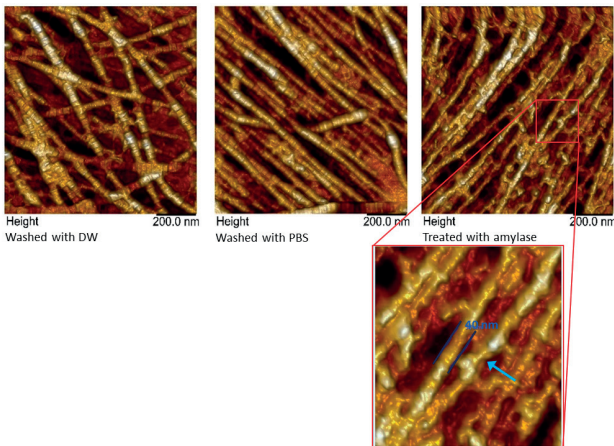
Fig. 2. Topographical images of corneal samples showing collagen fibrils.

DMTModulus   200.0 nm
Washed with DW

DMTModulus   200.0 nm
Washed with PBS

DMTModulus   200.0 nm
Treated with amylase
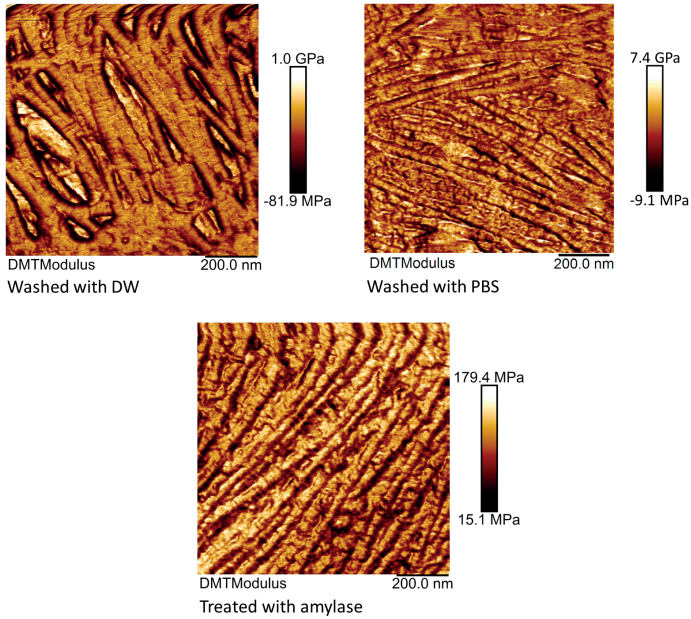
Fig. 3. Elastic modulus images of corneal samples
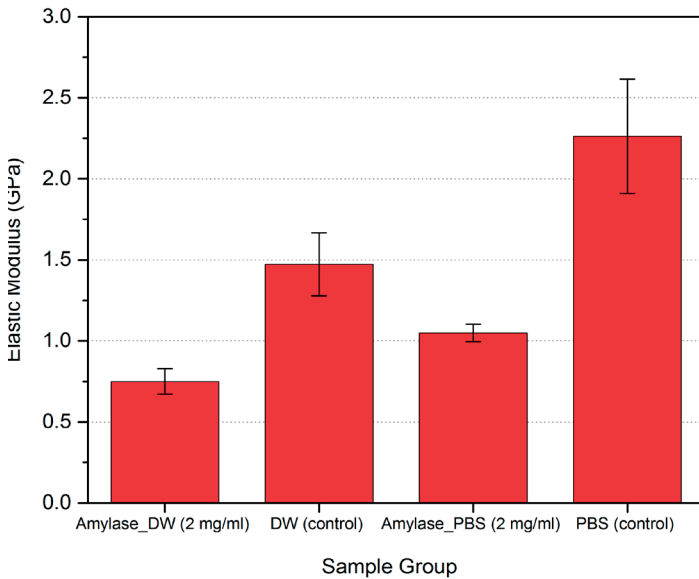
Fig. 4. Mean elastic modulus values of control group and amylase dissolved in DW (2 mg/ml) treated group.
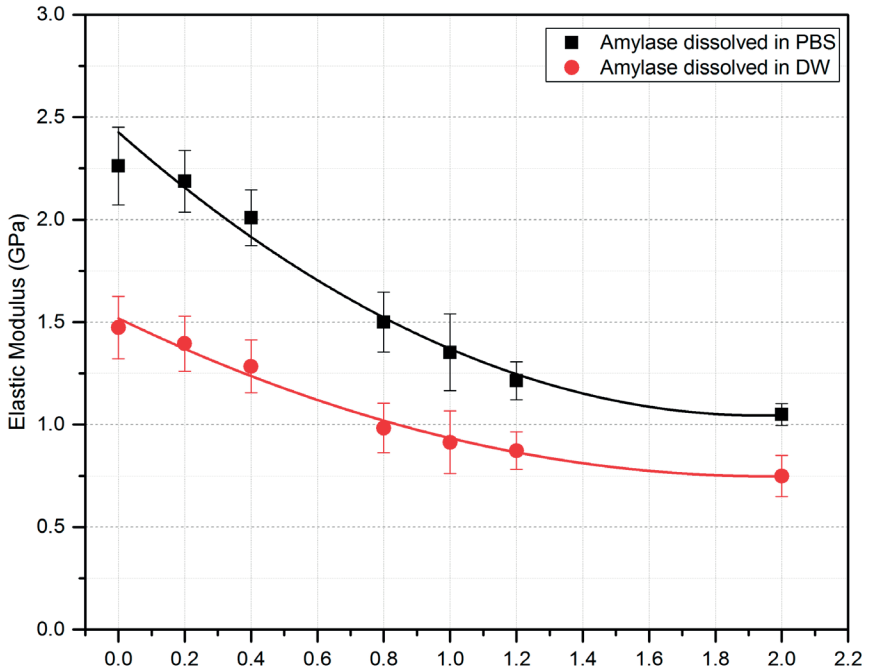
Fig. 5. Mean values of elastic modulus of corneal samples treated with varying concentrations of amylase.

3.2. Mechanical properties

Elastic modulus images of corneal samples in different solutions are shown in Figure 3. The elastic modulus was reduced by 37% for the samples washed by DW as compared to samples washed by PBS. The greatest reduction was seen following amylase (2 mg/ml) treatment. There was a 68% reduction in the elastic modulus as compared to samples washed by PBS, and a 49% reduction as compared with samples washed by DW (Fig. 4).

It was noticed that elastic modulus values decreased as the amylase concentration increased. The mean values of elastic modulus of corneal samples treated with varying amylase concentrations are shown in Figure 5. In both curves, the reduction seems to reach a steady state of proteoglycan digestion at higher amylase concentrations.

4. Conclusion

Amylasetreatment dramatically altered the collagen fibril structure and appeared to affect the surrounding proteoglycans, leading to deterioration of the mechanical

properties of the cornea. This enzymatic degradation method may serve as a model for understanding keratoconus.

Acknowledgements

References

1. Meek KM, Knupp C. Corneal structure and transparency. Prog Retin Eye Res. 2015;49:1-6.
2. Müller LJ, Pels E, Vrensen GF. The specific architecture of the anterior stroma accounts for mainte-nance of corneal curvature. Br J Ophthalmol. 2001;85(4):437-443.
3. Ambekar R, Toussaint KC, Johnson AW. The effect of keratoconus on the structural, mechanical, and optical properties of the cornea. J Mech Behav Biomed Mater. 2011;4(3):223-236.
4. Fischer AH, Jacobson KA, Rose J, Zeller R. Cryosectioning tissues. Cold Spring Harb Protoc. 2008;3(8). doi:10.1101/pdb.prot4991.
5. Papi M, Paoletti PA, Geraghty BR, Akhtar R. Nanoscale characterization of the biomechanical proper-ties of collagen fibrils in the sclera. App Phys Lett. 2014;104(10):103703.
6. Pittenger B, Erina N, Su C. Quantitative mechanical property mapping at the nanoscale with Peak-Force QNM. Application Note Veeco Instruments Inc. 2010;1-2.
7. Dokukin ME, Sokolov I. Quantitative mapping of the elastic modulus of soft materials with HarmoniX and PeakForce QNM AFM modes. Langmuir. 2012;28(46):16060-16071.

Multiscale modeling and simulation of neurovascular coupling in the retina

Riccardo Sacco[1], Aurelio G. Mauri[1], Alessandra Cardani[1], Brent A. Siesky[2], Giovanna Guidoboni[3], Alon Harris[2]

[1]Department of Mathematics, Politecnico di Milano (Polytechnic University of Milan), Milan, Italy; [2]Eugene and Marilyn Glick Eye Institute, Indiana University School of Medicine, Indianapolis, IN, USA; [3]Department of Mathematics, Indiana University and Purdue University, Indianapolis, IN, USA

Abstract

The role of nitric oxide (NO), usually considered as a potent vasodilator, in regulating retinal neurovascular coupling is still elusive. Measurements of flicker light-induced functional hyperemia (FH) in humans show that an increase of NO levels reduces vasodilation. This evidence has led to conjecture that such an increase may be responsible for suppressing flicker-evoked vasodilation in diabetic retinopathy. In this paper, we propose a mathematical model to theoretically investigate the effect of an increase in neural NO (nNO) on the vasodilation of retinal arterioles. Simulation results indicate that nNO increase may:

1. significantly affect vasoconstrictive agent production by glial cells; and
2. elicit vasoconstriction rather than vasodilation in retinal arterioles.

Model predictions seem therefore to support the conjecture that NO increase may be responsible for suppressing flicker-evoked vasodilation in diabetic retinopathy.

Keywords: mathematical modeling, retinal dysfunction, retinal regulation, visual neuroscience

---

Correspondence: Prof. Riccardo Sacco, Dipartimento di Matematica Politecnico di Milano, Piazza Leonardo da Vinci 32, 20133 Milano, Italy.
E-mail: riccardo.sacco@polimi.it

1. Introduction

The multiscale nature of the human body system covers a wide spectrum with respect to both time and space variables. The time scale ranges from nanoseconds to years, whereas the space scale ranges from nanometers to meters. Such hierarchical and complex structure is representative also of the eye as an organ, whose physiology in health and disease is still far from being fully understood.

In this article, we illustrate the simulation results obtained using the multiscale/multiphysics mathematical model proposed in Cardani[1] and presented in Sacco *et al.*,[2] with the goal of exploring the role of nNO, jointly with 20-hydroxyeicosatetraeonic acid (20-HETE) and epoxyeicosatrienoic acid (EET), in the regulation of retinal neurovascular coupling (NVC).

The analysis is motivated by experimental data on flicker light-induced FH in humans, indicating that increased NO levels mediated by 20-HETE reduce vasodilation.[3] The aim of our investigation is to employ the computational tool to provide quantitative predictions of the effect of an increase of nNO on the vasodilation of retinal arterioles in order to assess the validity of the conjecture that increased NO levels may be responsible for suppressing flicker-evoked vasodilation in diabetic retinopathy.[4]

2. Methods

The concept of multiscale modeling proposed to represent retinal microcirculation and regulation mechanisms is illustrated in Figure 1. Retinal vasculature is described by the equivalent electrical circuit illustrated in Figure 2. NVC is described by the interaction between vasoactive agents synthesized by active neurons, and astrocytes and smooth muscle cell (SMC) contraction/dilation. Model inputs are blood pressure at the central retinal artery and vein, intraocular pressure, nNO, and glutamate (GLU) postsynaptic levels. Kirchhoff current law is solved at each node of the circuit to determine the time evolution of nodal blood pressures and compartment diameters.

Model inputs are:

1. P_{in}, P_{out}: inlet/outlet retinal vasculature pressures. Baseline: P_{in} = 30 mmHg; P_{out} = 15 mmHg.
2. GLU: glutamate synthesized by post-synaptic terminal. Baseline: GLU = 0 μM.
3. nNO: NO synthesized by a nearby neuron. The amounts δ*nNO and (1 - δ)*nNO are delivered to astrocytes and SMCs, respectively. Baseline: nNO = 1 μM; δ = 0.99.

The neurochemical model block has been validated against results reported in Hadfield *et al.*,[5] whereas the model biomechanical block has been validated against results reported in Kudryashov and Chernyasvskii.[6]

(A) Macroscale   (B) Mesoscale   (C) Microscale
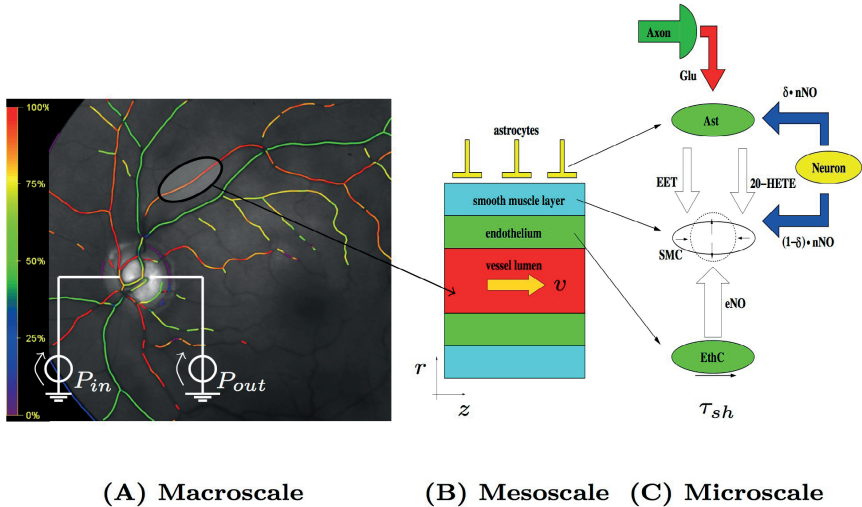
Fig.1. Multiscale model of retinal circulation utilized to assess the contributions of blood flow shear stress (τsh), nNO, 20-HETE, and EET on retinal NVC. Also shown: astrocytes (Ast); smooth muscle cell (SMC); endothelial cell (EthC). Microscale biochemistry adapted from Attwell *et al.*[7]
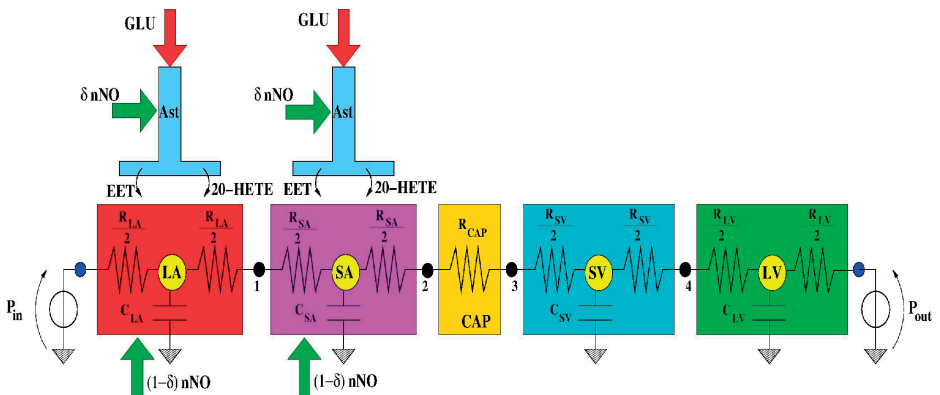
Fig.2. Equivalent electrical circuit for the simulation of retinal NVC. Among the five vascular compartments — large arterioles (LA), small arterioles (SA), capillaries (CAP), small venules (SV), and large venules (LV) — only LA and SA are active.

3. Results

We consider the experimental data set of Newman[3] on the response to flicker-light stimulation in humans. We use the model to investigate the conjecture of Metea and Newman[4] that NO increase may be responsible for suppressing flicker-evoked vasodilation in diabetic retinopathy.

3.1. Clinical data

FH in the retina of five healthy subjects was studied via arterial diameter response to flicker-light stimulation (signal frequency: 12.5 Hz; wavelength: 530–600 nm; duration: 20 s).[4] Maximum dilation was approximately 8%, whereas maximum constriction was approximately 4% (Figs. 4 and 5, black circles correspond to the clinical data). A conjecture was then proposed on how NO modulates NVC *in vivo*, particularly that NO increase may be responsible for suppressing flicker-evoked vasodilation in diabetic retinopathy.

3.2. Comparison between clinical data with model predictions

Figure 3 illustrates how flicker-light application is modeled by a triangular GLU stimulus of 0.07 µM for 20 s. Simulations were performed for the two different reported nNO levels (Fig. 3, black and red curves, bottom panel). Figure 4 shows a comparison of % LA mean diameter change between clinical data[3] (Fig. 4, black circles) and model simulations obtained when two different segments are vasoactive. Model predictions match data only if both LA and SA are vasoactive. Figure 5 shows a comparison of % LA mean diameter change between clinical data[3] (Fig. 5; black circles) and model simulations obtained for different nNO levels. Results show that elevated nNO may reduce vasodilation by a factor of 4.

4. Conclusion

Multiscale simulations of NVC in the retina indicate that:
1. NVC has a noticeable impact on functional hyperemia in the human retina, showing that only if both LA and SA are vasoactive, clinical data on flicker-light stimulation[3] can be correctly reproduced; and
2. nNO increase above baseline significantly affects EET production by glial cells (even by a factor of 4), contributing to elicit vasoconstriction rather than vasodilation, in agreement with data reported in Metea and Newman.[4]

Model predictions seem therefore to support the conjecture that increased NO levels may be responsible for suppressing flicker-evoked vasodilation in diabetic retinopathy.[4]
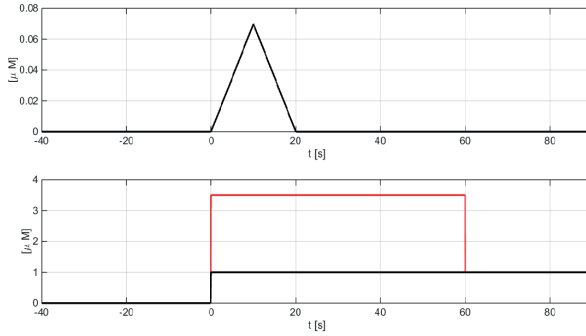
*Fig. 3.* Time evolution of GLU and nNO input signals.
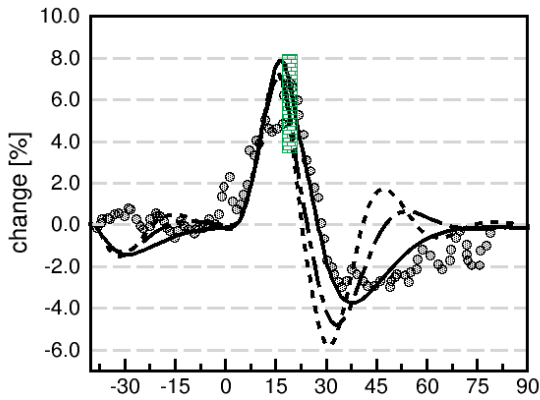
Fig. 4. Simulated effect of vasoactive segments on FH.
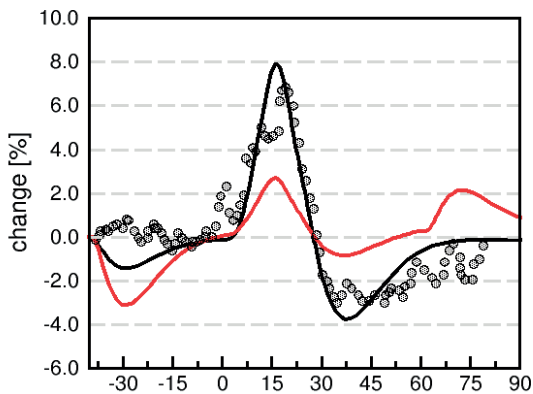
Fig. 5. Simulated effect of nNO level on FH.

Acknowledgements

References

1. Cardani A. Theoretical analysis of neurovascular mechanisms contributing to retinal blood flow regulation. Master Thesis, Politecnico di Milano, Italy, 2015.
2. Sacco R, Mauri AG, Cardani, A, Siesky BA, Guidoboni G, Harris A. Increased levels of nitric oxide may pathologically affect functional hyperemia in the retina: model and simulation. Posterboard Number 214 – B0245, Annual Meeting of the Association for Research in Vision and Ophthalmology, Baltimore MD, 2017.
3. Newman EA. Functional hyperemia and mechanism of neurovascular coupling in the retinal vasculature. J Cereb Blood Flow Metab. 2013; 33(11):1685–1695.
4. Metea MR, Newman EA. Glial cells dilate and constrict blood vessels: A mechanism of neurovascular coupling. J Neurosci. 2006; 26(11):2862–2870.
5. Hadfield J, Plank MJ, David T. Modeling secondary messenger pathways in neurovascular coupling. Bull Math Biol. 2013; 75(3):428-443.
6. Kudryashov NA, Chernyasvskii IL. Numerical simulation of the process of autoregulation of the arterial blood flow. Izvestiya Rossiiskoi Akademii Nauk, Mekhanika Zhidkosti i Gaza. 2008;43(1):38-56.
7. Attwell D, Buchan AM, Charpak S, Lauritzen M, MacVicar BA, Newman EA. Glial and neuronal control of brain blood flow. Nature. 2010;468(7321):232–243.

Polarimetric interferometry to objectively evaluate the optical properties of corneal stroma

Eugenio Lipari[1], Alessandra Sborgia[2], Mario Nubile[3], Leonardo Mastropasqua[3], Giovanni Alessio[2]

[1]Phronema SRL, Bari, Italy; [2]Department of Medical Basic Sciences, Neuroscience and Sense Organs, Ophthalmology Clinic, University of Bari "A. Moro", Bari, Italy; [3]Department of Medicine and Ageing Sciences, Ophthalmology Clinic, University of Chieti-Pescara "G. d'Annunzio", Chieti, Italy

Abstract

A new non-invasive method, based on the interferometric analysis of diffractive and polarizing effects related to the birefringent properties of corneal collagen fibrils, has been developed to objectively evaluate the optical properties of the stroma. The new method shows a relevant impact on corneal surgeries specifically for lamellar transplantation where, due to the polarizing properties of the stroma, the alignment between collagen fibrils of donor corneas with patient collagen fibril orientation has shown an improvement of visual acuity postoperatively. Further studies on the regularity of the corneal isogyre pattern are showing this new method has a strong impact in early-stage diagnosis of corneal disease.

Keywords: corneal cross, isogyre, melatope, birefringence

1. Introduction

The cornea has a dual function, optical and mechanical. The human cornea provides two-thirds of the refractive power of the eye and the requisite durability to maintain its shape, notwithstanding the action of the extraocular muscles and the internal force of the ciliary muscle. The latter mediates the change in lens shape in order

---

Correspondence: Eugenio Lipari, Phronema SRL, Via Junipero Serra n. 19, Bari, Italy.
E-mail: lipari@phronema.it

to adjust the focusing power of the eye, and has been shown to have a very small and optically negligible effect on corneal shape.[1] A fundamental characteristic for corneal function is that of transparency. The cornea is classically accepted as a five-layered structure: an epithelial and an endothelial layer at the anterior and posterior surfaces respectively; two membranes: Bowman's under the epithelium and Descemet's anterior to the endothelium; and a central and predominant stroma composed of collagen fibrils, which represent approximately 90% of corneal thickness.

The stroma is composed of approximately two successively stacked lamellae of type I collagen fibrils with a diameter of around 25-30 µm.[2] Within each lamella, the collagen fibrils run parallel to each other and show a regular interfibrillar spacing.[2-5] The orientation of the fibrils is constant within each lamella, but varies throughout successive layers.[6-9] The regular arrangement of the fibrils within each layer is considered to be responsible for the transparency of the tissue.[2,10,11] It is also an important factor for determining the mechanical properties of the cornea[12,13] as well as maintaining its shape.[14,15]

Such an organization contributes to characteristic patterns that are linked to highly ordered structures, such as crystals, which possess the property of birefringence.

These characteristic patterns seen when the structure is illuminated between crossed polarizers are a dark cross, the arms of which have been called isogyres, and colored rings or isochromatics. Whilst these formations, which are caused by the separation of refracted rays into ordinary and extraordinary components that travel at different velocities through the crystal depending on the atomic spacing in the plane of travel, can be explained in relation to crystal structure,[16] similar features have been noted over 200 years ago in eye lenses.[17-18] More recently, they have been noted in the cornea.[7,8,19-24] This cannot be explained on the same basis as crystals, given that ocular tissue is not highly ordered, but rather accords with the descriptions for elongated structures that arise in biology, such as cell layer arrangements.[25,26] The lamellar organization of the corneal stroma is akin to a Wiener body,[27] which gives rise to form birefringence due to the directional variations in refractive index: *i.e.*, differences along single fibers and across fiber layers.[27] It has also been shown that isogyres can be formed in curved structures made of amorphous materials that do not possess any birefringent properties.[21,28] The number of studies that have considered corneal birefringence show differences in findings,[19-24] and indeed it has been suggested that the random orientation of the central layers of the stroma results in no birefringence effects at the corneal apex.[8] Such variation is to be expected in a biological tissue that differs in shape and thickness between individuals and changes with age and pathologies. There has been a paucity of investigation into the use of polarization optics for the study of stromal structure. Stromal orientation is important for optical quality and differences between individuals may suggest that the particular orientation of lamellae is optimized

for image quality. In cases of corneal transplantation, the orientation of the donor cornea should therefore be considered. This study presents results of measurements on *in-vivo* corneal tissue using a new device that can determine the polarization properties of the cornea *in vitro* or *in vivo*. The instrument applies specialized software to determine the orientation of the corneal fibrils, offering the prospect of a detailed structural analysis which may have applications for clinical studies.

2. Scope

Development of a new non-invasive method to objectively evaluate the optical properties of the stroma, based on the interferometric analysis of diffractive and polarizing effects related to the birefringent properties of the stroma.

3. Method

Comparison between polarimetric interferometry image obtained by the interference between polarized light and stromal structure of human corneas using a new patented[29] medical device called Lumaxis® (Phronema SRL; Bari, Italy) with data published in the literature and obtained by x-ray, and second and third harmonic generation technique (SGH eTGH).
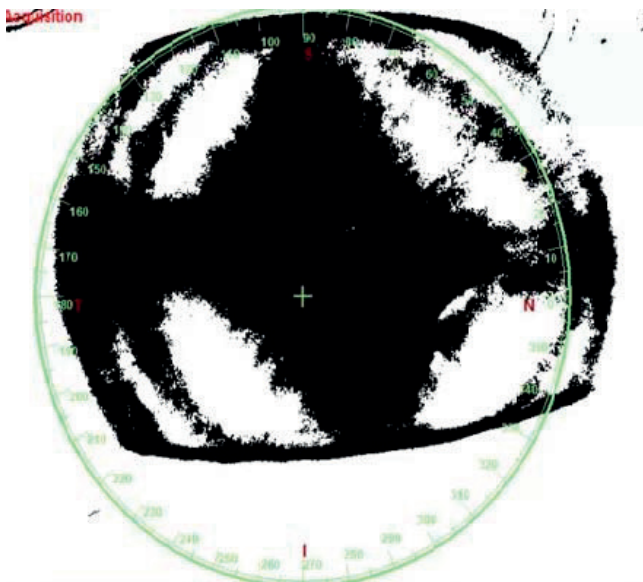
Fig. 1. Lumaxis isogyre acquisition.
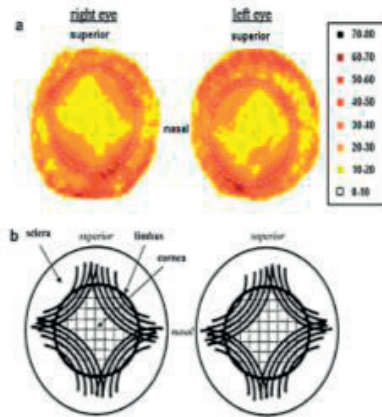
Fig. 2. (*a*) Contour maps of aligned collagen x-ray scatter from a left/right pair of normal human corneas . Note the high degree of body-line mirror symmetry. (*b*) Theoretical model of fibrillar arrangement based on (*a*). Reproduced from Boote *et al.*[30]

4. Results

Data obtained by the polarimetric interferometry showed a cross-like pattern (isogyre), shown in Figure 1, which perfectly correlates with the pattern obtained by the x-ray, THG, and SHG analysis (Figs. 2 and 3), confirming that deep stroma lamellae have two preferential alignments along the superior-inferior and nasal-temporal directions. The regular distribution of stromal lamellae allows the stroma to behave as a polarizer, which eliminates the diffractive effect of the light during its journey into the stroma.

5. Conclusions

In accordance with the importance of regularity and orientation of stromal lamellae distribution in the corneal refractive process, the importance of polarimetric inter-ferometry as a non-invasive technique to detect such orientation as a consequence of correlation/decorrelation between probe light polarization plane angle and stromal lamellae orientation becomes evident. Information from the cross-like pattern can be used for multiple applications in ophthalmology, such as corneal transplantation and diagnosis of corneal diseases due to stromal pathologies. This new technique represents a unique method to correlate the internal stromal structure and optical properties of the cornea. Recent studies have shown a new, intrinsic axis of the stroma, which can have very important refractive applications in ophthalmology.
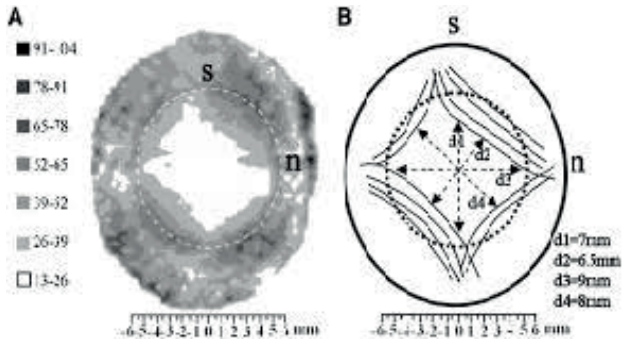
Fig. 3. (*a*) Contour map of aligned collagen x-ray scatter (a.u.) from a right human cornea. Superior, s, and nasal, n, positions are marked. Broken line denotes the limbus. Note the skewed diamond shape of the scatter contours, which displays mirror symmetry between the left and right eyes. (*b*) Proposed model of collagen fibril arrangement to explain the shape of the aligned scatter contours. The peripheral, oblique cornea is reinforced by chords of anchoring collagen of scleral origin. Figure modified from Boote *et al.*[31]

Acknowledgements

References

1. Pierscionek BK, Popiolek-Masajada A, Kasprzak H. Corneal shape change during accommodation. Eye. 2001;15:766-769.
2. Maurice DM. The structure and transparency of the corneal stroma. Physiol. 1957; 136:263-286.
3. Hart RW, Farrell RA. Light scattering in the cornea. J Opt Soc Am. 1969;59:766-774.
4. Farrell RA, McCally RL, Tatham PER. Wavelength dependencies of light scattering in normal and cold swollen rabbit corneas and their structural implications. J Physiol. 1973;233:589-612.
5. Fratzl P, Daxer A. Structural transformation of collagen fibrils in corneal stroma during drying: An x-ray scattering study. Biophys J. 1993;64:1210-121.
6. Komai Y, Ushiki T. The three dimensional organization of collagen fibrils in the human cornea and sclera. Invest Ophthalmol Vis Sci. 1991;32:2244-2258.
7. Naylor J. Polarized light studies of corneal structure. Brit. J. Ophthal., 1953; 37: 77E.
8. Stanworth A, Naylor EJ. The polarisation optics of the isolated cornea. Br J Ophthalmol. 1950;34:201-211.
9. Meek KM, Blamire ST, Elliott GF, Gyi TJ, Nave C. The organization of collagen fibrils in the human corneal stroma: A synchrotron x-ray diffraction study. Curr Eye Res. 1987;6:841-846.
10. Benedek GB. Theory of transparency of the eye. Appl Opt. 1971;10:459-473.
11. Twersky V. Transparency of pair-related, random distributions of small scatterers, with application to the cornea. Opt Soc Am. 1975;65:524-530.

12. Nyquist GW. Rheology of the cornea: Experimental techniques and results. Exp Eye Res. 1968;7:183-188.
13. Nash I, Greene P, Foster S. Comparison of mechanical properties of keratoconus and normal cornea. Exp Eye Res. 1981;35:413-423.
14. Asejczyk-Widlicka M, Śródka DW, Kasprzak H, Pierscionek BK. Modelling the elastic properties of the anterior eye and their contribution to maintenance of image quality: the role of the limbus. Eye. 2006;1-8. Available from: http://www.nature.com/eye/journal/vaop/ncurrent/pdf/6702464a.pdf.
15. Asejczyk-Widlicka M, Pierscionek BK. Elasticity and rigidity of the outer coats of the eye. Br J Ophthalmol. 2008;92:1415-1418.
16. Wood EA. An Introduction to Optical Crystallography. In: Wood EA. Crystals and Light. Princeton, New Jersey: D. Van Nostrand Company, Inc.;1964.
17. Brewster D. On the structure of the crystalline lens in fishes and quadrupeds as ascertained by its action on polarised light. Phil. Trans R Soc London 1816;106:311-317.
18. Brewster D. On the development and extinction of regular doubly refracting structures in the crystalline lenses of animals after death. Phil Trans R Soc London. 1837;127:253-258.
19. Cope WT, Wolbarsht ML, Yamanashi BS. The corneal polarisation cross. J Opt Soc Am. 1978;68:1139-1141.
20. Pierscionek BK, Weale RA. Is there a link between corneal structure and the 'corneal cross'? Eye. 1997;11:361-364.
21. Bueno JM, Jaronski JW. Spatially resolved polarization properties for in vitro corneas. Ophthalmic Physiol Opt. 2001;21:384–392.
22. Bueno JM, Vargas-Martın F. Measurements of the corneal birefringence with a liquid- crystal imaging polariscope Appl Opt. 2002;41:116–124.
23. Jaronski JW, Kasprzak HT. Linear birefringence measurements of the in vitro human. Ophthalmic Physiol Opt. 2003;23:361–9.
24. Knighton RW, Huang XR. Linear birefringence of the central human cornea. Invest Ophthalmol Vis Sci. 2002;43:82–86.
25. Perutz MF. Polarization dichroism, form birefringence, and molecular orientation in crystalline haemoglobins. Acta Crystallogr. 1953;6(11-12):859-864.
26. Bragg WL, Pippard AB. The form birefringence of macromolecules. Acta Crystallogr. 1953;6(11-12):865-867.
27. Oldenbourg R, Ruiz T. Birefringence of macromolecules. Wiener's theory revisited, with applications to DNA and tobacco mosaic virus. Biophys J. 1989;56(1):195-205.
28. Pierscionek BK, Chan DY. Refractive index gradient of human lenses. Optom Vis Sci. 1989 Dec;66(12):822-829.
29. Patent N. WO2014033697; WO2015011692.
30. Meek KM, Boote C. The use of X-ray scattering techniques to quantify the orientation and distribution of collagen in the corneal stroma. Prog Retin Eye Res. 2009;28(5):369-392.
31. Boote G, Kamma-Longer CS, Hayes S, et al. Quantification of collagen organization in the peripheral human cornea at micron-scale resolution. Biophys J. 2011;101(1):33-42.

Computational corneal biomechanics in the clinic

Miguel Ángel Ariza-Gracia[1,2], David Pablo Piñero Llorens[2], José Félix Rodríguez Matas[4], Begoña Calvo Calzada[1,5]

[1]*Applied Mechanics and Bioengineering (AMB), Aragón Institute for Engineering Research (i3A), University of Zaragoza, Zaragoza, Spain;* [2]*Institute for Surgical Technology and Biomechanics, University of Bern, Bern, Switzerland;* [3]*OFTALMAR, Vithas Medimar International Hospital, Alicante, Spain;* [4]*LaBS, Politecnico di Milano (Polytechnic University of Milan), Milan, Italy;* [5]*Center for Biomedical Research in Bioengineering, Biomaterials, and Nanomedicine (CIBER-BBN), Madrid, Spain*

Abstract

Corneal topographers and air-puff devices aim at completely characterizing so-called corneal biomechanics, a collection of features that describes corneal behavior. The European FP7 project (PopCorn) was born with the goal of integrating both technologies. Among the novelties, computational models were included as an integral part of the clinical assessment. Automatic patient-specific (P-S) reconstruction of the cornea, alongside material prediction based on finite element simulations, optimization, and fitting were used to strive forward in *a priori* surgical planning. Both methodologies show good performance in retrieving the P-S geometry of the cornea (error < 1%) and the maximum deformation amplitude of a non-contact tonometry (error ~ 5%). Nevertheless, physiological and non-physiological corneas cannot be classified solely in terms of material, at least with a single experiment. Eventually, and due to the interplay of different factors (geometry, material, and pressure), results coming from air-puff devices should be handled with care.

Keywords: corneal biomechanics, material characterization, non-contact tonometry, patient-specific

Correspondence: M.Á. Ariza-Gracia, Edificio i3A, Campus Río Ebro Calle Mariano Esquillor Gómez s/n, C.P. 50.018, Zaragoza, Spain.
E-mail: mariza@unizar.es

1. Introduction

Corneal biomechanics is an emerging topic in ophthalmology. Non-contact tonometers aim at determining the intraocular pressure of the eye (IOP) and characterizing the mechanical properties of corneal tissue by applying a short air jet (approximately 20 ms) on the cornea. Different corneal biomarkers are recorded as the cornea deforms, establishing an interesting framework to determine the mechanical properties of the corneal tissue by means of inverse optimization processes.[1] The PopCorn European project was born as an effort to combine non-contact tonometers, imaging techniques (*i.e.*, plenoptic imaging), and computational methods to reconstruct the P-S geometry and predict the P-S material. The data from this project will be essential to reach the ultimate objective: personalized surgical simulations.

2. Material and methods

First, a theoretical *in-silico* study on an average cornea was designed to shed light on the interaction between different corneal features (geometry, material, and IOP) (Fig. 1, upper left).[2] Second, two algorithms were developed: an automatic P-S reconstruction of the cornea using clinical data[3] and an automatic P-S material predictor based on clinical biomarkers[4] (Fig. 1, bottom panels). The geometric algorithm reconstructed the 3-D finite element (FE) model including: the patient's topography (*i.e.*, point cloud describing the corneal geometry); an average orthogonal distribution of collagen fibers; the anisotropic hyperelastic response of the corneal tissue (*i.e.*, a non-linear isotropic behavior related to the extracellular matrix, plus an exponential orientation-dependent anisotropic behavior related to the fibers);[5] and a free-stress algorithm that allows for recovering the natural pre-stress due to the IOP. Furthermore, the automatic non-supervised pipeline allows integrating a geometrical P-S simulation after the reconstruction process (*e.g.*, a non-contact tonometry or surgery). The material predictor combined our former P-S geometric algorithm with *in-silico* simulations of a non-contact tonometry to sweep a range of P-S geometries, IOPs, and material properties (*i.e.*, in the framework of anisotropic elasticity), building a dataset of ~9.000 FE simulations. The dataset contained the mechanical response of the cornea to inflation experiments in humans[6] and the kinematic response of the cornea to an air puff.[7] After filtering those by physiological response (Fig. 1, upper right), the predictors of the material model were set using four mathematical strategies: support vector regression (SVR), multiple layer perceptron (MLP), quadratic response surface (QRS), and a clustering technique based on the K nearest neighbors (K-nn). Once the models were trained, three clinical biomarkers were used to predict the three material constants of our proposed model:[4] the maximum corneal displacement of the non-contact
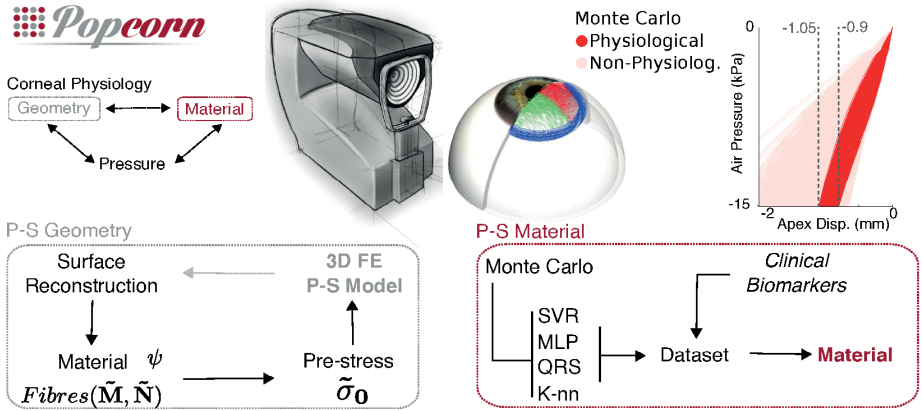
Fig. 1. Methodology pipeline (*upper left*). Interplay between corneal features (*bottom left*). Patient-specific geometric reconstruction (*bottom right*). Patient-specific material prediction (*upper right*). Monte Carlo simulations for the normal population. Physiological behavior after filtering (*dark red*) vs non-physiological behavior (*light red*). Topographer concept (*center*).

tonometry test (Umax), the corneal thickness (CCT), and the IOP. To validate our protocol, we performed a closed-loop validation using new unknown healthy and diseased real cases. First, the material parameters were predicted based on real clinical biomarkers (Umax, IOP, and CCT). Second, the automatic reconstruction algorithm reconstructed the P-S model (including IOP, geometry, and predicted material properties). Third, we performed the simulation of a generic non-contact tonometer to obtain the simulated displacement (Unum). Finally, the accuracy of the protocol was determined by the difference between both displacements, actual (Umax) and numerical (Unum).

3. Results

First, we highlight that an interplay exists between different corneal features (CCT, IOP, and material stiffness) when an air-puff diagnosis test is applied. The maximum apical displacement presents an inverse linear relation with IOP, but an inverse cubic relation with CCT. Meaning that, for similar geometrical features, a compliant (soft) cornea with a high IOP could behave as a stiff cornea with a low IOP.[2] Second, the automatic geometric algorithm showed that the accuracy of the P-S reconstruction had an error of less than 1%. Disregarding the free-stress configuration of the eye could lead to up to a 10% of error in the prediction of the displacement (Unum). Not only that, but the sensitivity analysis using P-S features also showed an interplay between the aforementioned variables, supporting the

outcomes outlined with average models.[3] Third, regarding the material predictor, a Monte Carlo approach requires significant computational resources to build a reliable dataset, but at the same time, provides great flexibility. After filtering the data to those satisfying the physiological response in inflation and air-puff tests, the distribution of the material parameters was not parametric (*i.e.*, not normal). Moreover, when studying the combinations of material parameters, IOP, and CCT that lead to the same displacement (Unum), the result demonstrates the interplay between parameters: different combinations of IOP and CCT gave the same response depending on the material. Finally, the average validation error of the methodology (*i.e.*, the difference between numerical and real displacement) was approximately 5%, even for diseased eyes (*i.e.*, eyes with keratoconus).[4]

4. Conclusion

A computational tool applicable to clinical situations was developed. From P-S reconstruction to the prediction of corneal tissue stiffness, all clinical requests were covered. Due to the interplay of different corneal features (IOP, geometry, and material), physiological and non-physiological eyes cannot be differentiated solely in terms of material, at least not with a single diagnostic test. Therefore, results from non-contact tonometry tests must be handled with care to avoid misdiagnosing. However, this work is not exempt of limitations: we do not include viscoelastic effects, since the test is extremely quick;[8] P-S distribution of fibers is disregarded, since nowadays it is unlikely to obtain them in the clinic; the internal structures of the eye (*i.e.*, lens and ciliary muscles) are disregarded, the internal humors are treated as a uniform pressure applied over the inner surface of the eyeball, and do not account for mass nor compressibility; and the simulations are assumed to be quasi-static. Next steps should involve a more complex behavior of the corneal tissue, and fluid-structure simulations, currently in the final stages of development. Nevertheless, as the proposed methodology presents a block-wise design, all these features could be introduced without modifying the pipeline.

Acknowledgements

References

1. Piñero DP, Alcón N. Corneal biomechanics: A review. Clin Exp Optom. 2015;98(2):107-116.
2. Ariza-Gracia MÁ, Zurita JF, Piñero DP, Rodriguez-Matas JF, Calvo B. Coupled biomechanical response of the cornea assessed by non-contact tonometry. A simulation study. PLoS One. 2015;10(3):e0121486.
3. Ariza-Gracia MÁ, Zurita J, Piñero DP, Calvo B, Rodríguez-Matas JF. Automatized patient-specific methodology for numerical determination of biomechanical corneal response. Ann Biomed Eng. 2016;44(5):1753–1772.
4. Ariza-Gracia MÁ, Redondo S, Llorens DP, Calvo B, Rodriguez-Matas JF. A predictive tool for determining patient-specific mechanical properties of human corneal tissue. Comput Methods Appl Mech Eng. 2016;317:226–247.
5. Pandolfi A, Holzapfel GA. Three-dimensional modeling and computational analysis of the human cornea considering distributed collagen fibril orientations. J Biomech Eng. 2008;130(6):61006. doi:/10.1115/1.2982251.
6. Elsheikh A, Alhasso D, Rama P. Biomechanical properties of human and porcine corneas. Exp Eye Res. 2008;86(5):783–790.
7. Huseynova T, Waring 4th GO, Roberts C, Krueger RR, Tomita M. Corneal biomechanics as a function of intraocular pressure and pachymetry by dynamic infrared signal and Scheimpflug imaging analysis in normal eyes. Am J Ophthalmol. 2014;157(4):885–893. doi:/10.1016/j.ajo.2013.12.024.
8. Simonini I, Angelillo M, Pandolfi A. Theoretical and numerical analysis of the corneal air puff test. J Mech Phys Solids. 2016;93:118–134. doi:/10.1016/j.jmps.2016.04.012.

Biomechanical evaluation of central and peripheral Descemet's membrane endothelial graft

Vito Romano[1,2], Zhuola[1], Zhuo Chang[3], Bernhard Steger[4], Hannah J. Levis[2], Stephen B. Kaye[1,2], Riaz Akhtar[3]

[1]Department of Ophthalmology, St. Paul's Eye Unit, Royal Liverpool University Hospital, Liverpool, UK; [2]Department of Eye and Vision Science, Institute of Ageing and Chronic Disease, University of Liverpool, Liverpool, UK; [3]Department of Mechanical, Materials and Aerospace Engineering, School of Engineering, University of Liverpool, Liverpool, UK; [4]Department of Ophthalmology, Medical University of Innsbruck, Innsbruck, Austria

Abstract

Corneal endothelial transplant is the gold-standard treatment in cases of corneal endothelial cellular dysfunction. Preparation, delivery, and unfolding of the graft are technically demanding. We assessed the biomechanical behavior of Descemet's membrane to better understand Descemet's membrane endothelial keratoplasty (DMEK) graft behavior, and to select the right diameter and donor age graft. The biomechanical behavior was tested using atomic force microscopy (AFM) on five corneas unsuitable for transplantation. The peripheral cornea was found to be stiffer than the central cornea (3171.89 MPa and 2837.20 MPa, respectively). The elastic modulus of both the central and peripheral cornea exhibited a trend to decrease with age. In addition, the central cornea becomes stiffer than the peripheral cornea in older patients, while the peripheral cornea was stiffer in younger patients. AFM is a suitable technique for evaluating biomechanical behavior of DMEK grafts. One interpretation of this varied behavior is that the type and quantity of collagen changes with age and location.

Keywords: atomic force microscopy (AFM), biomechanical behavior, corneal transplant, endothelial keratoplasty

Correspondence: Vito Romano, MD, Department of Corneal and External Eye Diseases, St Paul's Eye Unit, Royal Liverpool University Hospital, Prescot Street, Liverpool, L7 8XP, UK. E-mail: vito.romano@gmail.com

1. Introduction

Over the last twenty years, significant advances have been made in corneal transplantation techniques. The treatment of corneal pathologies has evolved from the replacement of full-thickness cornea to replacing only the diseased corneal endothelium.[1] During the past several years, new surgical techniques have been reported, endothelial keratoplasty being the gold standard. Posterior lamellar keratoplasty, either Descemet's stripping automated endothelial keratoplasty (DSAEK) or DMEK, eliminate surface corneal incisions or sutures, maintain much of the cornea's structural integrity, and induce minimal refractive change, suggesting distinct advantages over standard penetrating keratoplasty. DMEK represents the final iteration of endothelial keratoplasty (EK), producing near-pure anatomic replacement therapy for patients with endothelial dysfunction, stromal edema, and Descemet's membrane disfigurement. Although the visual results after DMEK are better on average than the published visual results after DSAEK, DMEK has not overtaken DSAEK because it is a technically demanding surgical procedure.[2] Handling the DMEK graft is difficult, making loading, delivery, and unfolding very challenging, thus taking up surgical time.[3-7] In order to better understand DMEK graft behavior and to select the right diameter and donor age graft, we studied the biomechanical behavior of the Descemet's membrane graft.

2. Purpose

To characterize the biomechanical behavior of Descemet's membrane, its parts, and the DMEK graft.

3. Design

Laboratory study.

4. Methods

Five corneas unsuitable for transplantation were collected from the Manchester Eye Bank Foundation, UK, with a written consent to be used for research from the donor's next of kin. The donor corneas did not show indications of any systemic disease, dystrophy, or infections. The corneas were not suitable for transplant due to low endothelial cell count.

The average age of the donors was between 54 and 77 years. The tissues were preserved in organ culture medium (OCM) for 20 days.

All the corneas (n = 8) were centered on the base of a trephine punch using the peripheral holes of the suction area as reference. A 9.5-mm diameter punch (Moria, SA: Antony, France) was used to create a superficial cut by gently tapping the endothelial surface (cut edge) of the tissue. The endothelium was submerged in the OCM. The membrane was lifted using a cleavage hook throughout the circumference to limit the peripheral tearing of the very fragile DMEK tissue. Using acute forceps (E. Janach SRL; Como, Italy), the membrane was stripped with a longitudinal movement from three sides, ensuring that no torsions were generated during this phase.

The nanomechanical properties were measured with AFM using PeakForce Quantitative Nanomechanical Mapping (QNM) in air mode. The AFM probe had a 5 N/m of nominal spring constant of the cantilever and 8 nm of nominal tip radius. The resonant frequency was 150 kHz. For each sample, three random areas (5 μm^2) were imaged in the center and periphery of the corneas. The DMEK grafts were tested with the corneal endothelium facing downwards, to expose Descemet's membrane to the probe.

For the nanoindentation measurements, the Peak Force set point was fixed at 0.05 V, which gives rise to a maximum force of about 5 nN. For the data processing and elastic modulus calculation, unloading curves were utilized. It is worth pointing out that negligible hysteresis was observed during the approaching-retraction cycles, reasonably because of the absence of cells on the non-endothelial side of the membrane.

Statistical analysis was performed using Stata (StataCorp; College Station, Texas, USA) and a Student's t-test was performed, deeming $p < 0.05$ statistically significant.
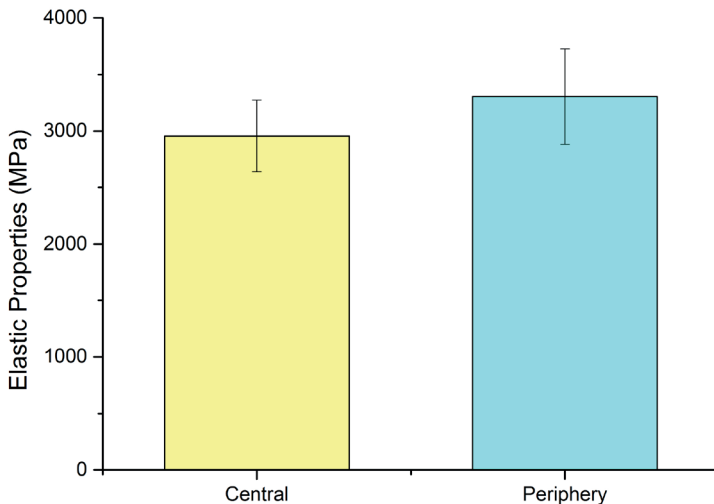

Fig. 1. Elastic properties in MPa of the central and peripheral cornea.
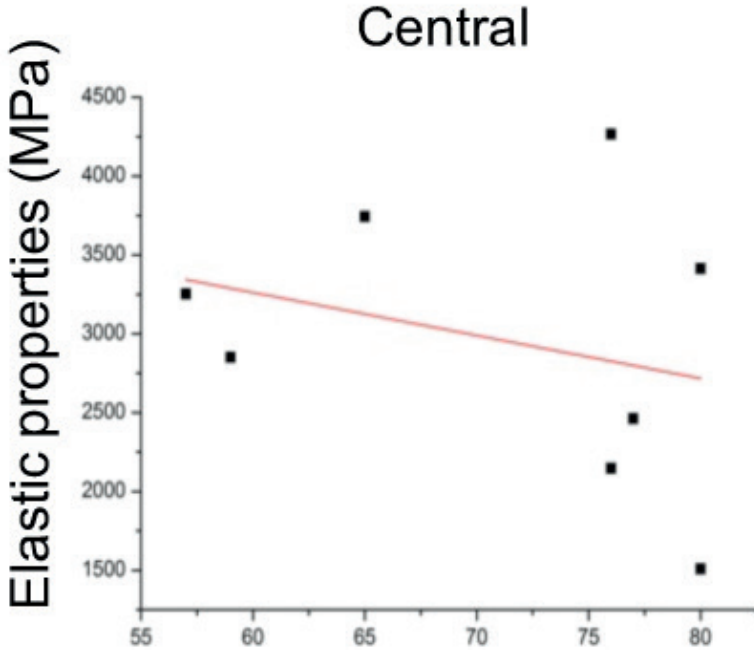
*Fig. 2.* Elastic modulus of the central cornea.
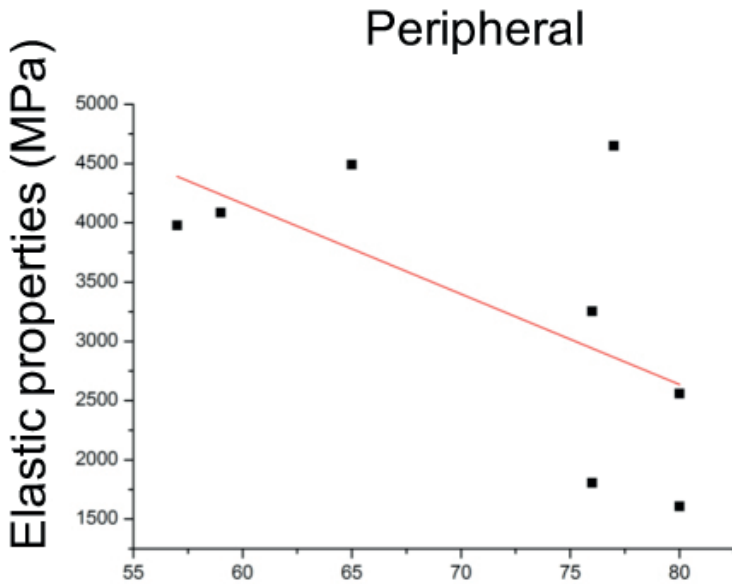
Fig. 3. Elastic modulus of the peripheral cornea.

5. Results

The periphery of the cornea was stiffer than the center ($E_{periphery}$ = 3171.89 MPa; E_{center} = 2837.20 MPa) (Fig. 1). The elastic modulus of both the central and peripheral cornea exhibited a trend to decrease with age. Interestingly, we found that the center was stiffer than the periphery in older patients (75 - 80 years) (Fig.2), while the periphery was stiffer in younger patients (55-70 years) (Fig.3).

6. Conclusion

Peakforce AFM is a suitable technique for evaluating DMEK grafts. The limitation of the present study is the limited number of samples considered, which reduces the statistical significance of the results, and thus, the lack of stratification on a larger sample that can include a variability in age. Nevertheless, the study clearly showed different behaviors between the central and peripheral DMEK graft, which can be explained in terms of a different distribution in collagen quantity and quality. These findings provide some interesting areas for consideration and future research on the characterization of the biomechanical properties of the cornea for identification of potential risk factors in donor selection for DMEK surgery, allowing a potential reduction in complication rates and improved graft survival.

References

1. Anshu A, Price MO, Tan DT, Price FW, Jr. Endothelial keratoplasty: a revolution in evolution. Surv Ophthalmol. 2012;57(3):236-252.
2. Dapena I, Ham L, Melles GR. Endothelial keratoplasty: DSEK/DSAEK or DMEK--the thinner the better? Curr Opin Ophthalmol. 2009;20(4):299-307.
3. Dapena I, Moutsouris K, Ham L, Melles GR. Graft detachment rate. Ophthalmology. 2010;117(4):847-.e1.
4. Fernandez Lopez E, Baydoun L, Gerber-Hollbach N, Dapena I, Liarakos VS, Ham L, et al. Rebubbling techniques for graft detachment after Descemet membrane endothelial keratoplasty. Cornea. 2016;35(6):759-764.
5. O'Brien PD, Lake DB, Saw VP, Rostron CK, Dart JK, Allan BD. Endothelial keratoplasty: case selection in the learning curve. Cornea. 2008;27(10):1114-1148.
6. Parekh M, Ruzza A, Ferrari S, Ahmad S, Kaye S, Ponzin D, et al. Endothelium-in versus endothelium-out for Descemet membrane endothelial keratoplasty graft preparation and implantation. Acta Ophthalmol. 2017;95(2):194-198.
7. Romano V, Parekh M, Ruzza A, Willoughby CE, Ferrari S, Ponzin D, et al. Comparison of preservation and transportation protocols for preloaded Descemet membrane endothelial keratoplasty. Br J Ophthalmol. 2017. doi: 10.1136/bjophthalmol-2017-310906.

The effect of serum proteins on dynamic interfacial properties of silicone oils in vitrectomized eyes

Irene Nepita[1], Libero Liggieri[3], Eva Santini[3], Francesca Ravera[3], Mario R. Romano[2], Jan O. Pralits[1], Rodolfo Repetto[1]

[1]Department of Civil, Chemical and Environmental Engineering, University of Genoa, Genoa, Italy; [2]Department of Biomedical Sciences, Humanitas University, Milan, Italy; [3]Institute for Condensed Matter Chemistry and Energy Technologies, National Research Council, Genoa, Italy

Abstract

The formation and stability of emulsions in vitrectomized eyes is linked to the properties of the silicone oil-aqueous humor interface, in particular the surface tension. In the presence of natural surfactants, such as serum and plasma, the value of the surface tension is likely to change, but little quantitative information is presently available.

To this end, we perform accurate experiments measuring the interfacial properties of the Siluron 1000 (Fluoron GmbH, Ulm, Germany) silicone oil with an aqueous solution in the presence of endogenous-like proteins. It is found that the surface tension is significantly reduced when physiologically realistic concentrations are used. Moreover, the values obtained for the dilational viscoelastic modulus are compatible with the formation of stable emulsions.

Keywords: emulsion, silicone oil, surface tension, vitrectomy

1. Introduction

High-viscosity silicone oils (SO) are used in ophthalmology in a variety surgical procedures involving vitrectomy. This is the second most frequent surgical inter-

Correspondence: Irene Nepita, Department of Civil, Chemical and Environmental Engineering, University, of Genoa, Via Montallegro 1, 16145 Genoa, Italy.
E-mail: irene.nepita@gmail.com

vention and is performed to treat several pathological or traumatic vitreoretinal conditions, such as retinal detachment, hemorrhage, inflammation, and infection in the eye.

The main complication associated with the use of SOs after vitrectomy is the tendency of the oil to emulsify in the aqueous solution produced in the eye, causing several postsurgical complications from moderate to serious. Hindering emulsification is therefore a mandatory step to improve the success of these surgical treatments.

The blood proteins produced by inflammatory processes have been identified as one of the co-factors responsible for the emulsification.[1-3] However, so far, the few available studies did not address the effects of these proteins on the key chemico-physical properties of the interface that are involved in the emulsion formation and stability. The present work is aimed at evaluating and characterizing the effects on the properties of the interface between SO and surfactant biomolecule aqueous solutions responsible for emulsification.

2. Methods

The interfacial tension (IT) and the interfacial dilational viscoelasticity (the response of interfacial tension to oscillatory perturbations of the interfacial area) have been measured at 35°C for the interface between SO and key serum proteins within the physiological concentration range in a Dulbecco alkaline buffer.[4-5]

The corresponding measurements have been performed in the proper characteristic time windows by using a Drop Shape tensiometer (PAT1; Sinterface, Berlin, Germany) that allows the control of the drop interfacial area. The shapes of liquid menisci result from the equilibrium between hydrostatic and capillary pressure at each point, according to the Young-Laplace Equation:

$$P_0 + \Delta\rho gz = \gamma \left[\frac{1}{R_1} + \frac{1}{R_2} \right] \tag{1}$$

where R_1 and R_2 are the curvature radii, γ the interfacial tension, P_0 a constant, $\Delta\rho$ the density difference, and g gravity. This relation for the axisymmetric profile of a drop, as shown in Figure 1, can be redrawn by the Bashforth-Adams equation for an axisymmetric drop as follows:

$$2 + \frac{\beta z}{b} = \frac{1}{R/b} + \frac{sin(\phi)}{x/b} \tag{2}$$

where b is the curvature radius at the apex, R the curvature radius of the axial section at the point P (Fig. 1), and β the shape factor. The IT is obtained by the best fit of Equation (2) to the drop profile acquired from images of the drop.
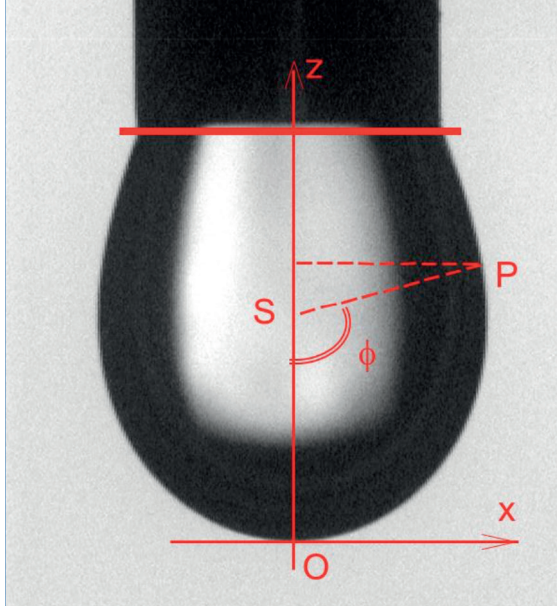
Fig. 1. Pendent drop with symbols used in Equation (2).

The dilational viscoelasticity, (Eq. (3) and Fig. 2), is measured according to the oscillating drop method, measuring the response of the IT to sinusoidal perturbations of the interfacial area, A. Here, A0 is a reference area and φ the phase.

$$E = \frac{d\gamma}{d\ln A} = A0 \frac{\Delta\gamma}{\Delta A} \exp(i\varphi) \tag{3}$$

3. Results

The presence of endogenous proteins affects the interfacial properties remarkably. For the investigated albumin concentrations, Figure 3 reports the ratio between the equilibrium values of IT in the presence of albumin and those with the bare buffer. The ratio decreases to approximately 0.3 for an albumin concentration of 70 g/L, which most likely increases the tendency to emulsify. The time to attain equilibrium IT decreases from two hours to a few minutes by increasing albumin concentration.

Moreover, a typical serum protein in concentrations close to the physiological ones increases the dilational viscoelasticity modulus (|E|) to significantly higher values (Fig. 4), which are compatible with emulsions that, once formed, are expected to be more stable against coalescence.
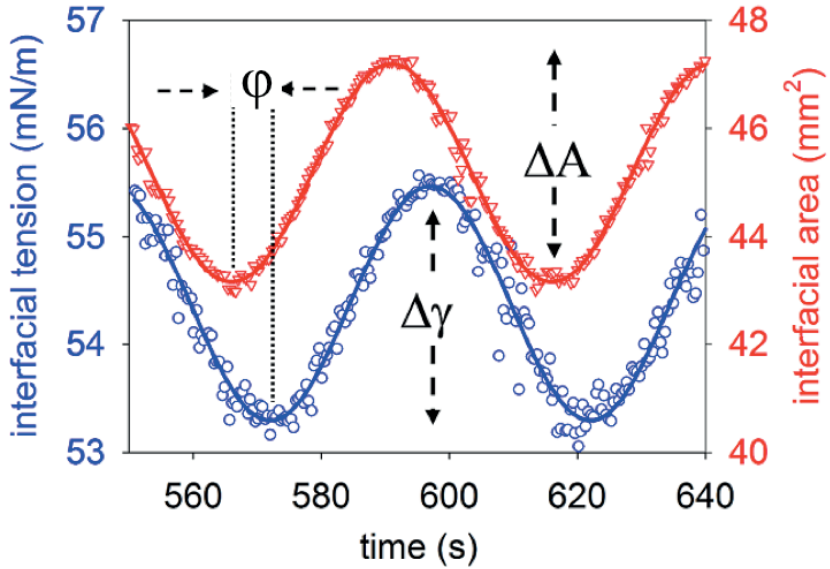
Fig. 2. Interfacial tension response to small amplitude harmonic perturbations of the interfacial area, A.
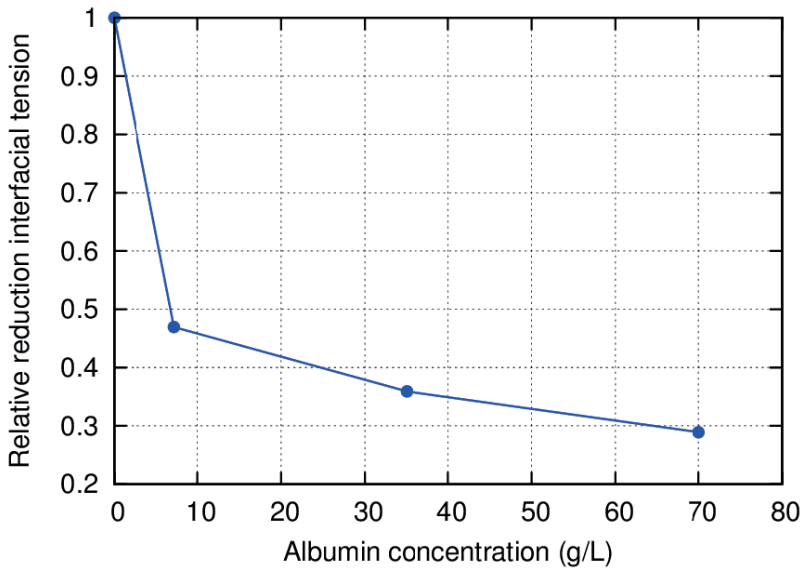
Fig. 3. The interfacial tension normalized with the value corresponding to pure SO-aqueous solution as a function of the albumin concentration.
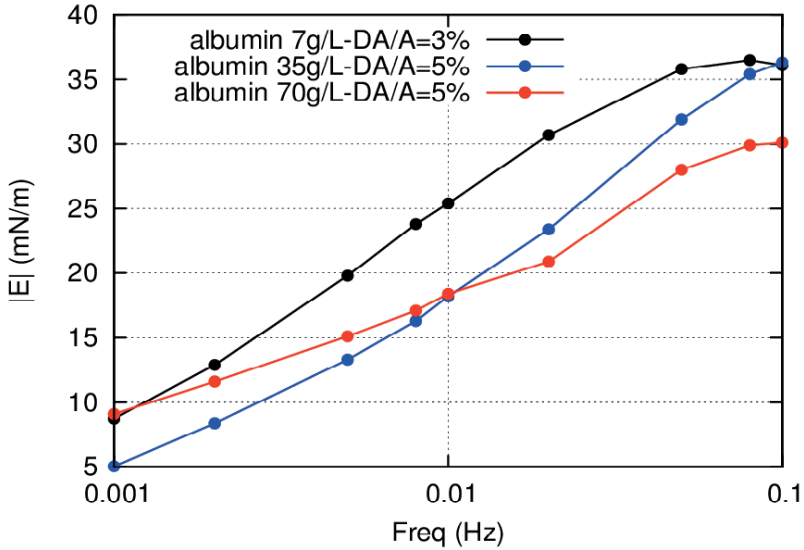
Fig. 4. Dilation viscoelasticity modulus at adsorption equilibrium measured as a function of the perturbation frequency for different albumin concentrations.

4. Conclusions

The adsorption of proteins at the liquid interface reduces the interfacial tension to values compatible with an increased tendency to emulsify and provides values of the dilational viscoelasticities compatible with a good stability for the resulting emulsions.

These observations are preliminary to design a wider study where different types of endogenous-like surfactants and their physiological blends will be investigated, suggesting possible strategies for the mitigation of the SO emulsification phenomena.

Acknowledgements

References

1. Nakamura K, Refojo MF, Crabtree DV. Factors contributing to the emulsification of intraocular silicone and fluorosilicone oils. Invest Ophthalmol Visual Sci.1990;31(4):647-656.
2. Caramoy A, Hagedorn N, Fauser S, Kugler W, Groß T, Kirchhof B. Development of emulsification-resistant silicone oils: can we go beyond 2000 mPas silicone oil?. Invest Ophthalmol Visual Sci. 2011;52(8):5432-5436.
3. Zelisko PM, Flora KK, Brennan JD, Brook MA. Water-in-silicone oil emulsion stabilizing surfactants formed From native albumin and α, ω-triethoxysilylpropyl-polydimethylsiloxane. Biomacromolecules. 2008;9(8);2153-2161.
4. Loglio G, Pandolfini P, Miller R, Makievski AV, Ravera F, Ferrari M, Liggieri L. Novel methods to study interfacial layers. Stud Interface Sci. 2001;11:439.
5. Ravera F, Ferrari M, Santini E, Liggieri L. Influence of surface processes on the dilational visco-elasticity of surfactant solutions. Adv Colloid Interface Sci. 2005;117(1-3):75-100.

A stochastic model of stroma: interweaving variability and compressed fibril exclusion

Marcello Vasta[1], Alessio Gizzi[2], Anna Pandolfi[3]

[1]Department of Engineering and Geology, University of Chieti-Pescara, Chieti, Italy; [2]Department of Engineering, University Campus Bio-Medico of Rome, Rome, Italy; [3]Departament of Civil and Environmental Engineering, Politecnico di Milano (Polytechnic University of Milan), Milan, Italy

Abstract

Hyperelastic constitutive models of the human stroma accounting for the stochastic architecture of the collagen fibrils and particularly suitable for computational applications are discussed. The material is conceived as a composite where a soft ground matrix is embedded with collagen fibrils characterized by non-homogeneous spatial distributions typical of reinforcing stromal lamellae. A multivariate probability density function of the spatial distribution of the fibril orientation is used in the formulation of the lamellar branching observed on the anterior third of the stroma, selectively excluding the contribution of compressed fibrils. The physical reliability and the computational robustness of the model are enhanced by the adoption of a second order statistics approximation of the average structure tensors typically employed in fiber reinforced models.

Keywords: compressive fibril exclusion, hyperelasticity, lamellar branching, second order structure tensors

1. Introduction

The cornea is the external lens of the eye and carries out concerted protective, structural, and refractive functions. Since the cornea provides one-third of the total

Correspondence: M. Vasta, Dipartimento INGEO, Università di Chieti-Pescara, Viale Pindaro 42, Pescara, Italy.
E-mail: mvasta@unich.it

refractive power of the eye and due to its accessibility, it stands as the privileged site for surgical interventions to correct conditions such as myopia, presbyopia, and astigmatism. Corneal refractive surgery demands accurate diagnostic and surgical plans, but the outcomes are not always optimal.[1] Advanced numerical models of the cornea have been developed in recent years with the aim of supporting refractive surgery,[2,3] although they are still far to be an active part of the current clinical practice since they fail to be patient-specific models. Indeed, patient-specific models derive only from the combination of advanced diagnostic imaging, correct interpretation of optical and mechanical experimental observations, and efficient computational models. For one, the interpretation of the most promising *in-vivo* dynamical test (contactless air-puff tonometer) calls for the description of features of the stromal tissue that are not of relevance under more traditional quasistatic loading. The present study is thus concerned with the definition of accurate material models of the stromal tissue, based on the description of the collagen fibril architecture according to its statistical distribution, characterized by a different degree of interweaving across the thickness[4] and inactivity of the fibrils under compressive loading. Starting from a second order approximation of the strain energy density of a statistical distribution of collagen fibrils,[5] a multivariate probability density function (PDF)[6] is introduced to incorporate recent experimental data.[7]

2. Hyperelastic fibril distributed models

2.1. Second order structure tensor approach
Stochastic models for fiber reinforced tissues[8] derive from the seminal work of Lanir,[9] where the contribution of fiber orientation to the mechanical response of soft tissues is formulated from a theoretical point of view. The computational challenge of describing the microstructural properties in a reliable manner motivated the development of several approximations.[10-18] The present study departs from the second order approximation of the strain energy density ψ_f^* of the collagen fiber distribution illustrated in Pandolfi and Vasta.[5] The approximation is based on the second order Taylor expansion of the fiber strain energy density about the fourth pseudo-invariant $\overline{I}_4 = \overline{\mathbf{C}} : \mathbf{A}$, where $\mathbf{A} = \mathbf{a} \otimes \mathbf{a}$ is the structure tensor associated to the mean direction $\mathbf{a}$ of the fiber distribution, *i.e.*, ψ:

$$\psi_f^* \simeq \psi_f^0 + \overline{\psi}_f^* \left(1 + K^* \sigma_{I_4}^2\right) \tag{1}$$

with

$$\psi_f^0 = -\frac{k_1}{2k_2} \qquad \psi_f^* = \frac{k_1}{2k_2}\exp\left[k_2(I_4^* - 1)^2\right]$$

$$I_4^* = \langle \overline{I}_4 \rangle = \mathbf{H} : \overline{\mathbf{C}}, \; \sigma_{I_4}^2 = \langle (\overline{I}_4 - I_4^*)^2 \rangle = \mathbb{H} : \overline{\mathbf{C}}$$

and $\boldsymbol{H}$ and $\mathbb{H}$ define the second and forth order averaged structure tensors, respectively. The model provides a closed form expression of the second Piola-Kirchhoff stress tensor:

$$\overline{S}_f^* \simeq \alpha\left(I_4^*, \sigma_{I_4}^2\right)\boldsymbol{H} + \beta\left(I_4^*, \sigma_{I_4}^2\right)\mathbb{H} : \overline{\boldsymbol{C}} \tag{2}$$

which is effective and robust in computational applications.[14,15,18]

2.2. Computational modeling of interweaving variability

The collagen fibril architecture of the stroma is characterized by a regular variation across the thickness, with a marked interweaving in the anterior third and a predominant surface tangent (planar) orientation distribution in the posterior third.[4,7] The organization of the fibrils can be modelled through a multivariate von Mises distribution, ruling both the in-plane and transverse orientation of the fibrils. Using the spherical angles $[\Theta, \Phi] \in [0, \pi], [0, \pi]$ the generic orientation $\boldsymbol{a}$ is:

$$\boldsymbol{a} = \sin\Theta \cos\phi\, e_1 + \sin\Theta \sin\phi\, e_2 + \cos\Theta\, e_3 \tag{3}$$

The corresponding PDF, $\rho(\alpha)$, decomposes in out-of-plane term $\rho_\theta(\theta)$ and in-plane term $\rho\phi(\phi)$ as $\rho(\boldsymbol{a}) = \rho\theta(\theta)\rho\phi(\phi)$:

$$\begin{aligned}\rho\theta(\theta) &= N_\theta \exp\left[b_\theta \cos 2\theta\right] \\ \rho\phi(\phi) &= N_\phi \exp\left[b_\phi \cos(\phi - \pi/2)\right]\end{aligned} \tag{4}$$
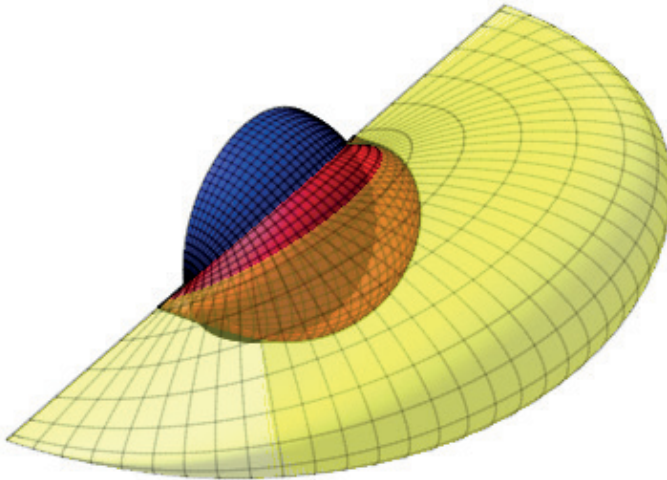

Fig. 1. Representative example of the multivariate von Mises PDF for three different combinations of the material parameters, b_θ, b_ϕ.
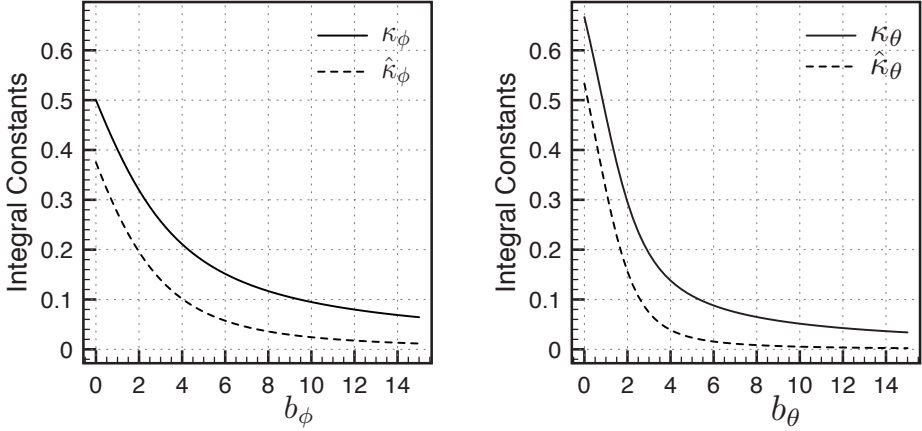
Fig. 2. Representative example of the integral coefficients derived from the multivariate PDF varying with the parameters b_θ and b_ϕ. (*Left*) κ_θ, $\widehat{\kappa}_\theta$ versus b_θ. (*Right*) κ_ϕ, $\widehat{\kappa}_\phi$ versus b_ϕ.

The decomposition preserves the simple structure tensor form of the approximated strain energy density. A representative example of multiple combinations is provided in Figure 1.

The formulation allows:

1. to characterize complex spatial PDF by means of only two material parameters, b_θ, b_ϕ; and
2. to recover a diagonal form for the averaged structure tensor.

The remarkable computational implication of the approach is that the averaged structure tensors **H** and $\mathbb{H}$ depend exclusively on four integral coefficients:

$$\kappa_\theta = \frac{1}{N_\theta} \int_0^\pi \rho_\theta \sin^3\theta \, d\theta \qquad \widehat{\kappa}_\theta = \frac{1}{N_\theta} \int_0^\pi \rho_\theta \sin^5\theta \, d\theta$$

$$\kappa_\phi = \frac{1}{N_\phi} \int_0^\pi \rho_\phi \sin^3\phi \, d\phi \qquad \widehat{\kappa}_\phi = \frac{1}{N_\phi} \int_0^\pi \rho_\phi \sin^5\phi \, d\phi \qquad (5)$$

A representative example of the novel behavior induced by the multivariate PDF is provided in Figure 2 with respect to different values of the concentration parameters b_θ, b_ϕ.

2.3. Fibril exclusion under compression

A full statistical approach has a great potential to exclude fibrils in compression.[15,19] By applying the random variable transformation rule, from the PDF of θ, ϕ it is possible to derive the PDFs of $\bar{I}_4$, $\rho_{I_4}(I_4)$ and of Ψ, $\rho_\Psi(\Psi)$. Moreover, by using a principal reference frame,[20] it is possible to obtain a closed form expression of $\rho_{I_4}(I_4)$ with the

a priori knowledge of the physical integration range. This notable result leads to the correct statistical exclusion of compressed fibers in the mechanical response of the tissue.

3. Conclusion

A material model for fiber reinforced soft materials characterized by stochastic distributions of the fibers is discussed. The approach allows for the description of local smooth variability of the spatial distribution of fibril interweaving, as the one observed across the thickness of the corneal stroma. Moreover, in a principal reference frame description, the knowledge of the portion of compressed fibers is achieved *a priori* and easily accounted for in numerical calculations. The statistical material model formulation proposed results well suited for multiscale generalization in the context of soft collagenous tissues.[21,22]

Acknowledgements

References

1. Renna A, Pandolfi A, Martinez FC, Aliò JL. Myopic surface ablation in asymmetrical topographies: refractive results and theoretical corneal elastic response. Am J Ophtalmol. 2017;177:34-43.
2. Pandolfi A, Manganiello F. A model for the human cornea: constitutive formulation and numerical analysis. Biomech Mod Mechanobiol. 2006;5:237-246.
3. Simonini I, Pandolfi A. Customized finite element modelling of the human cornea. PLoS One. 2015;10:e0130426.
4. Petsche SJ, Pinsky PM. The role of 3-d collagen organization in stromal elasticity: a model based on x-ray diffraction data and second harmonic-generated images. Biomech Mod Mechanobiol. 2013;12:1101-1113.
5. Pandolfi A, Vasta M. Fiber distributed hyperelastic modeling of biological tissues. Mech Mater. 2012;44:151-162.
6. Gizzi A, Pandolfi A, Vasta M. A generalized statistical approach for modelling fiber-reinforced materials. J Eng Math. 2017;1-16. doi:10.1007/s10665-017-9943-5.
7. Abass A, Hayes S, White N, Sorensen T, Meek KM. Transverse depth-dependent changes in corneal collagen lamellar orientation and distribution. J Roy Soc Interface. 2015;12:20140717.
8. Sacks MS. Incorporation of experimentally-derived fiber orientation into a structural constitutive model for planar collagenous tissues. J Biomech Eng – Trans ASME. 2003;125:280-287.
9. Lanir Y. Constitutive equations for fibrous connective tissues. J Biomech. 1983;16:1-12.

10. Organ CO, Saccomandi G. A new constitutive theory for fiber-reinforced incompressible nonlinearly elastic solids. J Mech Phys Solids. 2005;53:1985-2015.
11. Federico S, Herzog W. Towards an analytical model of soft tissues. J Biomech. 2008;41:3309-3313.
12. Gasser TC, Ogden RW, Holzapfel GA. Hyperelastic modeling of arterial layers with distributed collagen fibre orientations. J Roy Soc Interface. 2006;3:15-35.
13. Federico S, Gasser TC. Nonlinear elasticity of biological tissues with statistical fibre orientation. J Roy Soc Interface. 2010;7:955-966.
14. Vasta M, Gizzi A, Pandolfi A. On three-and two-dimensional fiber distributed models of biological tissues. Prob Eng Mech. 2014;37:170-179.
15. Gizzi A, Pandolfi A, Vasta M. Statistical characterization of the anisotropic strain energy in soft materials with distributed fibers. Mech. Mater. 2016;92:119-138.
16. Hashlamoun K, Grillo A, Federico S. Efficient evaluation of the material response of tissues reinforced by statistically oriented fibres. ZAMP. 2016;67:113.
17. Holzapfel GA, Niestrawska JA, Ogden RW, Reinisch AJ, Schriefl AJ. Modelling non-symmetric collagen fibre dispersion in arterial walls. J Roy Soc Interface. 2015;12:20150188.
18. Gizzi A, Vasta M, Pandolfi A. Modeling collagen recruitment in hyperelastic bio-material models with statistical distribution of the fiber orientation. Int J Eng Sci. 2014;78:48-60.
19. Latorre M, Montáns FJ. On the tension-compression switch of the Gasser–Ogden–Holzapfel model: Analysis and a new pre-integrated proposal. J Mech Behav Biomed Mater. 2016;57:175-189.
20. Li K, Ogden RW, Holpzafel GA. Computational method for excluding fibers under compression in modeling soft fibrous solids. Eur J Mech A/Solids. 2016;57:178-193.
21. Maceri F, Marino M, Vairo G. A unified multiscale mechanical model for soft collagenous tissues with regular fiber arrangement. J Biomech. 2010;43:355-363.
22. Marino M, Vairo G. Stress and strain localization in stretched collagenous tissues via a multiscale modelling approach. Comput Method Appl Mech Eng. 2014;17:11-30.

Mathematical modeling of ocular and cerebral hemo-fluid dynamics: application to VIIP

Fabrizia Salerni[1], Rodolfo Repetto[2], Alon Harris[3], Peter Pinsky[4], Christophe Prud'homme[5], Marcela Szopos[5], Giovanna Guidoboni[6]

[1]Mathematical, Physical and Computer Science, University of Parma, Parma, Italy; [2]Department of Civil, Chemical and Environmental Engineering, University of Genoa, Genoa, Italy; [3]Ophthalmology, Indiana University School of Medicine, Indianapolis, IN, USA; [4]Mechanical Engineering, Stanford University, Stanford, CA, USA; [5]Institute for Advanced Mathematical Research, UMR 7501, National Center for Scientific Research, University of Strasbourg, Strasbourg, France; [6]Department of Electrical Engineering and Computer Science, University of Missouri, Columbia, MO, USA

Abstract

This work aims at investigating the interactions between the flow of fluids in the brain and eyes, and their potential implications in the development of visual impairment and intracranial pressure (VIIP) syndrome in astronauts. We propose a reduced (0-D) mathematical model of fluid circulation in the eyes and brain, which is embedded into a simplified whole-body circulation model. This model allows us to predict fluid redistribution in the upper body vasculature as well as variation of the intracranial (ICP) and intraocular (IOP) pressures. The model results suggest that, by taking into account some effects of microgravity, it is possible to observe, on one hand, an increase in IOP, and on the other, a decrease in blood flow circulation in the choroid and ciliary body. These findings provide clues for the role that vascular components may play in VIIP pathogenesis, for which astronauts could be screened on Earth and in-flight.

Keywords: blood flow, intracranial pressure, intraocular pressure (IOP), visual impairment, intracranial pressure (VIIP) syndrome

Correspondence: Fabrizia Salerni, Department of Mathematical, Physical and Computer Science, University of Parma, Parco Area delle Scienze 7/A, 43124 Parma, Italy.
E-mail: fabrizia.salerni@studenti.unipr.it

1. Introduction

Long-term exposure to microgravity leads to several functional changes in the human body, among which one of the most serious is loss of visual function.

The many factors hypothesized to contribute to VIIP are: upper body fluid shift, alterations in IOP, ICP, cerebrospinal fluid (CSF) pressure, tissue deformation, and blood flow.[1]

Due to the difficulty of singling out each of these factors using *in-vivo* studies, we present a novel mathematical model to evaluate the interactions between the flow and pressures of fluids in the brain (blood, CSF, and interstitial fluid) and eyes (blood and aqueous humor), and their mathematical implications in VIIP.

As suggested in the literature, the effect of microgravity is accounted for by:
1. considering zero hydrostatic pressure;
2. imposing zero central venous pressure;
3. decreasing the blood/aqueous humor oncotic pressure difference ($\Delta\pi$); and
4. increasing the blood-brain barrier permeability.[2]

2. Methods

The physiological system is subdivided into a number of linked, interacting compartments in the brain and eyes, each of which contains a single physical constituent. An electrical analogue representation of the model is schematically shown in Figure 1.

The coupling between brain (adapted from Lakin and Stevens)[2] and eye (adapted from Guidoboni *et al.*, Szopos *et al.*, and Kiel *et al.*)[3-5] models allows us to account for the following mechanisms that we believe to be relevant in VIIP:
1. blood volume changes in the brain cause variations of the ICP and affect the pressure in the retrobulbar subarachnoid space;
2. blood volume in the ocular tissue has a direct impact on IOP:
3. deformation of the lamina cribrosa influences ocular blood perfusion as a result of the combined IOP, CSF pressure, and scleral tension; and
4. increase of aqueous humor production is triggered by changes in oncotic pressures.

By writing the Kirchoff law of currents at the circuit nodes, we obtain a set of non-linear algebraic equations. The non-linearity is a consequence of the fact that, in some compartments, resistances are assumed to depend on the pressures. Following Guidoboni *et al.*[3] and Pedley,[6] we model these deformable tubes as Starling resistors, reflecting the physiological high collapsibility of these vessels when the transmural pressure becomes negative.

The model is forced by the pressure drop between the central arteries (PA) and the central veins (PV) by the active secretion of aqueous humor in the eyes and by the production of CSF in the brain.
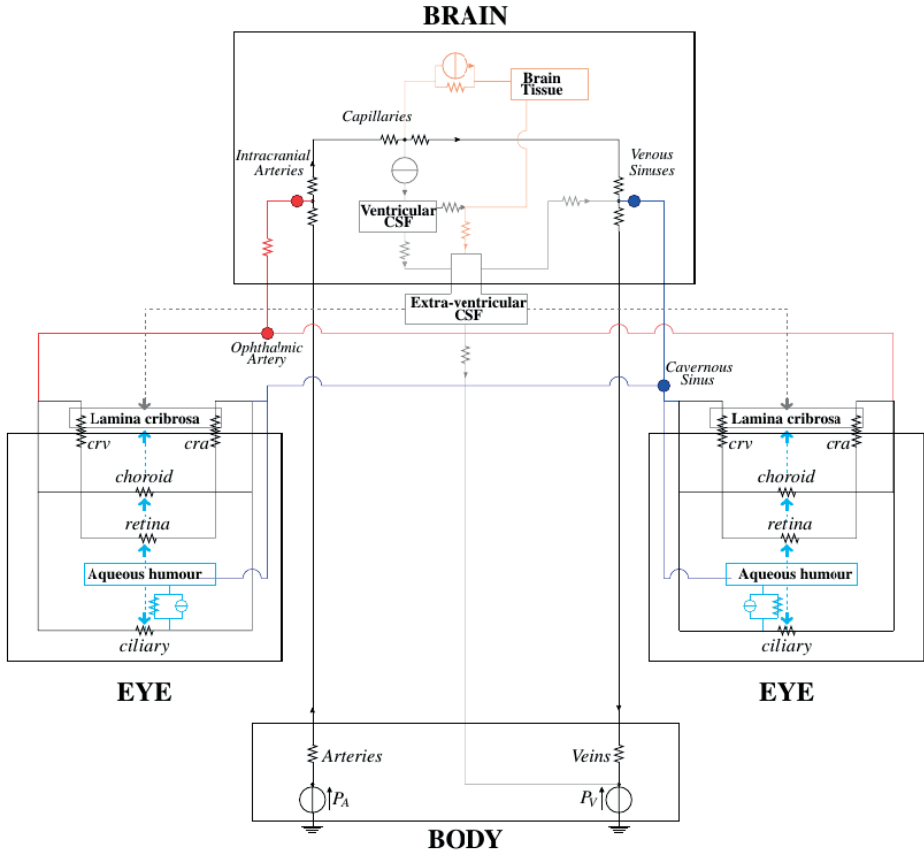
Fig. 1. 0-D model for the Body-Brain-Eyes system: blood vasculature (*black portion*), CSF network (*grey portion*), interstitial fluid network (*tan portion*), and aqueous humor network (*cyan portion*). The nodes correspond to the connection between the brain and eye models (*blue* arterial supply; *red*, venous drainage); the green and cyan arrows represent the pressures acting on both sides of the lamina cribrosa.

In this work, we focus on steady simulations, neglecting, in particular, time variations occurring on the time scale of heart beat. We also neglect autoregulation mechanisms, since we wish to keep the model relatively simple in order to understand its basic behavior. Moreover, little information exists about autoregulation mechanisms in orbit except that they might be altered due to high CO_2.[7]

This is the first time that all these model parts are combined into a single one. In order to assess the validity of the assumptions related to the coupling between the various components, we compared qualitatively and quantitatively the results provided by the whole model with several clinical findings:
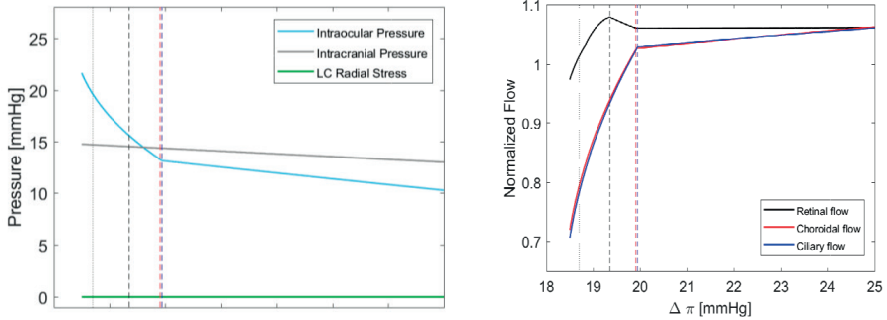
Fig. 2. (*Left*) Simulated IOP, ICP, and laminar compressive stress (LC radial showing that a decrease in Δπ in microgravity leads to a linear increase in ICP and a non-linear increase in IOP. This is due to the venous collapse: as the transmural pressure becomes negative, the Staring resistors collapse, giving rise to a significant increase in the resistance of the compartment). (*Right*) Simulated normalized blood flow in retinal, choroidal, and ciliary circulations. Dotted lines indicate Δπ values in microgravity, which differ from the physiological value on Earth of 25 mmHg. Dashed lines indicate Δπ values for which veins collapse in retinal (*black*), choroidal (*red*), and ciliary (*blue*) circulations.

1. choroidal venous pressure approximately equals IOP;
2. central retinal artery blood velocity decreases as IOP increases; and
3. IOP and ICP moderately increase with blood pressure, and the comparisons showed satisfactory agreement with experimental data.

3. Results

The model is used to simulate fluid shift from the limbs to the upper body, inducing changes in the plasma colloid osmotic pressures. Changes in the blood osmotic pressure modify both the brain pressure and IOP, owing to changes in the aqueous production rate.

Furthermore, the model predicts that ocular blood flow decreases markedly in the choroid and ciliary circulations when vessel collapse occurs (Fig. 2, right). Before venules collapse, the flux in the retina remains almost constant. This suggests that the particular architecture of the retinal vasculature provides a sort of mechanical (*i.e.*, purely passive) blood flow regulation when changes in IOP occur. When venules collapse in the ciliary and choroidal circulation, the flux in the retina initially grows, and only once the central retinal veins collapse, blood flow in the retina starts to drop significantly.

4. Conclusion

The model results suggest that:
1. IOP and ICP increase in microgravity conditions, but their respective trends may be different;
2. the venous segments play a fundamental role in controlling pressures and fluxes in the ocular circulation, owing to the possibility of their collapse; and
3. retinal circulation is less susceptible to microgravity-induced alterations than choroid and ciliary circulation.

These findings point towards further clinical assessment of ocular venous function in microgravity as a potential determinant factor for VIIP extensions.

Acknowledgements

References

1. Sigal IA, Flanagan JG, Tertinegg I, Ethier CR. finite element modeling in optic nerve. Invest Ophthalmol Vis Sci. 2004;45(12):4378–4387.
2. Sigal IA, Hongli Y, Roberts MD, Burgoyne CF, Downs CJ. IOP-induced lamina cribrosa displacement and scleral canal expansion: an analysis of factor interactions using parameterized eye-specific models. Invest Ophthalmol Vis Sci. 2011;52(3):1896–1907.
3. Sigal IA, Grimm JL, Jan NJ, Reid K, Minckler DS, Brown DJ. Eye-specific IOP-induced displacements and deformations of human lamina cribrosa. Invest Ophthalmol Vis Sci. 2011;55(1):1–15.
4. Causin P, Guidoboni G, Harris A, Prada D, Sacco R, Terragni S. A poroelastic model for the perfusion of the lamina cribrosa in the optic nerve head. Math Biosci. 2014;(257):33–41.
5. Guidoboni G, Harris A, Carichino L, Arieli Y, Siesky BA. Effect of intraocular pressure on the hemodynamics of the central retinal artery: a mathematical model. Math Biosci Eng. 2014;(11):523–546.
6. Biot MA. General theory of of three-dimensional consolidation. J Appl Phys. 1941;(12):155–164.
7. Biot MA. Theory of finite deformations of porous solids. Ind Univ Math J. 1972;21:597–620.
8. Larchè F, Cahn JW. Linear theory of thermomechanical equilibrium solids under stress. Acta. Metall. 1973;21:1051–1063.
9. Larchè F, Cahn JW. The interactions of composition and stress in crystalline solids. J Res Natl Bur Stand. 1984;89:467–500.
10. Honga W, Zhaoa X, Zhoua J, Suo Z. A theory of coupled diusion and large deformation in polymeric gels. J Mechan Phys Solids. 2008;56:1779–1793.
11. Eshelby JD. Elastic energy momentum tensor. J Elasticity. 1975;5:331–335.

A mesh-free approach to cornea-aqueous humor interaction during tonometry tests

Andrea Montanino[1], Maurizio Angelillo[2], Anna Pandolfi[1]

[1]Department of Civil and Environmental Engineering, Politecnico di Milano (Polytechnic University of Milan), Milan, Italy; [2]Department of Engineering, University of Salerno, Fisciano, Italy

Abstract

The dynamic tonometer test (air-puff test) is an *in-vivo* investigative procedure routinely utilized in ophthalmology to estimate the intraocular pressure (IOP). A rapid, localized air jet applied on the anterior surface induces the inward motion of the cornea, which interacts with the aqueous humor — filling the narrow space between cornea and iris — and has a strong influence on corneal dynamics. Potentially, this quick and painless test could be combined with inverse analysis methods to characterize the patient-specific mechanical properties of the human cornea. As a step towards this aim, the present study describes a fluid-structure interaction (FSI) approach based on a simplified geometry to simulate the anterior chamber of the eye undergoing the air-puff test. We regard the cornea as a non-linear, elastic, and isotropic membrane described through an analytical model, discretizing the weakly compressible Newtonian fluid with a mesh-free particle approach. Numerical analyses reveal a marked influence of the fluid on corneal dynamics. Additionally, we investigate the possibility of using the test dynamics to estimate IOP.

Keywords: air-puff test, collocation methods, fluid-dynamics, fluid-solid interaction, mesh-free methods, particle methods

Correspondence: Andrea Montanino, Politecnico di Milano, Dipartimento di Ingegneria Civile ed Ambientale, Piazza Leonardo da Vinci 32, 20133 Milano, Italy.
E-mail: andrea.montanino@polimi.it

1. Introduction

Experimental data on the human cornea obtained from *in-vivo* tests are of paramount importance for the design and implementation of predictive numerical methods in support of customized corneal refractive surgery. Patient-specific material properties must be determined necessarily by means of non-damaging tests performed on the anterior surface of the cornea. The most promising tests are based on the dynamic deformation of the cornea induced by a localized pressure following an assigned time history. During the test, the cornea snaps from the original convex shape to a locally concave shape and back. The inward deflection is contrasted by the presence of filling fluids (aqueous humor). In normal physiological conditions, fluids exert a uniform IOP on the posterior surface of the cornea, but during a dynamic test, the fluid pressure changes locally and loses uniformity. Advanced optical instruments (such as the Ocular Response Analyzer [Reichert Inc.; Buffalo, NY, USA] and the Corvis ST [Oculus Optikgerate GmbH; Wetzlar, Germany]) use a single rapid air jet applied at the center of the cornea to provide an estimate of the IOP together with diagrams of the evolution of the corneal apex displacement in the direction of the optic axis. Current numerical approaches to model the air-puff test are based on finite element technology. They use advanced solid models that reflect the complex collagen structure of the stroma and adopt anisotropic fiber reinforced material models for the solid parts.[1-7] Regrettably, the aqueous humor is always disregarded. A few attempts to account for the presence of the fluid include the use of spring-like elements or added fluid masses.[8,9] In this study, the interaction between aqueous humor and cornea is modeled explicitly to elucidate the influence of eye fluids on air-puff test dynamics.

The model comprises a membrane structure for the cornea and a mesh-free discretization (modified finite particle method, MFPM) for the fluid domain.[10] The dynamics of the anterior chamber of the eye undergoing an air-puff test are modelled as a FSI problem. For the sake of simplicity, axial symmetric conditions are considered and a non-linear isotropic material model is assumed for the solid. The solution is based on a partitioned approach. The simplified approach is the starting point for the development of an advanced 3-D model that will be employed to estimate the IOP and material properties by means of inverse analysis of multiple tests.

2. Model and results

2.1. Simplified model of the cornea and aqueous humor
The cornea is approximately a spherical cup (Fig 1a), but for modeling the air-puff test, a simplified axisymmetric configuration can be considered. Thus, the cornea reduces to a circular line, and the anterior chamber that contains the aqueous
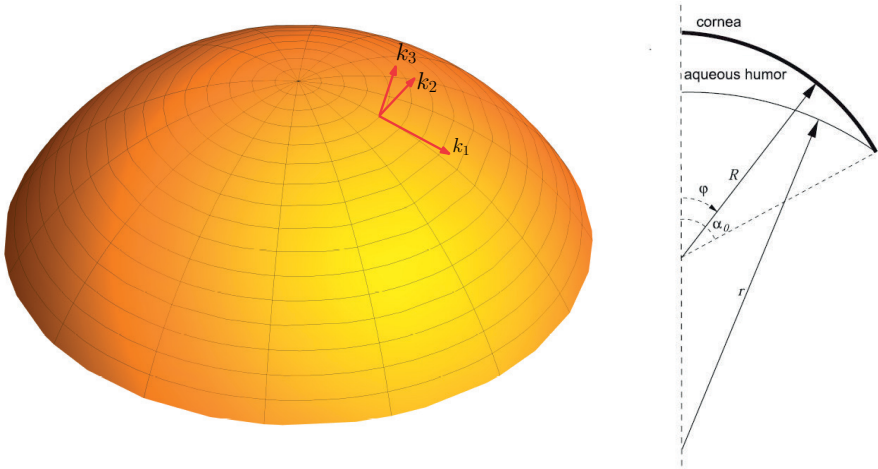
Fig. 1. (*a*) 3-D cornea spherical cup. (*b*) 2-D axis-symmetric approximation of the geometry of the cornea and anterior chamber.

humor becomes a closed surface (Fig. 1b). The posterior surface of the chamber, corresponding to iris and lens, is considered rigid.

The cornea is assumed to follow a classic isotropic hyperelastic material model able to capture the main non-linearities of biological tissues:

$$W = A \left[e^{\mathbf{C}(\mathbf{E}-\mathbf{E}_o)\cdot(\mathbf{E}-\mathbf{E}_o)} - 1 \right] \tag{1}$$

where A is a material constant with the dimension of an elastic modulus, $\mathbf{C}$ denotes a dimensionless fourth order elasticity tensor, and $\mathbf{E}$ the Green-Lagrange strain. The strain energy attains a minimum at the reference configuration $\mathbf{E}_0$, where the corresponding stress is null. The physiological state is characterized by $\mathbf{E} = \mathbf{0}$ and non-zero values of energy and stress. Corneal dynamics is governed by a non-linear equation of motion, solved with finite differences in space and an explicit Newmark algorithm in time.

The aqueous humor is modeled as a Newtonian, weakly compressible fluid, and its behavior is described by mass and linear momentum balance equations. Within the MFPM approach, the fluid domain is discretized in a finite number of nodes where the differential operators of the fluid equations are approximated. The FSI solution strategy adopted in the present study is based on a partitioned algorithm. The solid and fluid problems are solved independently, and coupling is enforced by means of an iterative procedure involving the actions at the boundaries where solid and fluid interact.
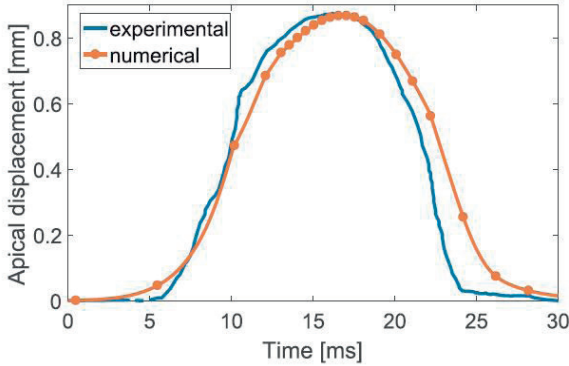
Fig. 2. Apex displacement vs time. Comparison between experimental data and numerical calculation.[7]
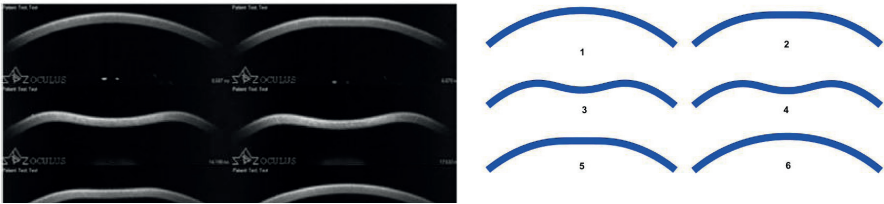

Fig. 3. Comparison between experimental and numerical results for the air-puff test at six different times. (*a*) Images of the Corvis ST output (http://www.healio.com). (*b*) Simulation results of the air-puff test with the present model.

2.2. Air-puff test simulation

The portion of the anterior surface of the cornea in proximity to the optic axis is loaded with the air-jet pressure, with a time history and a spatial distribution expressed by the equation:

$$p(t, \varphi) = p_{max} \exp[-a \sin^2 \varphi] \exp\left[-b \frac{(2t-T)^2}{4T^2}\right] \tag{2}$$

where T (duration) is 30 ms, p_{max} (peak pressure) is 10 kPa, and the constants are set, $a = 21.5$ and $b = 25$, respectively.

Figure 2 shows a comparison between the experimental data provided by the Corvis ST and the numerical simulation of the present model in terms of time history of the apex displacement.

A qualitative comparison between the images recorded by the Corvis ST (http://www.healio.com) during an air-jet test and a few snapshots of the simulation are shown in Figure 3. The numerical and experimental shapes of the cornea profiles at different times of the test compare rather well.

3. Conclusions

The model captures two important features of the time history of the apex displacement:
1. the delay in corneal response, *i.e.*, the displacement of the apex occurs at a distinct time interval after the action of the air-jet pressure over the whole process; and
2. the lack of symmetry of the apex displacement history.

These features must be attributed to the motion of the fluid. In fact, in the case of dynamic analysis without explicit modeling of the fluid, both effects appear less marked.[8,9] Evidently, the presence of the fluid causes a general deceleration of corneal motion due to the time needed by the speed front to cross the fluid domain, which possesses its own inertia. Note that, in the interpretation of the air-puff test, response delays, which are dynamic effects, are often mistakenly associated to a viscous behavior of the corneal material.

The approach presented here is oversimplified, given that it is based on sweeping assumptions of axis-symmetric geometry and isotropy of the material. Therefore, it is far from possessing any predictive ability. Nonetheless, it represents the very first application of a mesh-free method to the study of corneal dynamic behavior. In its simplicity, the model is sufficiently advanced to demonstrate the need for modeling the filling fluid in the dynamic analysis of the cornea undergoing the air-puff tests in order to avoid a wrong estimate of the material properties of ocular tissues.

References

1. Simonini I, Pandolfi A. Customized finite element modelling of the human cornea. PLoS One. 2015; 10(6):e0130426.
2. Sanchez P, Moutsouris K, Pandolfi A. Biomechanical and optical behavior of human corneas before and after photorefractive keratectomy, J Cataract Refr Surg 2014;40(6):905-917.
3. Ariza-Gracia MA, Zurita JF, Pinero DP, Rodriguez-Matas JF, Calvo B. coupled biomechanical response of the cornea assessed by noncontact tonometry. A simulation study. PLoS One. 2015; 10(3):e0121486
4. Ariza-Gracia MA, Zurita J, Pinero DP, Calvo B, Rodriguez-Matas JF. Automatized patient-specific methodology for numerical determination of biomechanical corneal response. Ann Biomed Eng. 2016;44(5):1753-1772.
5. Ortilles A, Rodriguez-Matas JF, Ariza-Gracia MA, Pascual G, Calvo B. Why non-contact tonometry tests cannot evaluate the effects of corneal collagen cross-linking. J Refract Surg. 2017;33(3):184-192.
6. Lanchares E, Del Buey MA, Cristobal JA, Calvo B, Ascaso FJ, Malve M. Computational simulation of scleral buckling surgery for rhegmatogenous retinal detachment: On the effect of the band size on the myopization. J Ophthalmol. 2016;2016:3578617.
7. Pandolfi A, Fotia G, Manganiello F. Finite element simulations of laser refractive corneal surgery. Eng Comput. 2009;25(1):15-24.

8. Simonini I, Pandolfi A. The influence of intraocular pressure and air jet pressure on corneal contactless tonometry tests. J Mech Behav Biomed. 2016;58:75-89.
9. Simonini I, Angelillo M, Pandolfi A. Theoretical and numerical analysis of the corneal air puff test. J Mech Phys Solids. 2016;93:118-134.
10. Asprone D, Auricchio F, Montanino A, Reali A. A modified finite particle method: Multi-dimensional elasto-statics and dynamics. Int J Numer Meth Eng. 2014;99(1):1-25.

Fluid structure interaction of the non-contact tonometry test

Miguel Ángel Ariza-Gracia[1], Wei Wu[2], Mauro Malve[3], Begoña Calvo[1], José Félix Rodriguez Matas[4]

[1]Mechanical Engineering Department, University of Zaragoza, Zaragoza, Spain; [2]Mechanical Engineering Department, University of Texas at San Antonio, San Antonio, TX, USA; [3]Mechanical Engineering Department, University of Navarra, Navarra, Spain; [4]Laboratory of Biological Structure Mechanics, Department of Chemical, Materials and Chemical Engineering, Politecnico di Milano (Polytechnic University of Milan), Milan, Italy

Abstract

The study of corneal biomechanics has gained interest due to its applications on predicting refractive surgery outcomes and the study of a number of pathologies affecting the cornea. In this regard, non-contact tonometry (NCT) has become a popular diagnostic tool in ophthalmology and as an alternative method to characterize corneal biomechanics. Since identification of material parameters using NCT tests rely on the inverse finite element method, accurate and reliable simulations are required. In this work, we present a full fluid structure simulation of a NCT test accounting for the effect of the presence of the humors. The results indicate that when inertial effects are considered, not including humors may lead to overestimating corneal displacement, and therefore, to an overestimation of the actual corneal stiffness when using the inverse finite element method.

Keywords: corneal mechanics, fluid structure interaction (FSI), non-contact tonometry (NCT)

1. Introduction

NCT has recently gained interest as a diagnostic tool in ophthalmology and as

Correspondence: Miguel Ángel Ariza-Gracia, i3A, Campus Río Ebro, Calle Mariano Esquillor Gómez S/N, C.P. 50018, Zaragoza, Spain.
E-mail: mariza@unizar.es

an alternative method for characterizing the mechanical behavior of the cornea. In a NCT test, a high-velocity air jet is applied to the cornea for a very short time (< 30 ms), causing the cornea to deform, while corneal motion is recorded by a high-speed camera. A number of biomarkers associated with corneal motion, *i.e.*, maximum corneal displacement and time between first and second applanation, among others, have been proposed to characterize pre- and postoperative bio-mechanical changes.[1-4] Identification of the material parameters associated with corneal mechanical behavior by means of a NCT test is usually performed using the inverse finite element method.[5-6] Hence, an accurate simulation of the NCT test is required. In this regard, most approaches model the NCT test as a quasi-static problem, considering only the cornea subjected to a constant intraocular pressure (IOP), and neglecting the inner structures of the eye, *i.e.*, the lens, ciliary muscles, and most importantly, the aqueous and vitreous humors. Considering that, during a NCT test, the dynamic pressure on the anterior surface of the cornea rises from 0 to 9~15 kPa in approximately 10 ms — implying a loading rate of approximately 1 MPa/s — neglecting inertial effects may result in inaccurate results. In this work, we perform fluid structure interaction (FSI) simulations in a 2-D model of the eye accounting for inertial effects and evaluating the effect of considering or not the presence of the humors in the model of the eyeball. Results indicate that when inertial effects are accounted for in the simulations, neglecting the humors in the model will lead to non-physiological results.

2. Methods

An axisymmetric 2-D model of the eyeball including the crystalline and ciliary muscles as inner structures as well as both humors — vitreous and aqueous – have been considered, as shown in Figure 1.

The cornea was modeled as an isotropic material described by a strain energy function of the form:[5]

$$W_{cornea} = D_1 \left(e^{D_2(\bar{I}_1 - 3)} + 1 \right) + \kappa (J - 1)^2 \tag{1}$$

where $\bar{I}_1$ is the first invariant of the modified right Cauchy-Green tensor, $\bar{C}$, $J = \sqrt{\det C}$ is the elastic volume ration, $D_1 = 7.56e\text{-}5$ MPa and $D_2 = 99.2$ are material constants chosen such that they fit inflation test experiments,[7] and κ is the bulk modulus. The sclera and ciliary muscles were also modeled as isotropic materials with strain energy function:

$$W_{sclera} = C_{10} (\bar{I}_1 - 3) + C_{20} (\bar{I}_1 - 3)^2 + C_{30} (\bar{I}_1 - 3)^3 + \kappa (J - 1)^2 \tag{2}$$

where $C_{10} = 0.81$ MPa, $C_{20} = 56.05$ MPa, and $C_{30} = 2{,}332.26$ MPa. The lens and the
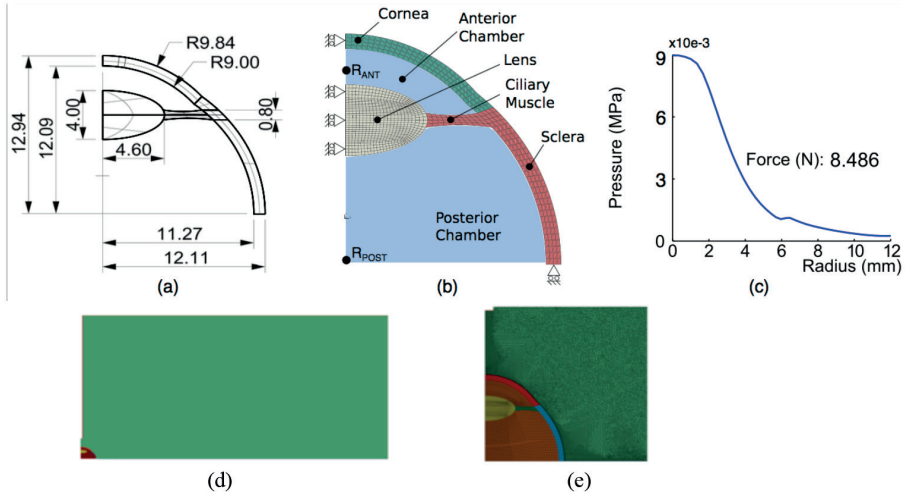
Fig. 1. Eyeball model. (*a*) Geometry. (*b*) Main parts. (*c*) Resulting pressure profile of the cornea. (*d*) Computational domain. (*e*) Detail of the finite element mesh.

muscle have been modeled as linear elastic materials with E = 1.45 MPa and E = 0.35 MPa, respectively, both considered highly incompressible (v = 0.47). The humors were considered as water.

　The air jet was applied as a ramp from 0 to 135 m/s in 10 ms and then back to zero velocity in 15 ms. Zero pressure was imposed as the outflow condition, and a turbulent flow model was used for the simulations. An IOP of 2 kPa was applied before initiating the air jet (Fig. 1). A mesh-sensitivity analysis was performed in the structural part in order to determine the minimum number of elements required for modeling the bending mode of the cornea. All simulations were performed using LS-DYNA Release 9.0 (LSTC, Livermore CA, USA and ANSYS, Inc., Canonsburg PA, USA) with Incompressible Computational Fluid Dynamics (ICFD) as fluid solver.

3. Results

The air jet caused a deflection in the cornea that reached its maximum value of 0.41 mm in correspondence with the peak velocity of the air jet (Fig. 2), as observed in actual application with the CorVis ST (OCULUS Optikgeräte GmbH Wetzlar, Germany) NCT.[4] During loading, the pressure in the anterior and posterior chambers of the eye (aqueous and vitreous humors) increased by three times (from 2 kPa to approximately 6 kPa), indicating that IOP changes due to the air-jet loading. In addition, as shown in Figure 2, the dynamic pressure exerted by the air jet is concentrated in an area of 6 mm in diameter with a Gaussian type spatial dis-
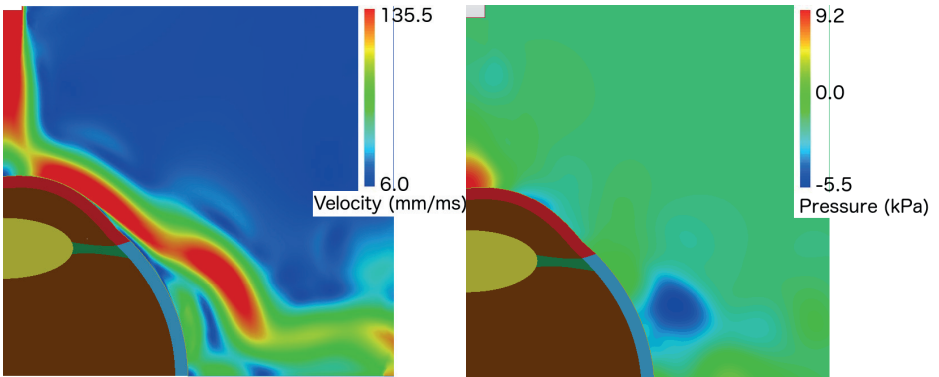
Fig. 2. Velocity field (*left*) and pressure distribution (*right*) of the air jet when the maximum velocity (135 m/s) is reached. At the same time, the cornea reaches maximum concavity.
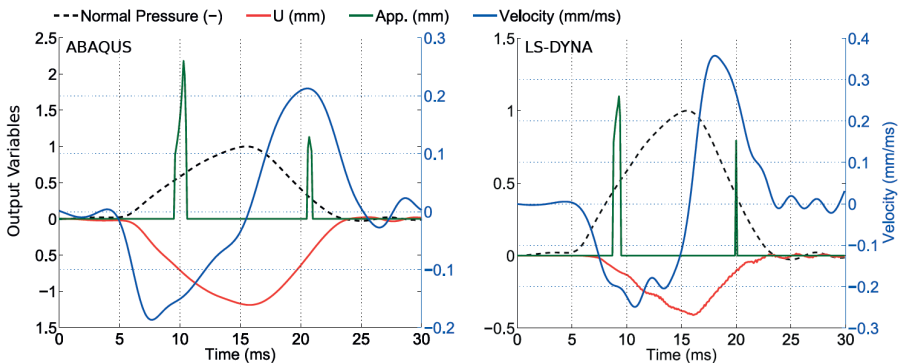

Fig. 3. Displacement and velocity of the apex of the cornea, and corneal applanation with and without humors. From 0 to 30 ms, both models are pressurized and stabilized at the IOP, after an air jet that lasted 25 ms.

tribution, and reaches the maximum value of 9.1 kPa, which is compatible with the theoretical value of 9.0 KPa.

The displacement experienced by the cornea is quite sensitive to the presence of humor in the model. If the simulation is performed without humor (using FSI and only structure analysis) with a constant IOP of 2 kPa, corneal displacement results five times greater (results not shown). If, on the contrary, a pure structural analysis is conducted, but allowing an increment of the cavity pressure with the deformation (fluid cavity feature in Abaqus), the maximum corneal displacement results three times greater with respect to the case of FSI with humors. These results indicate that humors are necessary in the model (Fig. 3).

4. Discussion and conclusions

NCT is gaining popularity as diagnosis tool in ophthalmology. A number of studies are considering this test as an alternative to characterize the mechanical behavior of corneal tissue.[3-5] However, in order to understand the contribution of the cornea to the mechanical response measured by the air jet, accurate simulations of the tests are required. Results from this study indicate that FSI simulations accounting for the presence of internal humors in the eye are required in order to accurately simulate the NCT test. Neglecting the humors and imposing a constant IOP during simulation lead to larger displacements of the cornea. In addition, these results indicate that most of the dynamic loading imposed by the air jet is absorbed by the humors, with minimal corneal contribution. Additional tests are required to study the sensitivity of the results (maximum corneal displacement) on the mechanical properties of the cornea and its thickness.

Acknowledgements

References

1. Lanza M, Iaccarino S, Bifani M. In vivo human corneal deformation analysis with a Scheimpflug camera, a critical review. J Biophotonics. 2016;9(5):464-477.
2. Ariza MA, Zurita JF, Piñero DP, Rodriguez Matas JF, B. Calvo B. Coupled biomechanical response of the cornea assesed by non-contact tonometry. A simulation study. PLoS One. 2016;10(3):e0121486.
3. Roy AS, Kurian M, Matalia H, Shetty R. Air-puff associated quantification of non-linear biomechanical properties of the human cornea in vivo. J Mech Behav Biomed Mater. 2015;48:173-182.
4. Hon Y, Lam AKC. Corneal deformation measurement using Scheimpflug noncontact tonometry. Optom Vis Sci. 2013;90(1):e1-e8.
5. Ariza-Gracia MA, Redondo S, Piñero D, Calvo B, Rodriguez Matas JF. A predictive tool for determining patient-specific mechanical properties of human corneal tissue. Comput Methods Appl Mech Eng. 2017;317:226-247.
6. Lago MA, Rupérez MJ, Martínez-Martínez F, et al. A new methodology for the in vivo estimation of the elastic constants that characterize the patient-specific biomechanical behaviour of the human cornea. J Biomech 2015;48(1):38-43.
7. Elsheikh A, Joda A, Abass A, Garway-Heath D. Assesment of the ocular response analyser as an instrument for measurement of intraocular pressure and corneal biomechanics. Curr Eye Res. 2015;40(11):1111-1119.

Thermodynamic derivation of a non-linear poroelastic model describing hemodynamics-mechanics interplay in the lamina cribrosa

Filippo Recrosi[1], Rodolfo Repetto[2], Amabile Tatone[3], Giovanna Guidoboni[4]

[1]GSSI, Gran Sasso Science Institute, L'Aquila, Italy, [2]DICCA, University of Genoa, Genoa, Italy, [3]DISIM, University of L'Aquila, L'Aquila, Italy, [4]Department of Electrical Engineering and Computer Science, University of Missouri, Columbia, MO, USA.

Abstract

In this paper we formulate a poroelastic model starting from a model of species diffusion in an elastic material. The model is applied to study the mechanics of the lamina cribrosa (LC) in the eye. The LC is a porous tissue at the head of the optic nerve. Deformation of this tissue and impairment of blood flow induced by tissue deformation are considered to be related to the pathogenesis of glaucoma.

The governing equations are derived from general thermomechanical principles. We carefully revise the role of the energy-stress Eshelby tensor, mutuated from the framework of tissue growth, in describing the hemo-mechanical behaviour of the tissue.

The model accounts for non-linear deformations of the solid matrix and deformation-induced changes in porosity and permeability. The model provides a qualitative better undertanding of the phatophysiology and pathogenesis of glaucoma in terms of coupling between tissue deformation and the resulting impaired hemodynamics inside the LC.

Keywords: blood perfusion, large deformations, poroelasticity, species diffusion

---

Correspondence: Filippo Recrosi, via Francesco Crispi 7, L'Aquila, Italy.
E-mail: filippo.recrosi@gssi.infn.it

1. Introduction

The LC is a part of the optic nerve head (ONH) acting as a scaold for collecting the retinal ganglion cells (RGC) axons. The optic nerve carries, through the axons, the signal generated by the retina to the brain. The LC is also a region crucial for blood supply to the whole optic nerve. An increased pressure inside the vitreous chamber (intraocular pressure, IOP) or a decreased pressure inside the subarachnoid space surrounding the optic nerve (cerebrospinal fluid pressure, CSFp) can generate a mechanical deformation of the LC, pinching the RGCs, possibly progressively leading to cell death. Further, lamina deformation can have an adverse effect on vascular perfusion of ocular tissue. Damages of the optic nerve are typical of glaucoma, a progressive optic neuropathy resulting in irreversible vision loss and blindness. A mathematical model able to describe the mechanics behind the pathogenesis of glaucoma would be invaluable, not only for diagnostic purposes by providing useful simulations and data, but also to support and guide, in the near future, the design of medical devices. Many researchers have worked on the mechanics of the ONH accounting for the complicated structure of the lamina. However, most of the literature focuses on the lamina deformation without accounting for the interactions with blood perfusion.[1-3] A possible strategy to eectively couple tissue deformation and blood perfusion is to model the tissue as a poroelastic material, where the saturated porosity stands for the vascular network made up of small vessels.[4,5] The aim of the present work is to study the interaction between porosity, tissue deformation, and blood perfusion.

2. Methods

We derive a poroelastic model[6,7] from a model of species diusion in an elastic material.[8,9] This derivation is formulated in the not common framework of virtual powers,[10] and it is carried out by transforming, in a natural way, quantities appropriate to a diusing species, such as concentration, chemical potential, and molar flux into the corresponding quantities which are appropriate to a saturated porous material, such as porosity, interstitial pressure, and discharge, while retaining the usual description for a non-linear elastic solid, based on deformation and stress.

We get a couple of power balance laws for the forces and for the mass of the fluid filling the pores:

$$\int_{P_o} \mathbf{b}_0 \cdot \mathrm{v}_0 dV + \int_{\partial P_o} \mathbf{t}_0 \cdot \mathbf{v}_0 dA = \int_{P_o} \mathbf{S}_0 \cdot \dot{\mathbf{F}}_0 \, dV \tag{1}$$

$$\int_{P_o} \breve{p}_0 \dot{\beta} \, dV = -\int_{\partial P_o} \breve{p}_0 \mathbf{q}_0 \cdot \mathbf{n}_0 dA + \int_{P_o} \mathbf{q}_0 \cdot \nabla \breve{p}_0 dV \tag{2}$$

where P_0 is any part of the referential body simultaneously showing the presence of both fluid and solid parts, v_0 is the velocity test field, $\dot{\mathbf{F}}_0$ is the time rate of the deformation gradient, $\mathbf{b}_0$ and to are respectively any volume and surface density of external forces, and $\mathbf{S}_0$ is the first Piola-Kirchho stress tensor. Moreover, $\breve{p}_0$ is the interstitial pore pressure, β is the determinant of the total deformation and $\mathbf{q}_0$ is the fluid flux.

Superimposing the contributions of both external power expenditures, the energy imbalance principle reads:

$$\mathbf{S}_0 \cdot \dot{\mathbf{F}}_0 + \breve{p}_0 \dot{\beta} - \mathbf{q}_0 \cdot \nabla \breve{p}_0 - \frac{d}{dt}\varphi \geq 0 \tag{3}$$

from which we state some constitutive prescriptions on the form of every dissipative term, together with a Darcy's law coupling tissue deformation with the flux:

$$q_0 = -\mathbf{K}_0 \nabla \breve{p}_0 \tag{4}$$

We assume a second order dependence of the permeability tensor $\mathbf{K}_0$ from the porosity, through a modified Carman-Kozeny equation, which should be appropriate to describe the capillary network. We emphasize how this characterization relies on the expression for the free energy, mutuated by tissue growth models, and in turn, on the stress energy function:

$$\mathbf{T} = \widehat{\mathbf{T}}^{\text{eff}}(\mathbf{F}_\iota, \beta) - \breve{p}_0 \mathbf{I} \mid = \left(\widehat{\mathbf{T}}^{\text{g}}(\mathbf{F}_\iota) + \left(\widehat{p}_\phi(\beta) + \phi_\iota(\mathbf{F}_\iota)\mathbf{I} \right) - \breve{p}_0 \mathbf{I} \right) \tag{5}$$

Table 1. Parameter values used in the simulations.

Description	Value
lamina thickness	0.02 cm
lamina external radius	0.095 cm
central retinal vessel passage radius	0.01 cm
shear modulus of the lamina	8×10^3 Pa
bulk modulus of the lamina	6×10^5 Pa
shear modulus of the sclera	11×10^5 Pa
reference porosity	0.01
max IOP	4666-4800 Pa
RLTp	1300 Pa
ciliary pressure	2000 Pa
central vein pressure	1000 Pa

where $\widehat{\mathbf{T}}^{\text{eff}}$ is the ective stress and $\phi_t(\mathbf{F}_t)$ is the spherical part of the Eshelby tensor.[11]

We perform numerical simulations on a three-D system - depicted in the background of Figure 1 - consisting in a curved disk embedded in a portion of peri-papillary slera (ppS). The LC is modelled as a non-linear poroelastic tissue, whose governing equations are (4) and (5), while the surrounding ppS is described as an hyperelastic incompressible medium. The blood supply is imposed by assigning the value of the ciliary pressure at the LC-ppS interface, aswell as the blood drainage by assigning the value of the central vein pressure on the hole surface, located at the center of the cap (Fig. 1). On the upper boundary of the LC (facing the vitreous chamber), we increase the IOP from physiological values (15 mmHg) to pathological ones (up to 35 mmHg), whereas on the lower surface (facing to the retrolaminar region) we assign a value of retrolaminar tissue pressure (RLTp). The most meaningful parameter values are reported in Table 1.
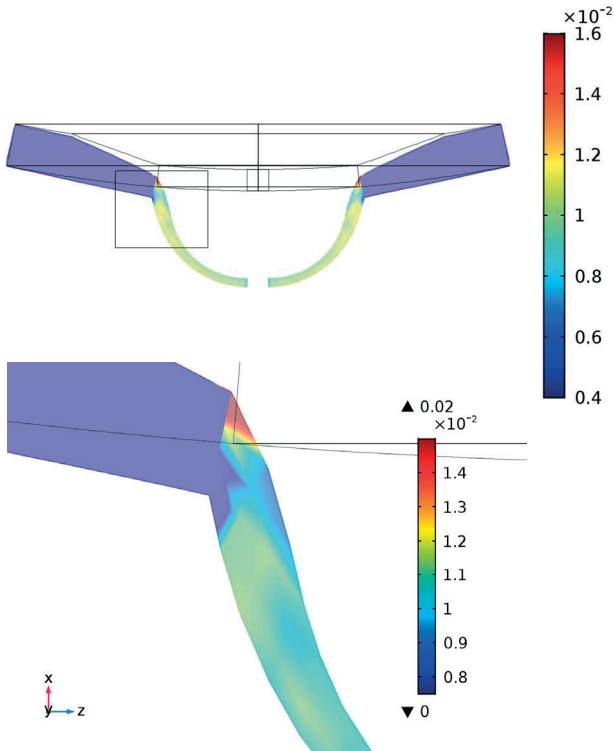

Fig. 1. Radial section of the LC-ppS system deformed under IOP = 35 mmHg. The colors show the value of the porosity field inside the LC: from low (*blue*) to high values (*red*). The boxed picture is a magnification of the interface region.
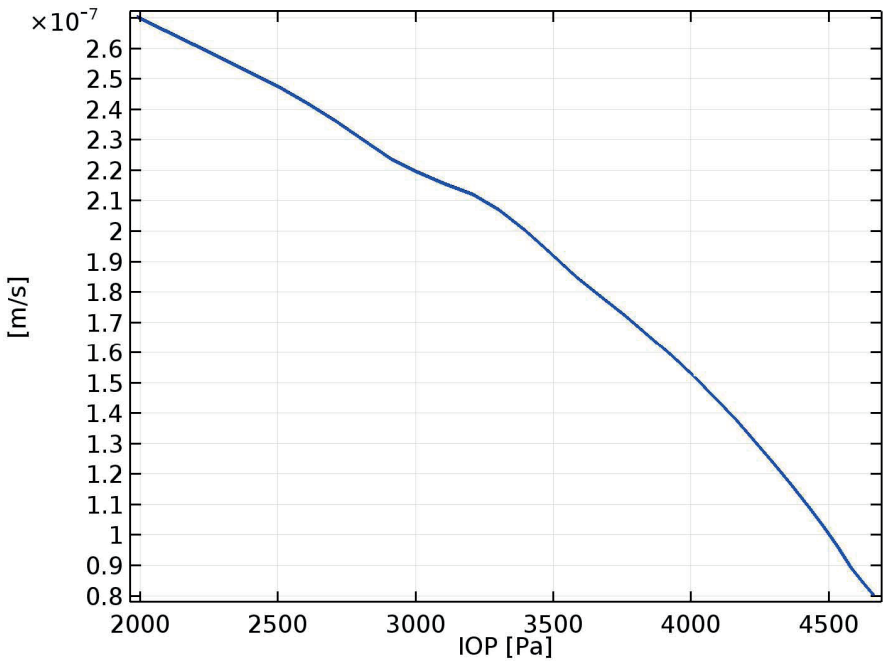
Fig. 2. Blood flux as a function of IOP.

3. Results

Figure 1 shows the porosity map, obtained for a high IOP value (35 mmHg), and the corresponding tissue deformation. A magnification of the LC-pps interface region is also shown, since this is where the most significant coupling between tissue deformation and changes in porosity occur, which strongly aects blood flow.

Figure 2 shows that the blood flux decreases for increasing values of IOP. IOP increases from physiological values (corresponding to 2000 Pa) towards increasingly more severe stages of glaucoma, up to IOP = 4666 Pa. The cause of such a decrease is related to the large deflection of LC portions close to the sclera, and the related appearance of a low porosity region crossing all the LC thickness (see the magnification of the interface region in Fig. 1).

4. Discussion

These preliminary results suggest that tissue deformation can influence blood flow significantly, at least in certain regions of the LC. The decrease in blood flow from

posterior ciliary arteries to the central retinal vein secondary to tissue deformation is far from being a minor adverse eect on the RGC axons, and it seems to be crucial for better understanding the pathogenesis of glaucoma.

References

1. Sigal IA, Flanagan JG, Tertinegg I, Ethier CR. finite element modeling in optic nerve. Invest Ophthalmol Vis Sci. 2004;45(12):4378–4387.
2. Sigal IA, Hongli Y, Roberts MD, Burgoyne CF, Downs CJ. IOP-induced lamina cribrosa displacement and scleral canal expansion: an analysis of factor interactions using parameterized eye-specific models. Invest Ophthalmol Vis Sci. 2011;52(3):1896–1907.
3. Sigal IA, Grimm JL, Jan NJ, Reid K, Minckler DS, Brown DJ. Eye-specific IOP-induced displacements and deformations of human lamina cribrosa. Invest Ophthalmol Vis Sci. 2011;55(1):1–15.
4. Causin P, Guidoboni G, Harris A, Prada D, Sacco R, Terragni S. A poroelastic model for the perfusion of the lamina cribrosa in the optic nerve head. Math Biosci. 2014;(257):33–41.
5. Guidoboni G, Harris A, Carichino L, Arieli Y, Siesky BA. Effect of intraocular pressure on the hemodynamics of the central retinal artery: a mathematical model. Math Biosci Eng. 2014;(11):523–546.
6. Biot MA. General theory of of three-dimensional consolidation. J Appl Phys. 1941;(12):155–164.
7. Biot MA. Theory of finite deformations of porous solids. Ind Univ Math J. 1972;21:597–620.
8. Larchè F, Cahn JW. Linear theory of thermomechanical equilibrium solids under stress. Acta. Metall. 1973;21:1051–1063.
9. Larchè F, Cahn JW. The interactions of composition and stress in crystalline solids. J Res Natl Bur Stand. 1984;89:467–500.
10. Honga W, Zhaoa X, Zhoua J, Suo Z. A theory of coupled diusion and large deformation in polymeric gels. J Mechan Phys Solids. 2008;56:1779–1793.
11. Eshelby JD. Elastic energy momentum tensor. J Elasticity. 1975;5:331–335.

Saccadic movement effects on intraocular drug delivery for a wet-AMD clinical case

Marco Ferroni[1], Matteo Cereda[2], Federica Boschetti[1]

[1]Department of Chemistry, Materials, and Chemical Engineering "Giulio Natta", Politecnico di Milano (Polytechnic University of Milan), Milan, Italy; [2]Department of Biomedical and Clinical Science Luigi Sacco, Sacco Hospital, University of Milan, Milan, Italy

Abstract

Nowadays, intravitreal injections are the gold standard for the treatment of age-related macular degeneration (AMD). The prediction of the transport mechanism for the injected anti vascular endothelial growth factor (anti-VEGF) is needed in order to understand its distribution and consumption after each injection. Thus, this study aims at implementing a full model of vitreous drug delivery. The main novelty of this work is the coupling between an experimental evaluation of the scleral permeability and a numerical analysis of the saccadic dependency of the transport phenomena.

Keywords: age-related macular degeneration (AMD), computational fluid-dynamics, saccade, vitreous drug delivery

1. Introduction

One of the main ocular diseases related to aging is the wet form of AMD, which is treated with anti-VEGF injections in the eye. This problem has been tackled with different computational approaches, considering either the influence of the tissues surrounding the posterior chamber or the saccadic movements.[1,2] No work combines saccadic movements, surrounding physiological conditions, and drug injection and

Correspondence: Marco Ferroni, LaBS, Chemistry Materials and Chemical Engineering Department "Giulio Natta", Piazza L. da Vinci 32, 20133 Milan, Italy.
E-mail: marco.ferroni@polimi.it

consumption in a single model for a specific case of wet-AMD. Furthermore, the hydraulic conductivity behavior of the sclera has not been evaluated yet. The aim of this work is to develop a complete model of drug delivery in the posterior chamber of patients suffering of wet-AMD, showing the influence of the combination of the saccadic movements, physiological boundary conditions, and drug consumption upon drug distribution inside the vitreous.

2. Materials and methods

2.1. Geometrical reconstruction, mesh, and computer code
The idealized geometry was reconstructed from orbital magnetic resonance imaging (MRI) images, representing the effective anatomy and shape of the human posterior chamber bounded by the hyaloid membrane, the lens, and the retina-choroid-sclera (RCS) complex (Fig. 1).
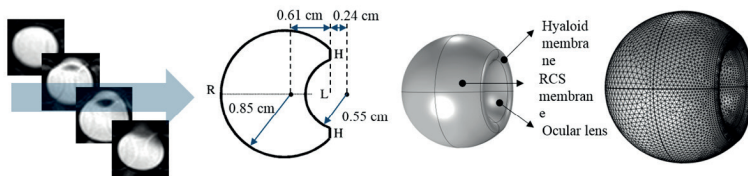

Fig. 1. MRI-based reconstruction and domain meshing.

The values of the radii of curvature of the retina and lens are equal to 0.85 cm and 0.55 cm, respectively. The retina and lens have two centers of curvature with respect to the hyaloid membrane, the posterior one of 0.61 cm, and the anterior one of 0.24 cm. The bolus that mimics the intravitreal drug injection was modeled as a sphere with a radius of 2.29 mm in order to recreate the clinical injected volume in cases of wet-AMD (0.05 mL). Structured meshes and all the simulations were performed using the commercial software Comsol Multiphysics 5.2 (COMSOL Inc.; Burlington, MA, USA) and built with at least 250,000 elements.

2.2. Characterization of scleral permeability
In a similar fashion to other experimental studies in the ocular field, we used bovine samples due to their high availability and similarity to human anatomy.[3] Cylindrical samples were prepared and tested within two days after slaughter and preserved at 4°C to slow the degradation process (Fig. 2).

The experimental setup consists of a closed chamber within which the sample is placed and constrained. The pressure drop is applied from the top and developed through a hydraulic head of saline solution that acts directly on the sample. From the bottom, the fluid flows into a graduated capillary in relation to its hydraulic con-
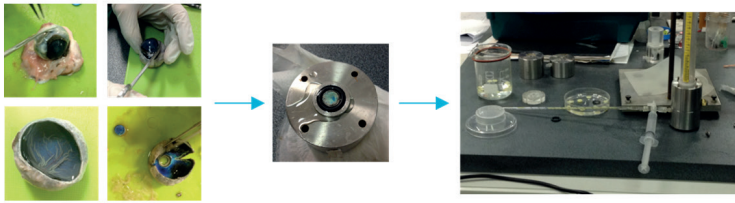
Fig. 2. Sample preparation and experimental setup for scleral permeability.

ductivity following Darcy's law, whereas its trend as function of the pressure drop is obtained through interpolation. This function is implemented in the modeled posterior chamber to describe the changes in the permeation of the vitreous humor in relation to the time changes of the pressure drop.

## 2.3. Computational fluid-dynamic modeling

The vitreous humor inside the eye was modeled as water at ocular temperature (T = 34°C)[4] due to the liquefaction occurring in the presence of wet-AMD; thus, the Navier-Stokes and the continuity equations for a 3-D unsteady, incompressible Newtonian flow were solved. The imposed boundary conditions allowed us to consider the posterior chamber surrounded by its biological environment: indeed, they mimic the pressure exerted by the anterior chamber (intraocular pressure, IOP = 15 mmHg) and the outflow of fluid through the RCS complex, governed by Darcy's law. In particular, we imposed:

1. no aqueous permeation through the lens;
2. IOP at the posterior hyaloid surface; and
3. normal velocity across the porous RCS membrane, defined by the hydraulic conductivity function experimentally evaluated.

In addition to these conditions, the saccades were implemented. This involuntary movement during the ocular focusing of an object was defined as a fifth-grade polynomial, considering the maximum angular displacement of a saccade (50°) without the introduction of a rest time in order to represent the most stressful condition *in vivo*.

2.4. Drug delivery modeling

In order to analyze the influence of the saccadic movements on the delivery of anti-VEGF, the law of conservation of mass, Fick's law, Navier-Stokes, and continuity equations were properly coupled with each other. The imposed drug concentration of the injected bolus was equal to 0.207 mol/m^3, as 0.5 mg is the standard quantity of the humanized monoclonal antibody fragment Ranibizumab, with a molecular weight of 48 kDa.[5] The drug reaction was imposed only at the retinal surface, as shown by clinical evidence, and implemented as a linear relation between the outflow from the RCS complex and the retinal drug concentration.[1]
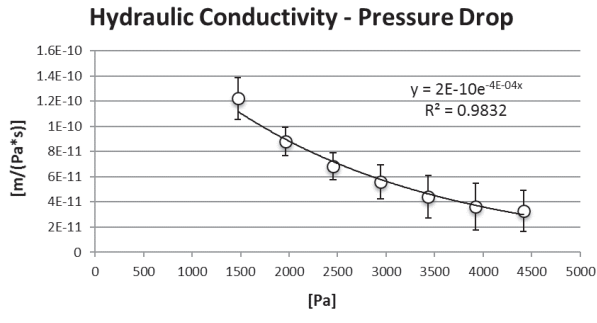
Fig. 3. Exponential decay for scleral hydraulic conductivity by varying acting pressure drop.
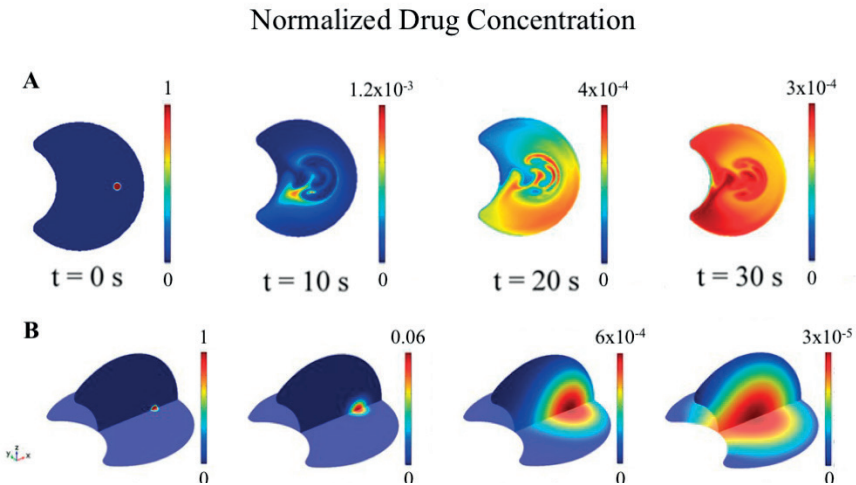
Fig. 4. Normalized concentration in the equatorial plane in case of saccade (*A*), and in the equatorial and vertical planes without saccade (*B*).

3. Results

The averaged trend of the permeability of the scleral samples related to the acting pressure drop is shown in Figure 3. The interpolation reported an exponential function, which is the typical trend for soft tissues.

The velocity distribution on the equatorial plane is purely dependent on the saccadic motion, with a slower volumetric flow rate (2.98 μL/min) if compared to the case without pure saccadic motion (5.32 μL/min), due to the mixing effect of the saccade. Streamline analysis shows two main stagnant regions on the equatorial
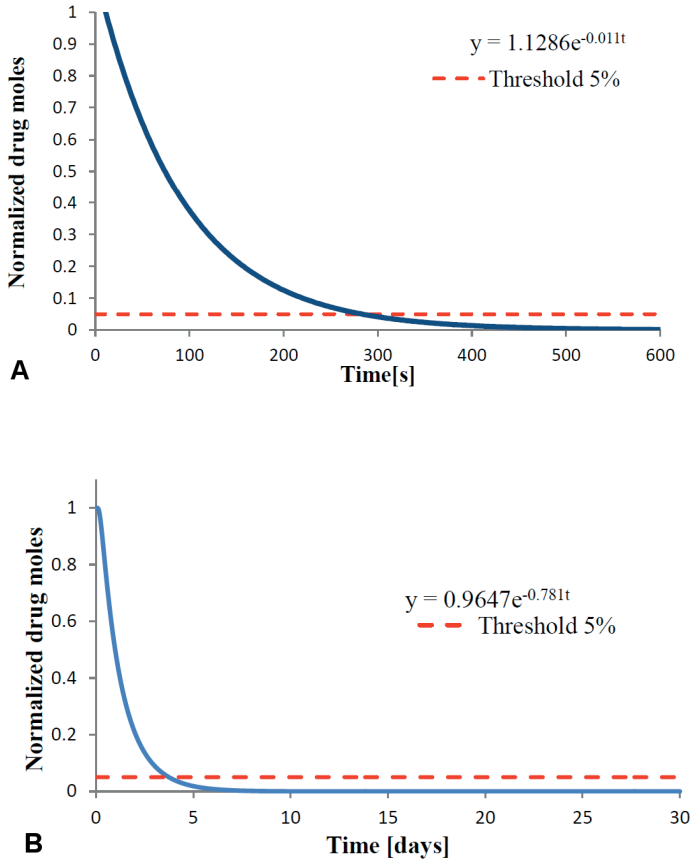
Fig. 5. Time decay of Ranibizumab in the presence (*A*) and absence of saccade (*B*).

plane. The distribution of the anti-VEGF in the equatorial and vertical planes, in the presence and absence of saccadic motion, is shown in Figure 4, underlining how the saccades allow a faster drug distribution. We interpolated the decay in time of the injected Ranibizumab with an exponential trend line in order to analyze the trend after the 120 seconds of simulation, imposing a threshold line of 5% under which the drug is considered totally consumed (Fig. 5A). In the absence of saccadic movements, drug uniformity is hard to reach, so its decay is considered under the 5% threshold almost four days after the injection (Fig. 5B).

4. Conclusion

This study shows that saccadic movements cannot be neglected due to their great influence on both the fluid-dynamic and drug delivery mechanism inside the posterior chamber of the eye under wet-AMD conditions. The drug tends to concentrate in the stagnant zones analyzed in the fluid-dynamic part, with a pattern strictly related to the saccade before reaching a type of uniform distribution. A complete characterization of the surrounding tissues is also mandatory in order to consider the changes in permeation across the RCS complex and the specific anti-VEGF consumption near the retinal surface. The experimental evaluation of the relation between permeability and applied pressure drop as well as its implementation in a computational fluid-dynamics model represents a novelty in this field.

References

1. Stay MS, Xu J, Randolph TW, Barocas VH. Computer simulation of convective and diffusive transport of controlled-release drugs in the vitreous humor. Pharm Res. 2003;20(1):96-102. Available from:http://www.ncbi.nlm.nih.gov/pubmed/12608542
2. Modareszadeh A, Abouali O, Ahmadi GG. Saccade movements effect on the intravitreal drug delivery in vitreous substitutes: a numerical study. Biomech Model Mechanobiol. 2013;12(2):281-290. doi:10.1007/s10237-012-0398-3
3. Xu J, Heys JJ, Barocas VH, Randolph TW. Permeability and diffusion in vitreous humor: implications for drug delivery. Pharm Res. 2000;17(6):664–669.
4. Romano MR, Vallejo-Garcia JL, Romano V, Angi M, Vinciguerra P, Costagliola C. Thermodynamics of vitreoretinal surgery. Curr Eye Res. 2013;38(3):371–374. doi:10.3109/02713683.2012.745160
5. Veurink M, Stella C, Tabatabay C, Pournaras CJ, Gurny R. Association of ranibizumab (Lucentis®) or bevacizumab (Avastin®) with dexamethasone and triamcinolone acetonide: An in vitro stability assessment. Eur J Pharm Biopharm. 2011;78(2):271–277. doi:10.1016/j.ejpb.2010.12.018

Assessment of the fluid dynamic performance of a vitreous cutter

Alessandro Stocchino[1], Rodolfo Repetto[1], Mario Romano[2]

[1]Department of Civil, Chemical and Environmental Engineering, University of Genoa, Italy; [2]Department of Biomedical Sciences, Humanitas University, Milan, Italy

Abstract

Vitreous cutters are surgical devices used during vitrectomy to remove the vitreous humor from the eye and replace it with tamponade fluids. The aim of the present work is to assess the performance of the EVA Phaco-vitrectomy System vitreous cutter (Dutch Ophthalmic Research Center (DORC) BV; Zuidland, The Netherlands) used with different needle sizes and blade shapes. The analysis is based on laboratory measurements of fluid flow performed using the particle image velocimetry (PIV) technique.

Keywords: particle image velocimetry (PIV), vitrectomy, vitreous cutter

1. Introduction

Vitreous cutters are surgical devices used during vitrectomy to remove the vitreous humor from the eye and replace it with tamponade fluids. A lot of attention has been devoted in recent years to optimize the shape of cutter needles with the aim of improving removal efficacy without generating excessive mechanical stress on the retina. The amount of mechanical stress on the retina during the vitrectomy procedure depends on the fluid flow generated during vitreous aspiration. Recently, Rossi *et al.* performed PIV measurements of fluid flow around the tip of various cutter blades and proposed a way of assessing the performance of the vitreous cutter.[1] In particular, they propose to evaluate the performance of the device making use of a diagram (see Fig. 8 of their paper),[1] in which they report the volumetric flux pumped by the cutter on the y-axis and the time derivative of the local fluid velocity,

Correspondence: Alessandro Stocchino, Dipartimento di Ingegneria Civile, Chimica e Ambiente, via Montallegro, 1, 16145 Genova, Italy.
E-mail: alessandro.stocchino@unige.it

$\partial\mathbf{u}/\partial t \equiv \dot{\mathbf{u}}$ (averaged over a certain spatial domain), on the x-axis. The rationale about the diagram is that, if a cutter is able to produce large fluxes, it is considered "efficient". Moreover, large values of $\dot{u}$ are considered "dangerous", while low values of $\dot{\mathbf{u}}$ are referred to as "safe". The quantity $\dot{\mathbf{u}}$ (or fluid acceleration, which also accounts for the convective acceleration, $(\mathbf{u}\cdot\nabla)\mathbf{u}$, is indeed a sensible kinematic quantity to consider, since it is likely to be closely related to fluid pressure, which in turn affects the stress on the retina.

In the present work, we perform systematic experiments on the EVA Phaco-vitrectomy System with different needle sizes and blade shapes to assess its performance.

2. Methods

We perform PIV measurements of the flow around the tip of vitreous cutters. Measurements are taken on two vertical planes orthogonal to each other, which are illuminated with a laser sheet. The time resolution of the measurements is such that we manage to resolve the fast oscillations of the flow induced by the high-frequency cutting rate.

We perform all measurements in balanced salt solution (BSS). We also plan to perform experiments in viscoelastic fluid in the near future.

We use cutters with three different diameters (23, 25, and 27 gauge), two different blade configurations (high-speed cutter [VC] and double cutter [TDC]), and two working modes ("core" and "shaving").

From the PIV measurements, we obtain instantaneous velocity fields, $\mathbf{u} = (u(\mathbf{x}, t),$ $v(\mathbf{x}, t))$. From these instantaneous fields, many other quantities can be obtained. In particular, we derive fluid acceleration, kinetic energy, vorticity, and rate of deformation. Moreover, for each kinematic quantity we perform:
1. spatial averages that give us information about the time evolution of the flow field;
2. time averages that provide a general picture of the averaged spatial distribution of the flow; and
3. time and space averages.

Since the flow is not exactly axisymmetric, it is not possible to obtain an accurate estimate of the volumetric flux from the PIV measurements taken on a plane, which would require a full 3-D reconstruction of the flow field around the tip of the needle. To overcome this difficulty, we employ a different technique. We illuminate a vertical plane of the whole reservoir containing the fluid, and track the position of the free surface in time. Knowing the cross-sectional area of the reservoir, we can evaluate the volumetric flux pumped by the vitreous cutter. We note that, with this approach, we cannot resolve the fast oscillations of the flux related to the cutting frequency.
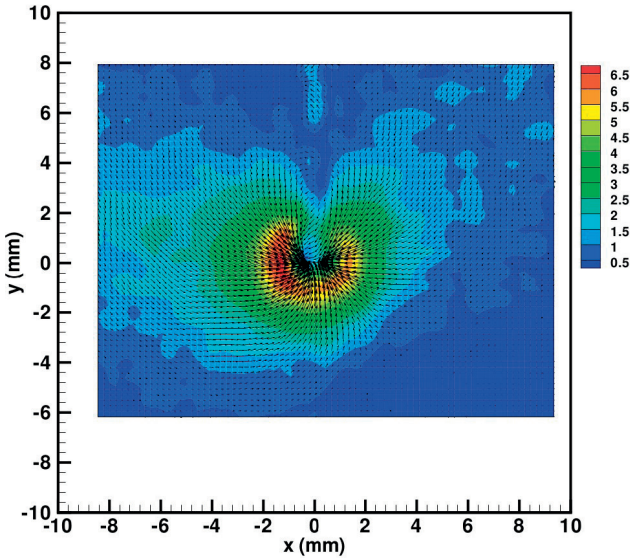
Fig. 1. Example of an instantaneous velocity field (*arrows*). The color map represents the velocity magnitude in mm/s.

3. Results

In Figure 1 we plot an example of a measured instantaneous velocity field, $\mathbf{u}(\mathbf{x},t)$, at a given time t. This is the basic output of the cross-correlation procedure that is performed to analyze the PIV images. The region depicted in the plot is a square with side ≈ 18 mm, and the quality of the images is such that we manage to compute ≈ 3600 velocity vectors on the measurement plane. The plane of measurement is not exactly in correspondence to the cutter needle, so that the whole image is occupied by the fluid. The magnitude of the velocity, |u|, is also reported in Figure 1. The velocity field is very regular and approximately symmetrical, as expected on this plane. Note that the slight departure from symmetry can be due to experimental errors, but also to the asymmetry of the suction needle.

In Figure 2 we show examples of the time evolution of the spatially averaged kinetic energy. The spatial average has been taken over a circle centered in correspondence to the cutter cleft with a radius of 3 mm. We note that, obviously, the values of the averaged quantities depend on the size of the region over which averaging is performed. Figure 2 also shows that the kinetic energy has fast oscillations about an average value . These oscillations are due to the cutting cycle, and therefore, have a dominant frequency equal to the cutting one.

In Figure 3 we report a plot that summarizes the main outcomes of the present
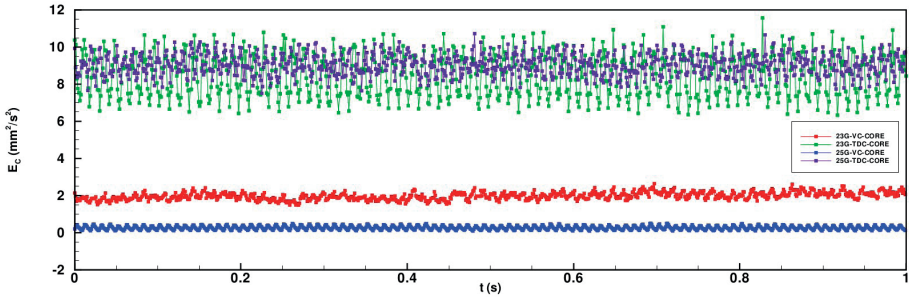
Fig. 2. Example of time evolution of the spatially averaged kinetic energy per unit mass.
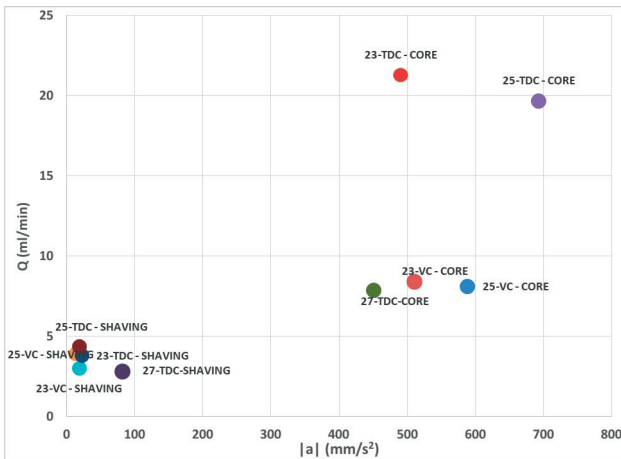

Fig. 3. Diagram showing, for each experiment, flux vs time and space-averaged magnitude of fluid acceleration.

analysis, analogous to Figure 8 in the paper by Rossi *et al.*[1] Each point in the plot identifies an experiment. On the x-axis, we report the magnitude of the time- and space-averaged fluid acceleration; on the y-axis, the volumetric flux. We note that in each experiment we used the cutter in conditions similar to those adopted in clinical practice.

4. Conclusion

The results show that, for a given cutter size and pressure, with the TDC, the velocity, and consequently, the flux, are significantly larger than in the corresponding VC cases. The accelerations, however, have a different behavior. In particular, for the 23-gauge case they are very similar in the TDC and VC cases, in spite of the fact

that in the former the flux is more than double. For the 25 gauge, the acceleration is greater in the TDC case. However, the difference between the accelerations is much smaller than the differences between the fluxes. These results show that, in the TDC case, the accelerations induced are significantly smaller for a given flux than in the VC case.

Acknowledgements

References

1.   Rossi T, Querzoli G, Angelini C, et al. Introducing new vitreous cutter blade shapes. Retina. 2014;34:1896-1904.

Effect of an iris-fixated intraocular lens on corneal metabolism: a numerical study

Peyman Davvalo Khongar[1], Jan Oscar Pralits[1], Xi Cheng[2], Peter Pinsky[2], Paolo Soleri[3], Rodolfo Repetto[1]

[1]Department of Civil, Chemical and Environmental Engineering, University of Genoa, Genoa, Italy; [2]Department of Mechanical Engineering, Stanford University, Stanford, CA, USA; [3]Ophtec BV, Groningen, Netherlands

Abstract

One of the possible risks associated with the implant of iris-fixated phakic intraocular lenses (pIOL) is loss of corneal endothelial cells. We hypothesize that this might be due to alterations in corneal metabolism secondary to the lens implantation. To verify the feasibility of this assumption, we propose a mathematical model of the transport and diffusion of metabolic species in the anterior chamber and the cornea, coupled to a model of aqueous flow. Results are obtained both with and without the pIOL in the case of closed eyelids. The results suggest that glucose availability may be significantly reduced at the corneal endothelium. However, it must still be verified whether this finding has clinical relevance.

Keywords: aqueous flow, corneal metabolism, intraocular lens

1. Introduction

In recent years, pIOL have gained widespread acceptance for the correction of visual acuity deficiencies, such as myopia. These lenses are implanted surgically into the anterior chamber of the eye and fixated to the iris by special claws. The procedure is considered very safe; however, a possible complication is the loss of corneal endothelial cells. We hypothesize that this might be due to alterations in

Correspondence: Peyman Davvalo Khongar, Department of Civil, Chemical and Environmental Engineering, University of Genoa, Via Montallegro 1, 16145, Genova, Italy.
E-mail: peyman.davvalo.khongar@edu.unige.it

corneal metabolism after pIOL implantation.

Although considerable research has been devoted to mathematical modeling of corneal metabolism, less attention has been paid to include the effect of metabolic species transport across the anterior chamber by the aqueous flow. In this study, we investigate corneal metabolism with and without a pIOL, accounting for aqueous flow in the anterior chamber. Since the cornea receives glucose mostly from the aqueous humor, and following the observation that the pIOL modifies aqueous flow characteristics,[1] we speculate that pIOL implantation may affect corneal metabolism.

When the eyelids are open, the thermal flow and the flow generated by eye rotations are likely intense enough so that the concentration of each metabolic species in the anterior chamber can be considered constant, and consequently, the effect of a pIOL in the delivery of metabolic species to the cornea can be neglected. On the other hand, when the eyelids are closed, aqueous flow is only induced by the production/drainage mechanism[1] and the resulting velocities are very small. Therefore, it is likely that the concentration of metabolic species will be variable across the anterior chamber and affected by the presence of the pIOL. Thus, we focus on the closed eyelid case.

2. Methods

In the present work, we adopt a model for oxygen, lactate, and glucose transport, based on that proposed in by Chhabra *et al.*[2] and Pinsky,[3] considering the role of aqueous humor flow in transporting metabolic species. We improve the previous models by using a sigmoidal oxygen consumption model, as proposed in Alvord *et al.*[4] We adopt an idealized axisymmetric shape of the anterior chamber and consider three superposed corneal layers (endothelium, stroma, epithelium) based on previous work (Fig. 1).[1,3] The geometry of the pIOL has been provided by Ophtec BV; Groningen, Netherlands.

Results are obtained by solving the Navier-Stokes equations for the fluid flow and the following advection-diffusion equations in the aqueous for oxygen tension (denoted by a subscript O), glucose (subscript G), and lactate (subscript L) concentrations:

$$k_O \frac{\partial p_O}{\partial t} + k_O (u \cdot \nabla) p_O - D_O k_O \nabla^2 p_O = 0 \tag{1}$$

$$\frac{\partial C_G}{\partial t} + (u \cdot \nabla) C_G - D_G \nabla^2 C_G = 0 \tag{2}$$

$$\frac{\partial C_L}{\partial t} + (u \cdot \nabla) C_L - D_L \nabla^2 C_L = 0 \tag{3}$$

where p_O, c_G, and c_L are the oxygen tension, glucose, and lactate ion concentrations,
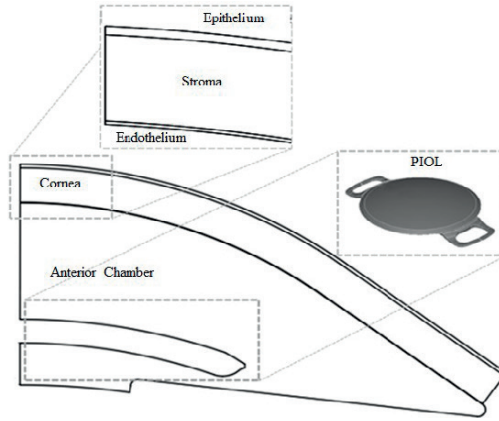
Fig. 1. Cross-section of the idealized anterior chamber with corneal layers and fixated pIOL.

respectively, and u is the flow velocity vector. D_i ($i = O, G, L$) are the diffusion coefficients and k_O is Henry's constant.

The transport of metabolic species in the cornea is described by the following equations:

$$k_O \frac{\partial p_O}{\partial t} - D_O k_O \nabla^2 p_O + Q_O = 0 \tag{4}$$

$$\frac{\partial C_G}{\partial t} - D_G \nabla^2 C_G + Q_G = 0 \tag{5}$$

$$\frac{\partial C_L}{\partial t} - D_L \nabla^2 C_L - Q_L = 0 \tag{6}$$

Here, Q_L and Q_G are the lactate production and glucose consumption rates, respectively,[2] and Q_O is the oxygen consumption rate given by:

$$Q_O = \frac{Q_{Qmax}^i}{1 + e^{\frac{-(p_O - P_{crt})}{R}}} \frac{C_G}{C_G + K_G^O} \left(1 + 0.8 \frac{7.6 - pH}{K_{pH} + 7.6 - pH}\right) \tag{7}$$

In the above expression p_{crt} and R are coefficients of the sigmoidal oxygen consumption model.[4] K_{pH} is set to be 0.1 and K_G^O is the glucose Monod dissociation equilibrium. Q_{Qmax}^i ($i = O,G,L$) is the saturation oxygen consumption rate.[2] For the closed eyelids case, we set $pH = 7.39$.[5]

3. Results

The results presented below refer to the case of closed eyelids. Steady-state simulations demonstrate that when the eyelids are closed, the presence of a pIOL
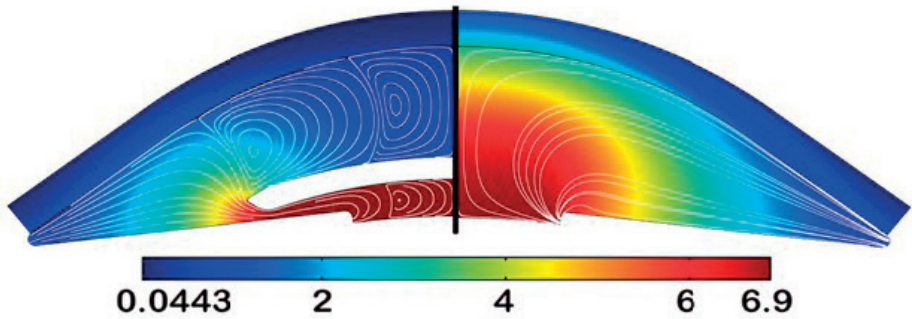
Fig. 2. Glucose concentration shown by colors and flow streamlines in white with (*left*) and without (*right*) a pIOL, in the case of closed eyelids.

has a strong influence on glucose availability on the cornea, as shown in Figure 2. Since the aqueous flow is diverted towards the periphery of the anterior chamber, glucose is depleted in a region anterior to the pIOL in comparison to the case with no pIOL.

Unsteady simulations have also been carried out, starting from conditions representative of open eyelids. As illustrated in Figure 3, glucose concentration at the center of the cornea declines progressively in time and asymptotically reaches the steady state. However, several hours are needed for this steady solution to be reached. During sleep, the typical time interval between successive rapid eye
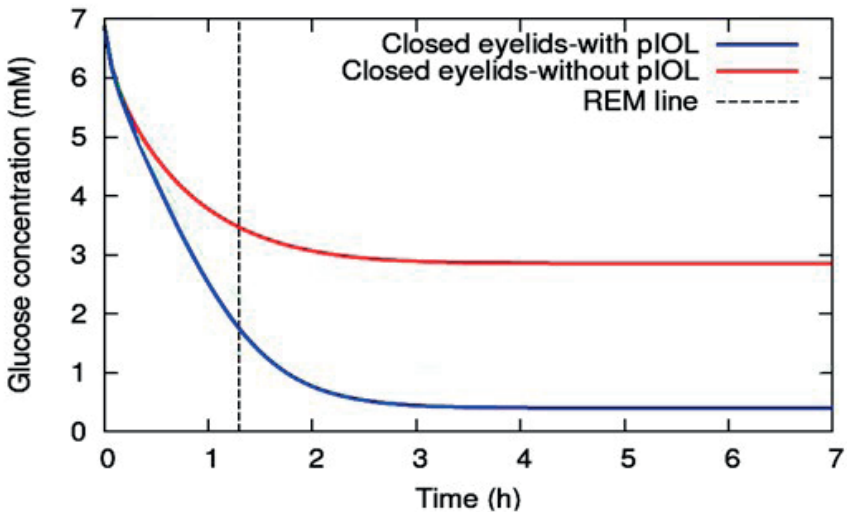

Fig. 3. Time evolution of glucose concentration at the center of cornea with (*blue*) and without (*red*) pIOL. The dashed line represents the REM time of 90 min.

movements (REMs) is 90 minutes. REMs are expected to make the glucose distribution more uniform due to the motion of aqueous humor. It can thus be conceivable that the steady state is unlikely to be ever reached. Nevertheless, the glucose reduction in the time intervals between successive REM phases is significant.

4. Conclusion

Our findings demonstrate that in the presence of an iris-fixated pIOL, when the eyelids are closed, glucose concentration at the corneal endothelium may decline significantly. It must be verified whether this has a clinical relevance.

Acknowledgements

References

1. Repetto R, Pralits, JO, Siggers, JH, Soleri P. Phakic iris-fixated intraocular lens placement in the anterior chamber: effects on aqueous flow. Invest Ophthalmol Visual Sci. 2015;56(5):3061–3068.
2. Chhabra M, Prausnitz JM, Radke CJ. Diffusion and monod kinetics to determine in vivo human corneal oxygen-consumption rate during soft contact-lens wear. J Biomed Mater Res B Appl Biomater. 2009;90(1):202–209.
3. Pinsky PM. Three-Dimensional modeling of metabolic species transport in the cornea with a hydrogel intrastromal inlay. Invest Ophthalmol Visual Sci. 2014;55(5):3093–3106.
4. Alvord LA, Hall WJ, Keyes LD, Morgan CF, Winterton LC. Corneal oxygen distribution with contact lens wear. Cornea. 2007;26(6):654–664.
5. Bonanno JA, Polse KA. Corneal acidosis during contact lens wear: effects of hypoxia and CO2. Invest Ophthalmol Visual Sci. 1987;28(9):1514–1520.